DEVELOPMENT AND TESTING OF A PROTOTYPE PILOT EXPANSION VALVE FOR VAPOR COMPRESSION SYSTEMS

A Thesis

by

EDWIN LARRY YOUMSI PETE

Submitted to the Office of Graduate and Professional Studies of
Texas A&M University
in partial fulfillment of the requirements for the degree of

MASTER OF SCIENCE

Chair of Committee,	Bryan Rasmussen
Co-Chair of Committee,	Jerald Caton
Committee Member,	Perla Balbuena
Head of Department,	Andreas Polycarpou

May 2015

Major Subject: Mechanical Engineering

ABSTRACT

The Vapor Compression Cycle (VCC) is the fundamental thermodynamic principle behind most Heating, Ventilation, Air Conditioning and Refrigeration (HVACR) systems. HVACR systems account for a vast majority of the energy used in residential and commercial buildings. There is a growing need to make these VCC systems and their respective components more energy efficient. This thesis proposes a prototype pilot expansion device. Preliminary results have shown that this prototype expansion valve outperforms most of the expansion devices currently being used in HVACR applications.

Valve hunting and superheat control are very important elements in the operation of expansion valves. They reduce system efficiency and increase energy consumption. To address these problems, the combination of conventional expansion valves with other expansion devices or components is still a relatively unexplored area. This approach has the potential to improve the energy efficiency of HVACR systems thus reducing cost of operation. This thesis discusses the development, design and proof-of-concept testing of a Prototype Pilot Expansion Valve (PPEV).

A number of tests were designed and carried out in order to objectively compare the performance of the PPEV to that of an Electronic Expansion Valve (EEV) and a Thermal Expansion Valve (TEV) under a variety of operational conditions. These tests involve a superheat change test, startup test and external fluid flow rate test, all carried

out at varying compressor speeds. The tests were carried out on a custom-built modulated water chiller system and a residential heat pump system.

The results obtained from these tests validated that the PPEV performed significantly better than the EEV and the TEV. It was able to provide more cooling, better superheat control and consistently higher Coefficient of Performance (COP). In addition, this thesis also provides and proves the validity of a mathematical model for the Prototype Pilot Expansion Valve.

Furthermore, an additional test was carried out to prove the possibility of an integrated design that will enable to PPEV to not rely on any external component to operate. This test demonstrates the possibility to use the compressor inlet and outlet to operate the PPEV thus confirming the possibility of a truly integrated design.

DEDICATION

This work is dedicated to my parents; Francois and Berthe Youmsi Mogtomo, to my siblings, Boris, Ariane and Pierre-Francois, and to all my friends and teachers.

ACKNOWLEDGEMENTS

I would like to thank my thesis adviser, Dr. Bryan Rasmussen for his teaching, guidance, financial and moral support over the course of this research work. I would also like to thank the members of my committee Dr. Jerald Caton and Dr. Perla Balbuena for all that they taught me and for serving on my thesis committee.

Furthermore, I would like to thank all the members of the Thermo-Fluids Control Lab; Erik Rodriguez, Kaimi Gao, Chao Wang, Chris Bay, Rohit Chintala, Chris Price, Rawand Jalal, Priyam Parikh, Franco Morelli, Trevor Terrill and Shuangshuang Liang for their help and advice. I would also like to thank all my professors and teachers at Texas A&M University, Sacred Heart College, Mankon and PNEU Douala.

Finally, I would like to thank my parents, my brothers, my sister and my friends for their constant support and encouragement.

ABBREVIATIONS

VCC	Vapor Compression Cycle
HVACR	Heating, Ventilation, Air Conditioning and Refrigeration
TEV	Thermal Expansion Valve
EEV	Electronic Expansion Valve
PPEV	Prototype Pilot Expansion Valve
AEV	Automatic Expansion Valve
psi	Pounds Per Square Inch

NOMENCLATURE

	Units	**Explanation**
P_i	[kPa]	Net inlet Pressure
P_s	[kPa]	Spring Force
P_e	[kPa]	Evaporator Pressure
A_d	[m^2]	Diaphragm Area
m_v	[kg/s]	Mass flow rate
x_0	[m]	Initial compression of spring
K_s	[N/m]	Spring Constant
δx	[m]	Net axial spring movement
P_0	[kPa]	Nominal Pressure
C_1	[m^2/N]	Valve parameter #1
C_2	[m^2/N]	Valve parameter #2
ρ	[kg/m^3]	Density
P_c	kPa	Condenser Pressure
A_1	[m^2]	Valve inlet area
A_2	[m^2]	Valve outlet area

TABLE OF CONTENTS

Page

LIST OF FIGURES

Page

LIST OF TABLES

Page

CHAPTER I

INTRODUCTION

As of 2013, the Department of Energy estimates that residential and commercial buildings account for 40% of the energy used in the United States [1]. Of these, air conditioning and refrigeration systems account for about 14% of the energy used in residential buildings and about 12% of the energy used in commercial buildings as shown in Figure 1 and Figure 2. This data only considers buildings and therefore does not account entirely for the use of HVACR system in the United States. HVACR systems are also heavily used in other sectors such as transportation and industry.

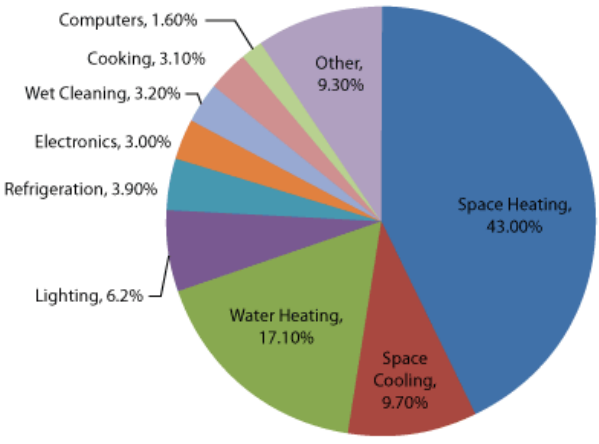

Figure 1: Energy consumption by end use in residential buildings [1]

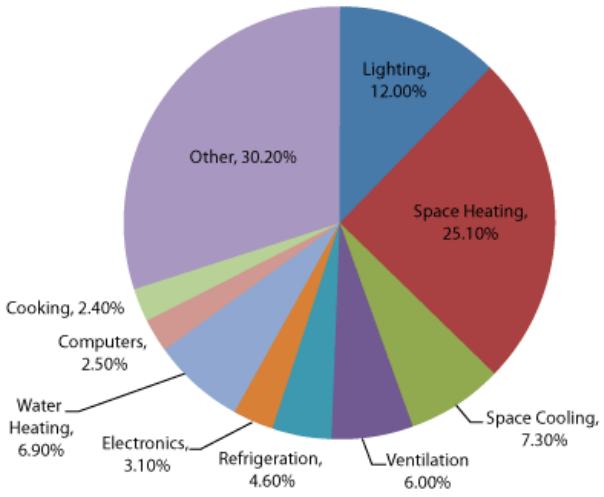

Figure 2: Energy consumption by end use in commercial buildings [1]

With increasing population growth and urbanization, there is a consequential increase in the demand for energy, but not an equivalent increase in the supply of this energy. As such, using the available energy efficiently is of great importance. This implies minimizing the amount of energy used in HVACR systems while meeting comfort, operational and user requirements.

Background

The Vapor Compression Cycle (VCC) is the fundamental thermodynamic principles behind most HVACR systems. The VCC consists of four main components; a compressor, a condenser, an expansion valve and an evaporator. The amount of energy consumed by a VCC system is directly dependent on the performance of these four

components. With the use of a refrigerant as a medium, the VCC absorbs and removes heat from a space to be cooled. This cycle operates from four main processes as shown in Figure 3.

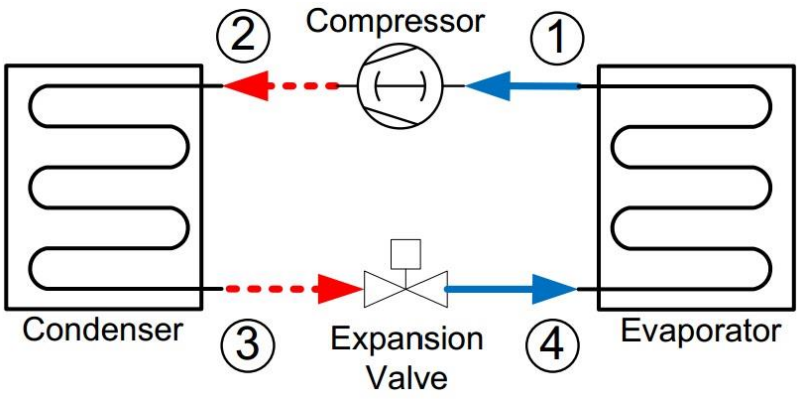

Figure 3: The vapor compression cycle [2]

From a pressure perspective, this cycle can be broken down into two sides; the high pressure side also referred to as high side and the low pressure side also referred to as low side. In Figure 3, the high side of the cycle goes from state 2 to state 3 and is represented by the red arrows while the low side goes from state 4 to state 1 and is represented by the blue arrows. The flow of refrigerant across the Vapor Compression Cycle shown is as described below.

- Process 1-2: Isentropic compression. A superheated vapor from the evaporator comes into the compressor where it is compressed and attains a higher pressure and consequently a higher temperature. It then enters the condenser.
- Process 2- 3: Isobaric condensation. The superheated from the compressor enters the condenser where heat rejection occurs and the superheated vapor refrigerant is condensed into a saturated liquid.
- Process 3-4: Isenthalpic expansion: The saturated liquid from the condenser is routed to the expansion valve where it goes through a throttling process. This expansion process reduces the temperature of the exiting liquid and vapor refrigerant mixture to the point where it is lower than the temperature of the enclosed space to be refrigerated. This expansion is achieved without the absorption or the rejection of heat.
- Process 4-1: Isobaric evaporation. The liquid and vapor refrigerant mixture at state 4 moves into the evaporator where a heat extraction process occurs and the refrigerant exits as a saturated vapor at state 1. This saturated vapor then once again enters the compressor where isentropic compression occurs and the cycle starts all over again.

This Vapor Compression Cycle can be represented by a Pressure-Enthalpy (P-h) diagram as shown in Figure 4. In this figure, the red curve represents the saturated liquid line on the left and saturated vapor line and the right. Under this curve, the refrigerant exists as a mixture of vapor and liquid. On the left of the saturated liquid line, the

refrigerant exists as a sub-cooled liquid while on the right of the saturated vapor line it exists as a superheated vapor. The line from 2 to 3 represents the cooling form of the refrigerant from being a superheated vapor to be a saturated liquid.

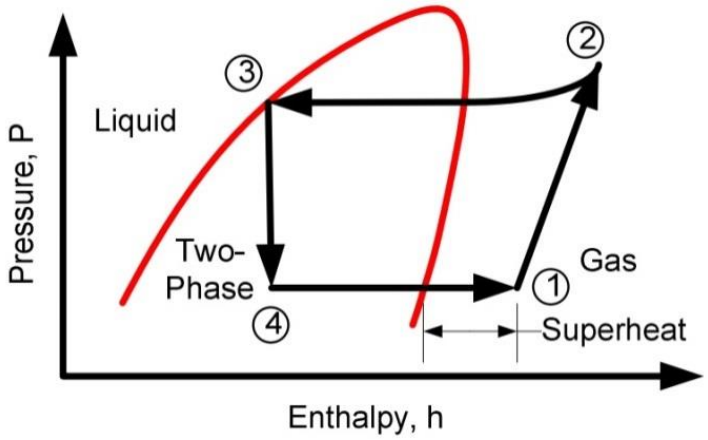

Figure 4: P-h diagram of the vapor compression cycle [2]

The expansion valve has two main roles: serve as a metering device for the flow of refrigerant through it and convert the high pressure liquid refrigerant at its inlet into low pressure two-phase refrigerant at its outlet. The roles of expansion valves have been potentially overlooked in the research to improve the energy efficiency of VCC [3]. This project seeks to capitalize on the opportunities for improvement of the energy efficiency of VCC systems which are provided by expansion valves.

One of the main issues affecting the performance of VCC systems is valve hunting. Valve hunting is a phenomenon whereby the expansion valve exhibits an oscillatory behavior in its opening as it tries to find a stable opening position. This behavior is highly undesirable and has been plaguing expansion valves from the beginning of their existence [4]. Valve hunting negatively affects the performance of the expansion valve as well as the energy efficiency of VCC systems [4].

Another factor which affects VCC systems is evaporator superheat control. Superheat refers to the difference between the temperature of the refrigerant at the outlet of the evaporator and the saturation temperature of the refrigerant. Through its metering role, the expansion valve is directly responsible for maintaining the level of superheat. A VCC system's cooling capacity is directly dependent on the two-phase flow to the evaporator, so controlling this flow effectively leads to better superheat control and system efficiency.

Expansion valves typically struggle to deal with the issues of superheat control and hunting. Both poor superheat control and hunting negatively affect the performance of VCC systems [5]. Yet, they are very common in the day to day operation of expansion valves [6]. The expansion valve developed in this project tackles both of these problems and provides considerable improvements to the performance of VCC systems as will be discussed later.

Literature Review

The basic concepts of air conditioning can be traced as far back as ancient Egypt [7]. At that time, the Egyptian people made use of evaporative cooling to cool the interior of their houses by hanging wet cloths and reeds on the doorways and windows. As wind blew through the doorway and windows, the air in the room would be cooled. Similarly, in ancient Rome, wealthy Roman citizens would build aqueducts in the walls of their houses through which cold water would flow in order to provide interior cooling [7]. Air conditioning slowly evolved throughout the centuries. A Chinese inventor named Ding Huane built a manually powered rotary fan in the second century [8] and in 1758 Benjamin Franklin carried out several experiments with evaporation and alcohol to attain freezing temperatures [8]. However, the industrial revolution of the 18^{th} century led to the inventions of the various parts and components of what are collectively known as Heating, Ventilation and Air Conditioning (HVAC) systems. The modern air conditioner is widely credited as an invention of Wills H. Carrier in 1902. Carrier's air conditioning system sent air through coils filled with cold water, cooling the air while at the same time removing moisture to control room humidity. During the 1950s and 1960s there was a rapid growth in the popularity of residential air conditioning systems in the United States and as of 2009, approximately 87% of the households in the country have been equipped with an air conditioner [9].

As the demand for HVAC systems soared, so did the amount of energy needed to operate them. However, the supply of this energy struggled to match the rapidly growing demand. This situation led to a widespread interest to make HVAC systems

more energy efficient. The energy efficiency of a VCC system is directly dependent on the performance of all of its individual components. However, expansion valves have been overlooked with regards to the potential they have to help improve the energy efficiency of VCC systems [3]. This project seeks to further explore the impact of expansion valve performance on VCC systems energy efficiency.

Superheat control is arguably one of the key factors affecting the performance and efficiency of VCC systems. By controlling the flow of refrigerant, expansion valves are also directly responsible for controlling the level of superheat. In the process of controlling superheat, expansion valves often experience hunting. Valve hunting is an oscillating behavior of valve opening (and refrigerant flow) in search of the desired superheat setpoint. This highly undesirable behavior has been plaguing expansion valves from the beginning of their existence. Expansion valves are known to exhibit less hunting behavior at higher superheat set points. However, just this information is not sufficient to solve the problem of valve hunting because of the other factors in play such as compressor speed and evaporator pressure. Operating valves only at relatively high superheat set points would considerably limit their use. This is because under these conditions high levels of cooling cannot be achieved thus leading to a loss in cooling capacity. Thermal expansion valve research has been geared towards modeling these expansion valves in order to prevent them from hunting. Broersen and Van der Jagt [4] discussed the undesirable impacts of valve of hunting and linked the hunting of the valve to the evaporator. Their proposed solution was to vary the heat resistance between the thermal expansion valve's sensing bulb and the evaporator wall. Their experiments

showed that increasing the resistance made the bulb dynamics slower and showed improvement in hunting behavior. The problem with this approach is that the added thermal resistance caused considerable problems for the system at startup. Further work to model the TEV and help curb the hunting of these devices was carried out by K. James [10] and by G. A. Ibrahim [11] who examined the effects of a deviation in the external parameters on a refrigeration system whose evaporator was controlled by a TEV. There has however been no experimental validation included in his study.

Electronic expansion valves soon emerged as a viable alternative to thermal expansion valves. Electronic expansion valve research has been geared towards improving superheat control. Outtagarts et al [12] investigated the behavior of an evaporator fed through an electronic expansion valve at transient conditions and compared its performance to that of one which was fed with a thermal expansion valve. These tests were carried out on a fixed refrigerating machine with a cooling capacity below 9 kW with constant condensation conditions and variable evaporating temperature and variable compressor speeds. Lazzarin et al [13] carried out a similar experiment by performing a one year experimental survey comparing the performances of TEVs and EEVs for use in supermarket refrigerator cabinets. The devices were installed in several different types of refrigeration cabinets and the superheating, subcooling, isentropic efficiency and pressure drop at suction and discharge lines data were recorded throughout the year for both types of device. Subcooling refers to the difference between the temperature of the refrigerant at the outlet of the condenser and the saturation temperature of the refrigerant. These tests were also carried out in different geographical

settings with different climates (cold, mild and hot) across the year. Both of these experiments ([12] and [13]) showed that that the EEV performance in superheat regulation was superior to that of the TEV. The EEV was shown to yield considerably higher energy savings than the TEV. The challenge with EEVs remains in their relative complexity, cost and fragility [14].

Nonetheless, while EEVs represented an upgrade to TEVs, there was still a considerable "gap" in the search for a device that would provide satisfactory superheat control and be free of hunting. Most of the research was geared towards modelling TEVs in order to eliminate hunting or control optimization of EEVs in order to have better authority over superheat. "Hybrid" valve designs involving the combination of conventional expansion valves with other expansion valves or components soon began to be researched as an alternative solution. Kim, Braun and Groll [15] proposed a hybrid-individual superheat control approach to improve the distribution of refrigerant in evaporators. The two approaches proposed by this method were upstream refrigerant flow balancing and downstream refrigerant flow balancing. These tests showed the benefits of controlling individual refrigerant flow rates for superheat control which were also validated by a simulation model. The problem with this test, however, is while it was very successful with upstream refrigerant flow balancing; it was not as successful with downstream refrigerant flow balancing control due to the large pressure drop at the end of the circuit.

Furthermore, Elliott et al [16] proposed a solution to the unending superheat control issues by the use of a hybrid device that uses two control mechanisms. An inner

mechanism that controls the pressure at the evaporator and an outer mechanism that adjusts the desired pressure to regulate evaporator superheat. This hybrid express valve (HEV) seemed to solve the problem of regulation at transient conditions because it made use of quantities (temperature and pressure) that address the two sources of superheat variation individually and also due to collocation of actuator for the pressure control loop. This HEV was not subject to valve hunting unlike TEVs. It did not flood or starve the evaporator at off conditions unlike AEVs, and required less control while providing a longer motor service life than EEVs. This valve provided a significant contribution but was big and clunky.

With advancements in technology, the use of microvalves like the one used in this project, have become more popular in the HVACR industry [17]. The strength of microvalves is their quick actuation time. The rise of this type of technology referred to as Micro Electro Mechanical Systems (MEMS) was discussed by Ameel et al. [17] and Henning [18]. Both of these publications discussed the opportunities brought by MEMS including increased performance, decreased size and increased reliability. They also discuss the challenges faced by these microvalves for HVAC and refrigeration applications. One of these challenges is that thermally activated microvalves have trouble operating with refrigerant liquids due to the fact that the refrigerant's thermodynamic state is prepared to be just on the edge of flashing and so the valve itself must impart little or no heat. Also, consideration of these scaling effects and the fabrication and material limitations often produce systems that are significantly different from their macroscale counterparts. Yet, if the potential of these microvalves was

harnessed properly, then the potential for significant improvement in superheat control was considerable.

DunAn Microstaq soon came up with a MEMS based Pilot Direct Acting Valve (PDAV) that attempted to provide solutions to several of the challenges faced by expansion valves [19]. The valve developed by Microstaq is compact, light, efficient, and compatible with all HCFC and HFC refrigerants. It also has a quick actuation time of about 250 milliseconds [20] compared to the Sporlan EEV which has a full motion transit time of 7.5 seconds [21]. This valve provides a good solution to the problems of size and actuation time but still faces some challenges including the fact that it does not work well with open loop systems, has no mechanical feedback mechanism, consumes more power when open and has a lower flow rate than conventional thermal expansion valves due to the smaller internal surface area required by the spool. This research project seeks to fill the gap left by this PDAV by proposing a valve design that makes use of the strengths of Microstaq's PDAV and conventional TEVs without the main challenges faced by these valves. The following sections will discuss in more details the objectives and tasks of these project as well as the methods, equipment used and results obtained.

There are several types of expansion valves used in HVACR applications. The most common types include; Thermal Expansion Valves which are also referred to as Thermostatic Expansion Valves (TEV), Automatic Expansion Valves (AEV) which are pressure regulating valves and Electronic Expansion Valves (EEV). TEVs struggle to deal with rapidly changing cooling loads (transient conditions) while AEVs tend to

starve the evaporators when the load is high due to their tendency to close (so as to maintain the outlet pressure) when the evaporator pressure increases [7]. EEVs are usually able to keep up with both rapidly and slowly changing conditions but are complex, expensive and subject to component failure [8]. The Prototype Pilot Expansion Valve (PPEV) developed in this project operates in a fashion similar to that of TEVs. Figure 5 shows a conventional TEV and Figure 6 shows the internal workings of a TEV.

Figure 5: Conventional thermal expansion valve

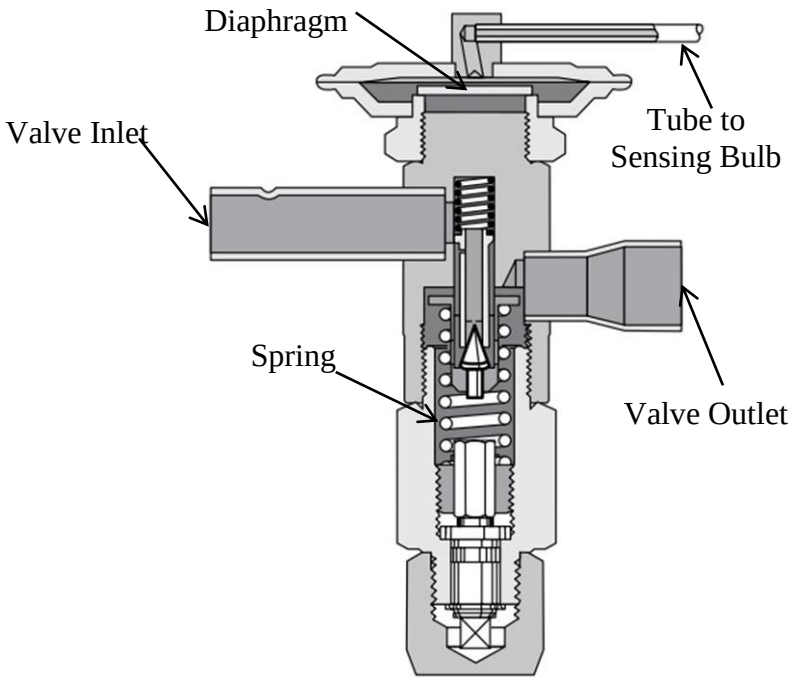

Figure 6: Internal workings of a conventional thermal expansion valve [23]

The TEV is used to control the flow of refrigerant into the evaporator and also convert high pressure liquid refrigerant from the condenser into lower pressure two-phase refrigerant which is then fed into the evaporator. It operates at varying pressures and temperatures. The flow of refrigerant across the TEV is achieved by the balancing effect of three forces of the diaphragm. Two of these forces act at the bottom of the diaphragm and through their action, they close the valve. These closing forces are created by the evaporator inlet pressure and the spring pressure. The third force acting on the top of the diaphragm arises as a result of the sensing bulb pressure on the spring. This is an opening force as it causes the valve to open. The sensing bulb is filled with a fluid similar to the refrigerant in the system. This sensing bulb is attached to the outlet of

the evaporator. When there is an increase in the temperature of the refrigerant at the outlet of the evaporator, the temperature and pressure of the fluid in the sensing bulb also increase. The increase in the pressure of the fluid inside the sensing bulb causes a force to act at the top of the diaphragm and this causes an increase in the valve opening and refrigerant flow rate across the valve. The increase in refrigerant flow across the expansion valve and into the evaporator will lead to a decrease in the temperature at the outlet of the evaporator and as that temperature decreases, so do the bulb pressure, valve opening and refrigerant flow rate until the system reaches a point of steady state. Through this operation, the TEV is able to operate over a wide range of loads and temperatures. It is also less adversely affected by variations in refrigerant charge, especially in smaller systems, than AEVs [23]. However, TEVs are often victims of hunting and they struggle to deal with rapidly changing conditions [6].

The PPEV consists of a combination of a conventional TEV and a pilot microvalve as shown in Figure 7. The flow of fluids across the Pilot Direct Acting Valve (PDAV) is regulated by a direct acting microvalve known as Ventilum chip as shown in Figure 8 [22]. The pilot microvalve used in this project is DunAn Microstaq's PDAV, which in addition to its fast actuation time [20], is small and would be ideal when moving to an eventual integrated design.

The PDAV is a pilot expansion valve which is electronically controlled and is based on Micro Electro Mechanical Systems (MEMS). This MEMS base consists of a pilot microvalve as shown in Figure 7 that is designed to control flow rate or pressure. The PDAV is a normally closed, single flow directional valve that is compatible with all

HCFC and HFC refrigerants. It provides effective closed loop control and has an actuation time of 0.25 seconds. Its two-stage hybrid valve design and aforementioned characteristics enable it to provide rapid response to changing loads and precise superheat control. However, the PDAV faces some challenges. It is designed to work with closed loop systems and so does not work well with open loop systems due to its dependence on an electronic feedback to operate. Thus it would not be a good option for a system in which the output is neither measured nor fed back for comparison with the input. This dependence on electronic feedback also means that the PDAV does not have any secondary (mechanical) feedback and so failure of electronic feedback would completely stop its operation. Furthermore the PDAV has a relatively lower flow rate due to the smaller internal area of its spool.

Figure 7: DunAn Microstaq's Proportional Direct Acting Valve (PDAV)

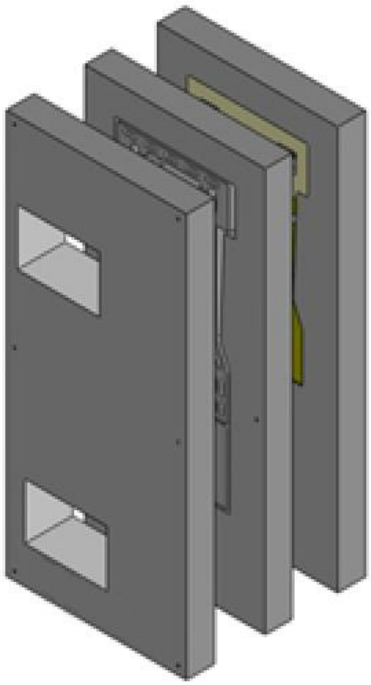

Figure 8: Direct acting ventilum chip inside PDAV [22]

In combining the PDAV with a conventional TEV, the PPEV is able to harness the strengths of the PDAV and the TEV but avoids the same challenges that they face individually. The PPEV provides both electronic and mechanical feedback and is able to achieve higher flow rates than the PDAV alone. The details of the PPEV's superior performances will be discussed later in this thesis.

Research Objectives and Tasks

The objective of this research project is to develop and test a proof-of-concept physical model Prototype Piloted Expansion Valve (PPEV). This PPEV consists of a

combination of a conventional Thermal Expansion Valve (TEV), developed and sold by Sporlan and a two Pilot Direct Acting Valves (PDAV) manufactured and sold by DunAn Microstaq. TEVs are responsible for regulating the level of evaporator superheat in Vapor Compression Cycle (VCC) systems and are widely used in industry alongside Electronic Expansion Valves (EEVs). The PPEV developed in this project operates in a fashion similar to that of TEVs.

This research project also endeavors to demonstrate the superior performance of the PPEV in comparison to TEVs and EEVs through modeling and experimental data. This will be achieved by carrying out a number of tasks. These tasks include developing a mechanism to be used by the PPEV, prototyping a design, developing and providing a proof-of-concept model, determining which tests are to be carried out to effectively evaluate PPEV performance and carrying out these tests to evaluate the PPEV's reaction to changes in system loads and operating condition. These tests will all be carried out on a modulated water chiller system and a direct exchange split heat pump system. These systems vary widely in terms of the refrigerant used, the operating pressure ranges, the available compressor speeds and other various conditions. These tests are intended to provide a fairly accurate picture of the how the PPEV compares to other valves. The tests described in the previous section were first carried out on a water chiller system and then on a residential split heat pump system and are summarized in Table 1.

The first test to be carried out is a superheat change test. This test is designed to assess the valve's speed of response. The superheat change test involves letting the system's superheat reach the designed setpoint from startup. Once it reaches the

superheat set point, the setpoint is then increased or decreased. This is done while keeping track of the system's response and how quickly it reaches the new setpoint. This test is carried out at different compressor speeds to further assess the system response under varying conditions. Reaching the superheat set point quickly and remaining there indicates a higher cooling capacity. For the modulated water chiller system, the initial superheat setpoint was 5°C; it was then progressively changed to 10°C, 15°C and back 10°C. This was all done at a compressor speed of (2,000 revolutions per minute (RPM). The same sequence (5°C to 10°C to 15°C to 10°C) was then carried out again. However, this time, the compressor speed was increased to 4,000 RPM. Both the EEV and PPEV were subjected to this test. The TEV was excluded from this test because it operates on mechanical, not electronic feedback. Furthermore, the superheat setpoint on a TEV is changed manually at the stem of the valve unlike the EEV and PPEV in which the superheat set point can be changed using computer software while the valve is operating.

Table 1: Summary of tests carried out

Test Number	Modulated Water Chiller System
1	Superheat change test for PPEV
2	Startup test for PPEV
3	External fluid flow rate change test for PPEV
4	Superheat change test for EEV

Table 1 Continued

Test Number	Direct Exchange Split Heat Pump System
5	Startup test for EEV
6	External fluid flow rate change test for EEV
7	Startup test for TEV
8	External fluid flow rate change test for TEV
	Direct Exchange Split Heat Pump System
9	Superheat change test for EEV
10	Startup test for EEV
11	External fluid flow rate change test for EEV
12	Startup test for TEV
14	Superheat change test for PPEV
15	Startup test for PPEV
16	External fluid flow rate change test for PPEV

This test is carried out on the direct exchange split heat pump system under the same conditions as with the water chiller system. The next test to be carried out is the startup test. This test is designed to evaluate the system's response from startup. VCC systems typically experience a spike in energy consumption at startup so they should be

able to reach operating conditions from start-up in the shortest amount of time possible. This translates to more cooling and less energy spent to achieve that cooling. For the water chiller system, after startup, the compressor was allowed to run for three minutes. After these three minutes, the compressor was shut down and was allowed to remain off another three minutes. This on-off cycle was repeated three times and all three valves were subjected to the test. For the direct exchange split heat pump system, the on cycle was nine minutes and the off cycle was one minute.

The third test to be carried out is the external fluid flow rate change test. This test is designed to evaluate the system's ability to respond to quick load changes. The change in external fluid flow rate simulates a change in the system load. In practical applications, most VCC systems are subject to random and sometimes rapidly changing loads. Consequently, they have to quickly adapt to these changing loads. Water is the external fluid for the water chiller system and air is the external fluid for the direct exchange split heat pump system. The water chiller system's heat pumps have a capacity of 115 gallons per hour (GPH). At startup, the water flow rate is set to 23 GPH and the compressor speed is set to 2000 GPH. The water flow rate is then progressively increased to 69 GPH and then to 115 GPM while the compressor's speed is kept at 2,000 RPM. At the end of this cycle, the water flow rate is changed back to 23 GPM and the compressor speed is increased to 4,000 RPM. The water flow rate is then once again progressively increased to 69 GPM and 115 GPM while the compressor speed is kept constant at 4,000 RPM.

For the direct exchange split heat pump system, at startup, the evaporator fan is set to produce and air flow rate of 1700 ft/min and the compressor speed is set to low (first stage). After 7 minutes, the air flow rate is then increased to 2200 ft/min while the compressor speed is kept at low. After another 7 minutes, the air flow rate is increased to 2700 ft/min while the compressor speed is kept at low. At the end of this cycle, the air flow rate is changed back to 1700 ft/min and the compressor speed is increased to high (second stage). The air flow rate is then once again progressively increased to 2200ft/min and 2700 ft/min while the compressor speed is kept constant at high. The PPEV, EEV and TEV were all subjected to this startup test on both systems.

Furthermore, an additional test was carried out to prove the possibility of an integrated design which will enable to PPEV to not rely on any external component to operate. In the aforementioned superheat change test, startup test and external fluid flow rate test, the PPEV relies on an external pressure source (a nitrogen tank), and the ability to vent the extra nitrogen to the atmosphere in order to operate. The final test for this thesis work demonstrates possibility of using the high pressure from the compressor outlet to provide the pressure needed to the PPEV to operate and that the extra refrigerant can be vented into the compressor inlet thus confirming the possibility of a truly integrated design.

CHAPTER II

EXPERIMENTAL SYSTEMS

Two experimental systems were used in this project; a custom-built modulated water chiller system and a direct exchange split heat pump system. The water chiller system is a three-evaporator system connected to a compressor and a condenser, while the direct exchange split heat pump system is a split system with an indoor and an outdoor component. This Chapter is intended to give an overview of both systems including the details of their components and the software and data acquisition systems used. The heat pump system is a standard unit manufactured and sold by Trane. Due to the fact that the modulated water chiller system is custom built, the next section will go into a more detail regarding the system's main components.

Modulated Water Chiller System

The modulated water chiller system is a custom-built system used to replicate the cooling process for a three-room system. It is equipped with three 0.5 ton evaporators. The refrigerant used here is R-134A and the system is equipped with a brushless DC variable speed compressor with a range of 1800 RPM to 6500 RPM. This system has a cooling capacity of 5.6 kW. Details regarding the components of this system are discussed later in this chapter. Figure 9 shows the water chiller system and Figure 10 shows a schematic of this system.

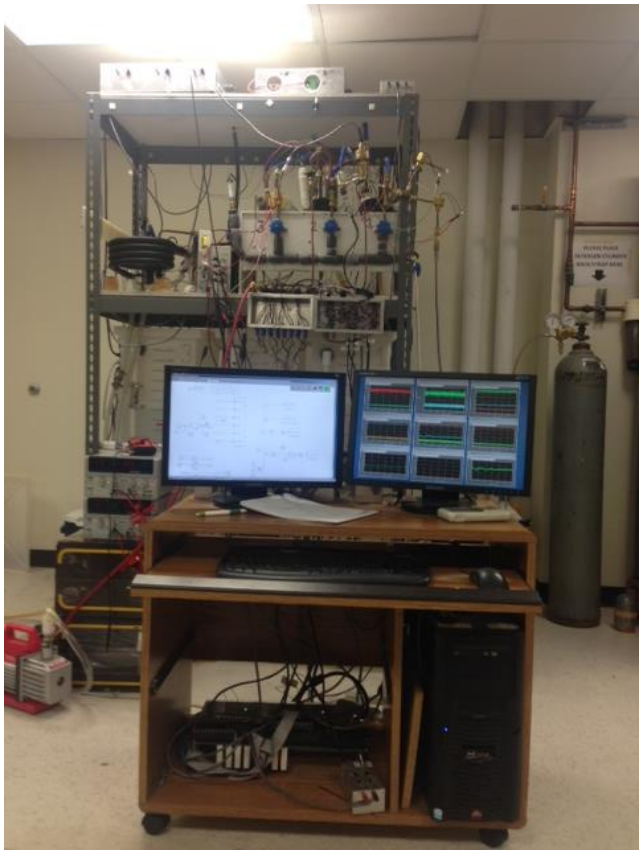

Figure 9: Modulated water chiller system

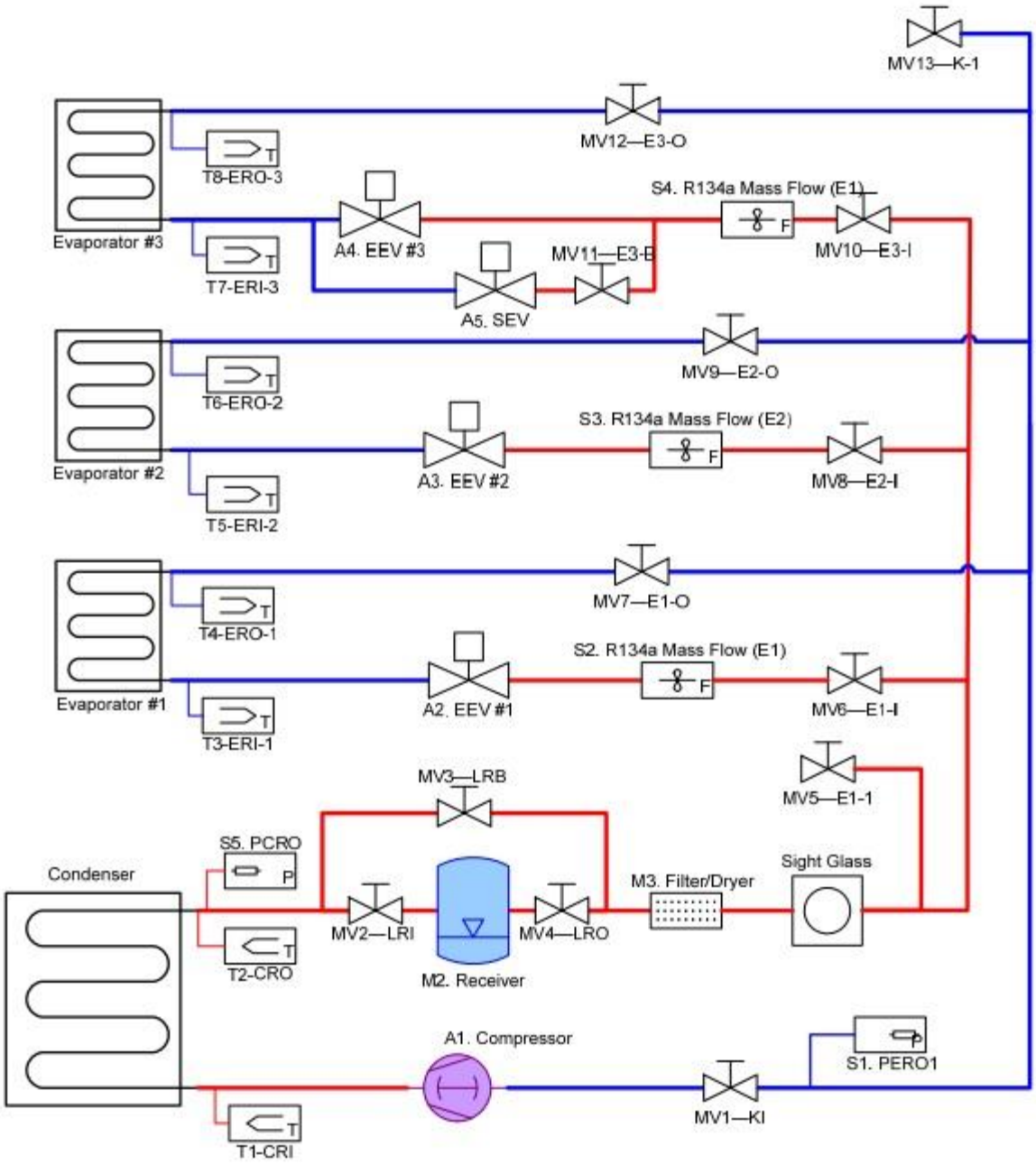

Figure 10: Schematic of modulated water chiller system [24]

Details of Modulated Water Chiller System Components

Compressor

The compressor installed on this system is a Masterflux compressor, specifically a Sierra model. It is intended for use with systems operating on R-134A, uses a 48 Volts direct current supply, voltage input and is a variable speed compressor with an operating range of 1800 RPM to 6500 RPM. It has a total cooling capacity of 1.5 tons. The compressor's tachometer provides active feedback regarding the compressor's speed. The tachometer does this by sending out a square wave signal which is directly proportional in frequency to the speed of the compressor which is measured. This square wave signal is later converted to a 0-5V DC voltage signal. The compressor is shown in Figure 11.

Figure 11: Masterflux sierra compressor

Thermocouples

The system is equipped with 12 type T thermocouples to measure the temperature at various points across the system. To do this, the thermocouples are immersed in the fluids whose temperature they measure. These thermocouples are connected to a PCI thermocouple board on the system's computer. They have an accuracy of ±1°C. One of the thermocouples is shown in Figure 12.

Figure 12: Type T thermocouple

Refrigerant Flow Transducers

There are three McMillan transducers in the system used to measure the flow of refrigerant across the system. These transducers have an operating range of 50-500mL/min, an output range of 0-5V and an accuracy of ±1%. One of these transducers is as shown in Figure 13.

Figure 13: McMillan refrigerant flow transducer

Pressure Transducers

There are five Cole-Parmer pressure transducers across the system. Three of them are used to measure the pressures at the outlet of the evaporators and have an operating range of 0-100 psig, one of them measures the pressure at the outlet of the condenser and the fourth measures the pressure of the PPEV diaphragm. The diaphragm pressure transducer and the condenser outlet pressure transducer both have an operating range of 0-300 psig. All five have a voltage output range of 1-5V and an accuracy of ±0.4%. One of the pressure transducers is as shown in Figure 14.

Figure 14: Cole-Parmer pressure transducer

Power Components

The system's compressor is powered by two 800 W DC power supplies. These power supplies receive a 208 Volts AC supply and output up to 16 amps at 48 Volts DC. These are connected in parallel to produce the power needed and used by the compressor and they are switched individually.

Furthermore a 24 Volts DC power supply is used to power the some of the system's transducers including the compressor current, differential pressure and refrigerant flow.

The water chiller system's main components are listed in Table 2.

Table 2: Main components of water chiller system

Component	Quantity	Manufacturer	Model Number
EEV	3	Sporlan	SEI 0.5-10-S
Compressor	1	Masterflux	Sierra 0.-0982Y3
Thermocouple	12	Omega	GTMQSS-062U-6
Mass Flow Meter	3	McMillan	102 Range 5
Pressure Transducer	6	Cole-Parmer	07356-04
DAQ Software	1	Quanser	WinCon 5.0

Direct Exchange Split Heat Pump System

The direct exchange split heat pump system is a 3 ton Trane XL 16i model. It provides two-stage cooling and has a Seasonal Energy Efficiency Ratio (SEER) rating of 16.0. It operates using R-410A refrigerant and has a cooling capacity of 36,000 BTU/H (10.5kW). This system is equipped with a two stage constant speed scroll compressor. The mass flow rate of air over the condenser and evaporator can be adjusted by varying the fan's speed. The compressor installed on this system is a Climatuff scroll compressor. It is a 230 volt, 160 Hz compressor which has two operating speeds. The system is equipped with a propeller outdoor fan with a diameter of 23 inches. It also has a direct-type drive with two speeds and its motor speed is a constant 825 RPM. The system is shown in Figure 15 while Figure 16 shows a schematic of the system.

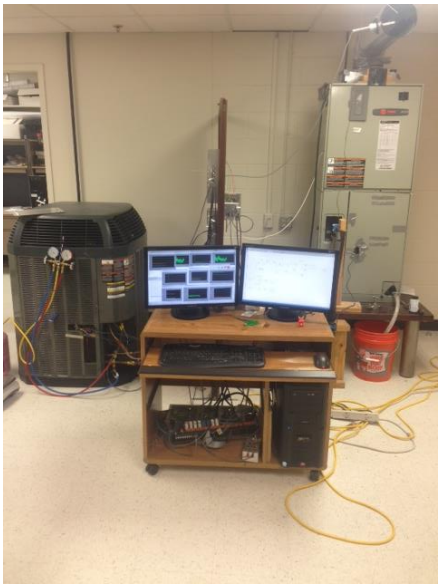

Figure 15: Trane XL16i direct exchange split heat pump system

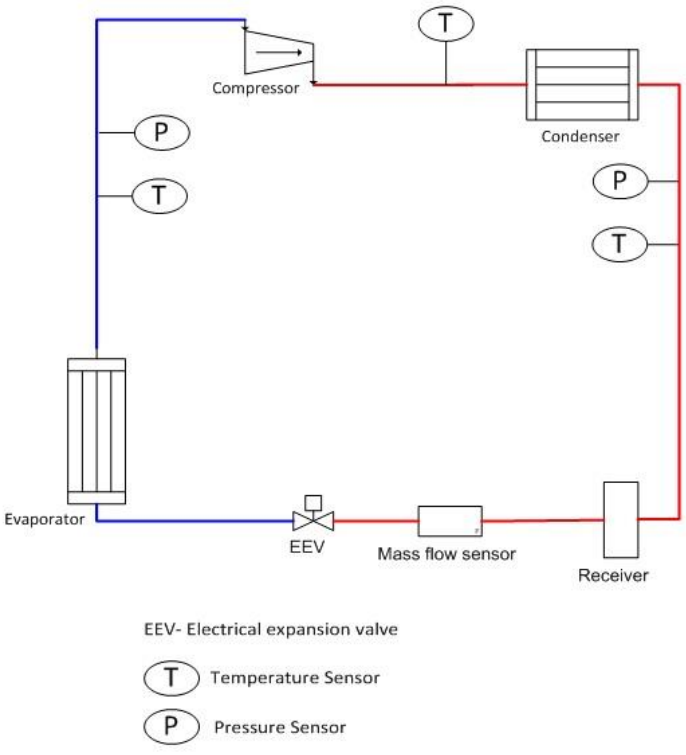

Figure 16: Schematic of Trane XL16i direct exchange split heat pump system

The system is also equipped with three thermocouples which are manufactured by Omega, three flow meters which are manufactured by McMillan, and two pressure transducers which are manufactured by Omega. The main components are listed in Table 3.

Table 3: Main components of direct exchange split heat pump

Component	Quantity	Manufacturer	Model Number
EEV	1	Parker	020432-00
Compressor	1	Climatuff	Sierra 0.-0982Y3
Thermocouple	3	Omega	GTMQSS-062U-6
Mass Flow Meter	3	McMillan	102 Range 8
Pressure Transducer	2	Omega	PX309-500G5V
DAQ Software	1	Quanser	WinCon 5.0

Data Acquisition and Software

Both systems use the same data acquisition system (DAQ) to record data and provide control. The system consists of four DAQ boards which are installed on a windows computer. The software used to run the experiments and record the data obtained is WinCon. WinCon operates simultaneously with Simulink and Matlab.

CHAPTER III

PROTOTYPE PILOT EXPANSION VALVE DESIGN

The Prototype Pilot Expansion Valve (PPEV) is a combination of a EBSSE2C Thermal Expansion Valve (TEV) by Sporlan and two Pilot Direct Acting Valves (PDAV) by DunAn Microstaq (DMQ). The PDAV has a relatively lower flow rate due to the smaller internal area of its spool. The PPEV is therefore able to use the PDAVs' fast response time and the TEV's ability to handle much larger flow rates than the PDAV. This Chapter will discuss the steps taken to design and implement the PPEV physical model used in this project.

Implementation of Prototype Pilot Expansion Valve Design

The first step in the process of building the PPEV is to cut the TEV's sensing bulb into two and void it of the sensing bulb fluid. The open end of the sensing bulb is then attached to a spool on which two PDAVs are fitted. The tube relaying the diaphragm to the sensing bulb is then cut in the middle and a Cole-Parmer 07356-04 pressure transducer was then fitted on it as shown in Figure 17.

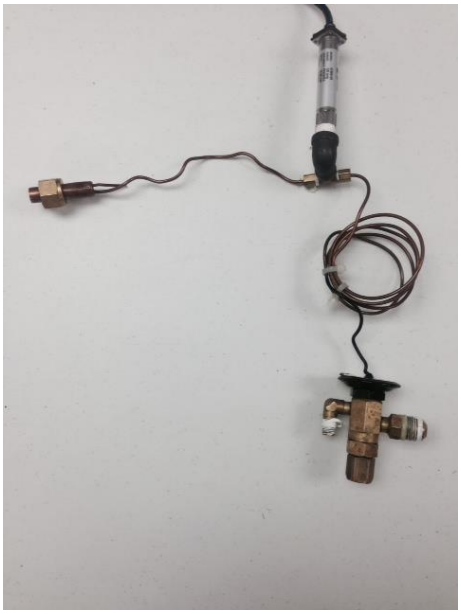

Figure 17: Pressure transducer inserted between cut sensing bulb and diaphragm

This pressure transducer was used to measure the measure the pressure acting on the top of the diaphragm. One of the two PDAVs was connected to a Nitrogen tank which provided the pressure that was regulated by the PDAVs as it acted on the top of the diaphragm. Figure 18 illustrates the PPEV setup and Figure 19 is a diagram showing the setup and working of the PPEV.

Figure 18: Picture of PPEV setup

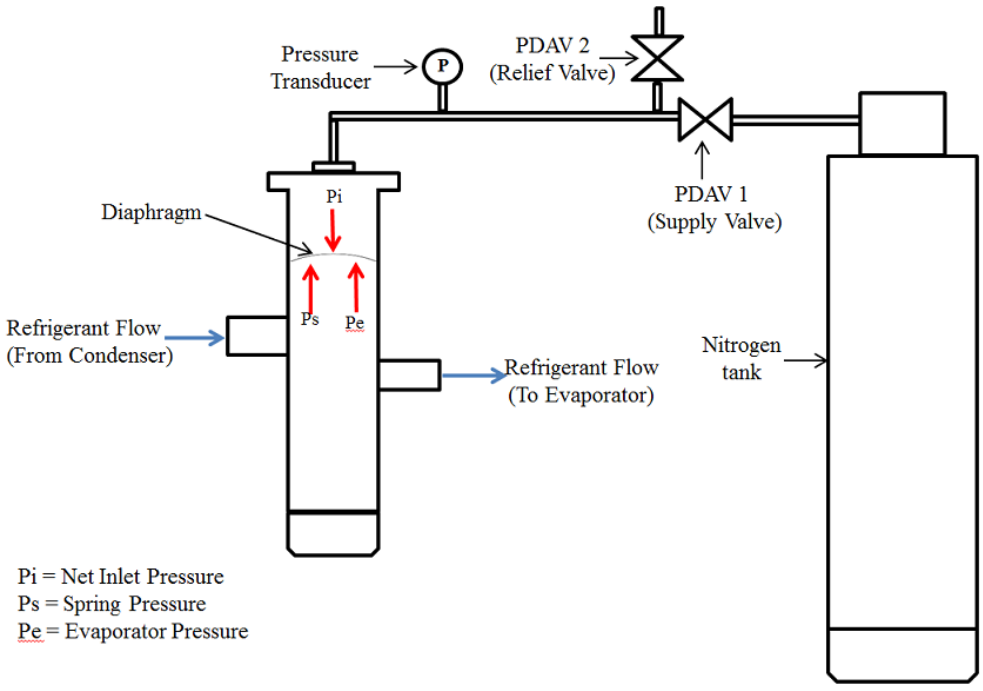

Figure 19: Schematic of PPEV setup and operation

The TEV's role of refrigerant flow control is directly dependent on the three forces acting on the diaphragm. The spring pressure (Ps) and evaporator pressure (Pe) both act at the bottom of the diaphragm and contribute to close the valve. The net inlet pressure (Pi) acts on the top of the diaphragm and is responsible for opening the valve and increasing the flow of refrigerant to the evaporator. The pressure balance on the diaphragm can be represented by the equation $Pi = Ps + Pe$. The two PDAVs were controlled by the use of two Model 400 Pulse-width Modulation (PWM) controllers which were set up to work with the DAQ as discussed in Chapter II. A controller was implemented on Simulink which controlled the opening of both PDAVs. The controller uses an electronic feedback mechanism which is based on the measured superheat of the system to adjust the opening of each of the valves. One of the PDAVs can be described as a supply valve (PDAV1) while the other can be described as a relief valve (PDAV2). The nitrogen tank was set to provide a fixed pressure of 150 psi. The net inlet pressure to the top of the diaphragm is then varied accordingly. The PPEV regulates the superheat as described below.

- Low superheat: When the system's superheat is lower than desired, the supply valve closes while the relief valve opens and vents the excess pressure. As the net inlet pressure to the diaphragm reduces, the flow rate of refrigerant into the evaporator decreases and the superheat increases. When the superheat reaches the desired level, the supply valve closes and the relief valve opens up accordingly to keep the rate of refrigerant flow constant. This constant flow keeps the superheat at the desired setpoint.

- High superheat: When the system's superheat is higher than desired, the supply valve immediately opens while the relief valve closes. These actions increase the net inlet pressure to the top of the diaphragm. As the net inlet pressure to the diaphragm increases, the flow rate of refrigerant into the evaporator increases and the superheat decreases. When the superheat reaches the desired level, the supply valve opens and the relief valve closes accordingly to keep the rate of refrigerant flow constant. This constant flow keeps the superheat at the desired setpoint.

Advantages of Prototype Pilot Expansion Valve Design

The PPEV design enables it to make use of the strengths of both the PDAV and the TEV without being handicapped by the same challenges that these valves face. The design provides several advantages over TEVs, EEVs, and AEVs. These advantages are as described below.

- Operation: The PPEV is simple to set up and operate. Once the PPEV is set up, it is able to provide automated control of refrigerant flow and superheat level. It is able to operate in a wide variety of environmental and load conditions. It can also be used with any HCFC or HFC refrigerant.
- Response: Due to the PDAV's quick actuation time (0.25 seconds), the PPEV is able to react very quickly to changes in load conditions or desired operating conditions.

- Superheat: The PPEV provides improved superheat control. Any deviation of the system's superheat from the desired level is quickly adjusted by varying the flow of refrigerant to the evaporator accordingly. It is able to reach low superheat set points without hunting, unlike the EEV and the TEV.
- Efficiency: The PPEV is more efficient than the EEV and the TEV. Due to its quick response time it is able to reach desired operating conditions in a considerable shorter time than the TEV, AEV or EEV. As a result of this, the compressor use is reduced and optimized thus saving energy.
- Robustness: The TEV operates using a mechanical feedback mechanism while the PDAV and EEV rely on an electronic feedback mechanism for their operation. However the PPEV relies on both mechanical and electronic feedback mechanisms. In case of failure of one of these mechanisms, the PPEV's operation is not completely compromised unlike the EEV, TEV or PDAV

These advantages will be illustrated in Chapter V of this thesis. Chapter V will discuss the experimental results of the tests carried out on the PPEV, TEV and EEV.

CHAPTER IV

MODELING APPROACH

The Thermal Expansion Valve (TEV) is responsible for regulating the level of evaporator superheat in a Vapor Compression Cycle (VCC) system. To do this, it uses a mechanical feedback mechanism which consists of a sensing bulb placed at the outlet of an evaporator. The Prototype Piloted Expansion Valve (PPEV) developed in this project operates in similar fashion. However, with the PPEV, refrigerant flow across the valve is not controlled by a sensing bulb. The PPEV consists of a combination of a conventional TEV and two PDAVs. The pilot valve is DunAn Microstaq's Proportional Direct Acting Valve (PDAV) which in addition to its fact actuation time is small and would be ideal when moving to an eventual integrated design. The schematic used for this derivation is as shown in Figure 19 in Chapter III.

Modeling Assumptions

This model is based on principles of the Bernoulli equation, the Continuity equation, Hooke's law and geometry. The PPEV model was based from the basic modeling principles of a TEV. However in this case, the bulb dynamics on the diaphragm is replaced by the net inlet pressure downstream of the two PDAVs. The following assumptions were taken to derive this model.

- Incompressible and laminar flow

- TEV inlet line (Thermal Sensing bulb and capillary tube) are horizontal and straight.
- The pipe wall friction is negligible.
- Fluid is non-viscous.
- No spring compression at start-up.
- At steady state conditions, force on diaphragm is equal to force on spring.
- TEV inlet and outlet areas are equal.
- Flow control between the TEV inlet and outlet modelled as flow through a gate valve.
- Refrigerant used is R-134A.

Model Derivation for the Prototype Pilot Expansion Valve

The derivation of this model requires that the thermodynamic properties of the refrigerant be known. In this case, the derivation is based on R-134A refrigerant. The valve's mechanism is modeled by carrying out a force balance at the diaphragm. The inlet pressure, is the net pressure acting at the top of the diaphragm as shown by the equation $P_i = P_{PDAV1} - P_{PDAV2}$. Table 4 shows the symbols and names of the parameters used in this model derivation.

Table 4: Parameters used in model derivation

Symbol	Name
P_i	*Net inlet Pressure*
F_s	*Spring Force*
P_e	*Evaporator Pressure*
A_d	*Diaphragm Area*
m_v	*Mass flow rate*
x_0	*Initial compression of spring*
K_s	*Spring Constant*
δx	*Net axial spring movement*
P_0	*Nominal Pressure*
C_0	*Valve parameter*
ρ	*Density*
P_c	*Condenser Pressure*
A_1	*Valve inlet area*
A_2	*Valve outlet area*

The force balance on the diaphragm is as follows:

$$P_i A_d = P_e A_d + K_s(x_0 + \delta x) \quad (1)$$

where:

$$\delta x = \frac{(P_i)A_d - (P_e)A_d}{K_s} \quad (2)$$

Recall that at a specific operating condition, the area of the valve opening is directing proportional to the displacement of the valve head. Thus;

$$A_v = c_0(x_0 + \delta x) \quad (3)$$

Assuming that at startup, there is no initial compression and considering equation 3, which is the equation for the net axial movement of the spring, the following equation is obtained:

$$A_v = c_0\left(0 + \frac{(P_i)A_d - (P_e)A_d}{K_s}\right) \quad (4)$$

This simplifies to:

$$A_v = c_0\left(\frac{P_b A_d}{K_s} - \frac{(P_e)A_d}{K_s}\right) \quad (5)$$

The equation for the mass flow rate through the valve's outlet orifice is as shown in equation 6 and equation 7 where:

Valve Inlet*:* $$m_{v1} = \rho A_1 v_1 \quad (6)$$

Valve Outlet: $$m_{v2} = \rho A_2 v_2 \quad (7)$$

Equation 8 is derived from Bernoulli's equation [25]:

$$gz_1 + \frac{P_1}{\rho_1} + \frac{v_1^2}{2} = gz_2 + \frac{P_2}{\rho_2} + \frac{v_2^2}{2} \quad (8)$$

where the left hand side of equation 8 represents the valve inlet (condenser outlet) and the right hand side of the equation represent the valve outlet (evaporator inlet). This simplifies to:

$$\frac{P_1}{\rho_1} + \frac{v_1^2}{2} = \frac{P_2}{\rho_2} + \frac{v_2^2}{2} \quad (9)$$

Thus:

$$v_2^2 - v_1^2 = 2\left(\frac{P_1 - P_2}{\rho}\right) \quad (10)$$

The following is obtained by performing a mass balance:

$$\rho_1 A_1 v_1 = \rho_2 A_2 v_2 \quad (11)$$

Considering that the density is constant:

$$v_1 = \frac{A_2}{A_1} v_2 \quad (12)$$

Substituting equation 12 in equation 10, the following equation is obtained:

$$v_2^2 - \left(\frac{A_2}{A_1}\right)^2 v_2^2 = 2\left(\frac{P_1 - P_2}{\rho}\right) \quad (13)$$

Equation 13 can be simplified to obtain equation 14:

$$v_2 = \sqrt{\frac{2(P_1 - P_2)}{\rho\left(1 - \left(\frac{A_2}{A_1}\right)^2\right)}} \quad (14)$$

The relationship between mass flow rate, evaporator pressure and condenser pressure is as can be obtained by combining equations 5, 7and 14:

$$m_{v2} = \rho c_0 \left(\frac{P_b A_d}{K_s} - \frac{(P_e) A_d}{K_s}\right) \sqrt{\frac{2(P_1 - P_2)}{\rho\left(1 - \left(\frac{A_2}{A_1}\right)^2\right)}} \quad (15)$$

Implementation of Model in Matlab/Simulink

The model derived was implemented into a single model consisting of a compressor and a heat exchanger. The details of the derivation of this model have in

included in Appendix A and Appendix B. The equations and model were implemented in Matlab and Simulink as shown in Table 5, Table 6, Table 7 and Table 8.

Table 5: Input variables

Variable	Description	Units
Pero	Evaporator Outlet Pressure	*kPa*
Pcro	Condenser Outlet Pressure	*kPa*
Tero	Evaporator Outlet Refrigerant Temperature	°*C*
Teri	Evaporator Inlet Refrigerant Temperature	°*C*
Tewo	Evaporator Outlet Water Temperature	°*C*
Tewi	Evaporator Inlet Water Temperature	°*C*
Tcro	Condenser Outlet Refrigerant Temperature	°*C*
Tcri	Condenser Inlet Refrigerant Temperature	°*C*
Teao	Evaporator Outlet Air Temperature	°*C*
Teai	Evaporator Inlet Air Temperature	°*C*
Tcao	Condenser Outlet Air Temperature	°*C*
Tcai	Condenser Inlet Air Temperature	°*C*
Pdia	Diaphragm Pressure	*kPa*

Table 6: Physical parameters

Variable	Description	Units
C1	Valve Parameter #1	-
C2	Valve Parameter #2	-

Table 7: Operating conditions

Variable	Description	Units
Pv_ri	Refrigerant pressure at valve inlet	*kPa*
Pv_ro	Refrigerant pressure at valve outlet	*kPa*
Hv_ri	Refrigerant enthalpy at valve inlet	*kJ/kg*
m_valve_exp	Refrigerant mass flow rate across valve	*kg/s*
Pv_diaphragm	Diaphragm pressure	*kPa*

Table 8: Support files

Variable	Type	Description
RefProp_R134a	mat-life	Refrigerant property maps for interpolation.

Validation of Model and Simulation Results

Two experimental systems are used in this thesis project. However, only the modulated water chiller system is used to validate the model. The model described in this Chapter is then implemented in Simulink and the results obtained are compared to that obtained from experimental tests carried out on the modulated water chiller system. These results are as shown in Figure 20.

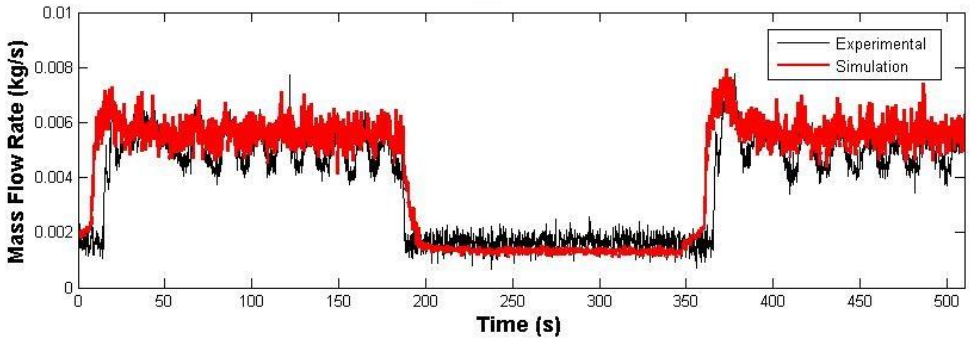

Figure 20: Refrigerant flow rate across valve in two startup cycles

CHAPTER V

EXPERIMENTAL RESULTS

As discussed in Chapters I and III, three tests are used to compare the performances of the PPEV, EEV and TEV relative to one another. These tests are carried out on two different systems; a modulated water chiller system which operates using R-134a refrigerant and a direct exchange split heat pump system which operates using R-410a. After the tests are complete, an analysis of each of the tests is done to determine and compare valve performances with regards to variables such as superheat, mass flow rate, evaporator outlet pressure, condenser outlet pressure and cooling capacity. The cooling capacity information is then used with the system's energy consumption to determine the coefficient of performance (COP). These are calculated as follows.

$$Cooling\ Capacity = Mass\ flow\ rate\ \times (h_{EvapOout} - h_{CondOut}) \quad (16)$$

For modulated water chiller:

$$COP = \frac{Cooling\ Capacity}{Mass\ Flow\ Rate \times (h_{CompOut} - h_{CompIn})} \quad (17)$$

For direct exchange split heat pump system:

$$COP = \frac{Cooling\ Capacity}{Electrical\ Energy\ Input\ to\ Compressor} \quad (18)$$

where:

$$H_{EvapOout} = Enthalpy\ of\ refrigerant\ at\ evaporator\ outlet$$

$$H_{CondOut} = Enthalpy\ of\ refrigerant\ at\ condenser\ outlet$$

$$H_{CompIn} = Enthalpy\ of\ refrigerant\ at\ compressor\ inlet$$

$$H_{CompOut} = Enthalpy\ of\ refrigerant\ at\ compressor\ outlet$$

The cooling capacity values show how much cooling of the external fluid is actually achieved by the system while the COP value shows how much work the compressor does to achieve this cooling. For the modulated water chiller system, the energy consumption used to calculate COP is determined by using the thermal work done by the compressor while on direct exchange split heat pump system, it is determined by using the electrical energy input to the compressor.

Superheat Change Test

This test is designed to assess how much superheat control the valve is able to offer. The superheat set point was changed progressively from 5°C to 10°C to 15°C and back to 10°C. This was done at 2,000 RPM then all over again at 4,000 RPM.

Modulated Water Chiller System

Figure 21 illustrates how the compressor speed signal changes throughout the superheat change procedure. The system responses comparing the superheat and superheat setpoint for the EEV and PPEV to these changes in superheat set point are as shown in Figure 22 and Figure 23 while Figure 24 and Figure 25 show the system's response comparing the superheat to the compressor speed for the same changes in superheat setpoint for the modulated water chiller.

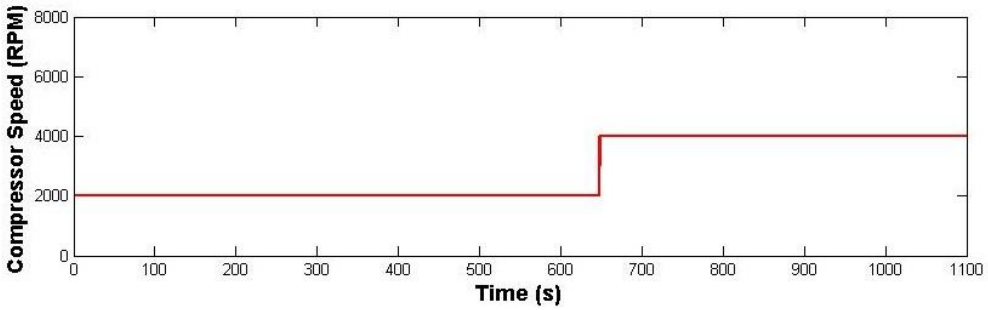

Figure 21: Superheat change test - compressor speed signal

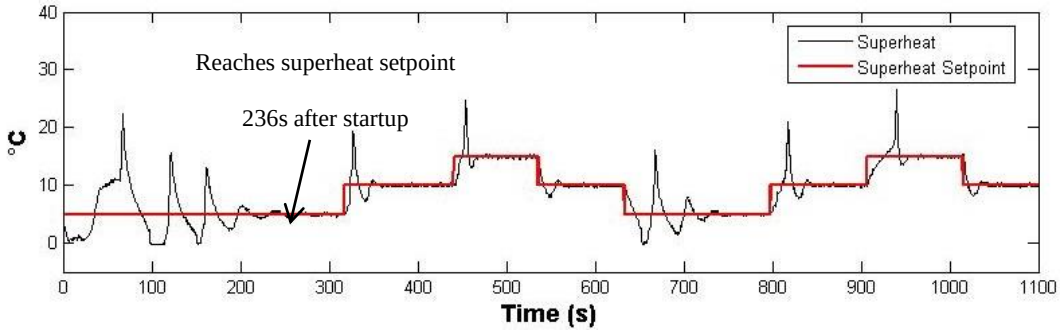

Figure 22: Superheat change test – superheat vs superheat setpoint using EEV on water chiller system

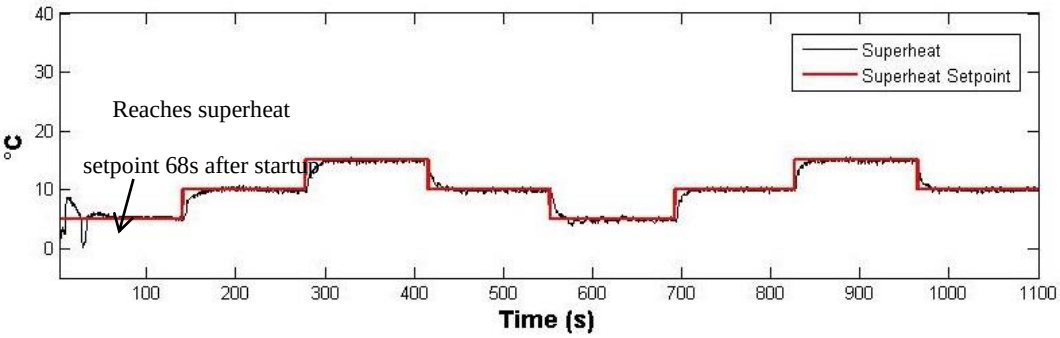

Figure 23: Superheat change test - superheat vs superheat setpoint using PPEV on water chiller system

From startup, the PPEV reaches the superheat setpoint 68 seconds after startup while the EEV reaches the superheat setpoint 236 seconds after start-up. This indicates a quicker response time and ability to reach operating conditions quicker thus minimizing compressor use. Figure 24 and Figure 25 illustrate how changing the compressor speed affects the level of superheat control by the valve. The compressor speed was 2,000 RPM for the first cycle and then it was increased to 4,000 RPM for the second cycle.

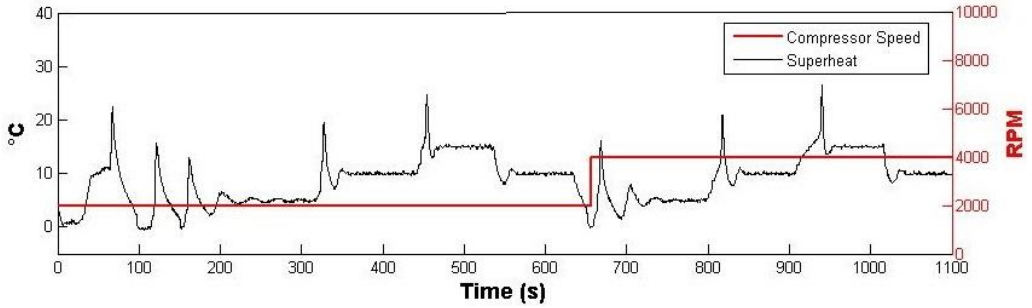

Figure 24: Superheat change test – superheat vs compressor speed using EEV on water chiller system

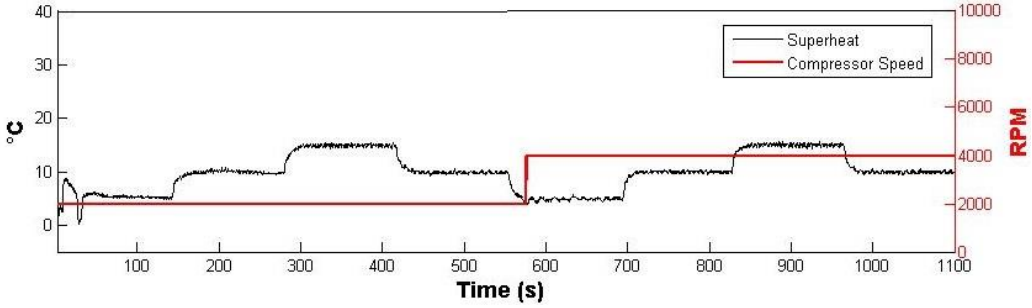

Figure 25: Superheat change test – superheat vs compressor speed using PPEV on water chiller system

As shown in Figure 24 and Figure 25, when the EEV is used and the compressor speed is increased, the system's superheat becomes disrupted and oscillates a little before finally settling back at the setpoint. This disruption causes a decrease in system efficiency. However, in the other case, the PPEV is able to respond fast enough to the change in the compressor speed that the level of superheat remains undisturbed in spite of the change in the operational conditions. The mass flow rates associated with these tests are as shown in Figure 26 and Figure 27.

As seen in these figures, the mass flow rate across the EEV fluctuates considerably while the mass flow rate across the PPEV is more stable. This translates into more efficiency and more energy savings as will be demonstrated in the evaluation of the respective COPs. The condenser outlet pressures and evaporator outlet pressures associated with these tests are as shown in Figure 28 and Figure 29. These figures also show that there are dips in the evaporator outlet pressure when the EEV is used. This is bad for the system as it indicates that more energy is used to maintain operating conditions. However, when the PPEV is used, these dips do not occur. The evaporator and condenser outlet pressures are more stable and consequently the system operates more efficiently.

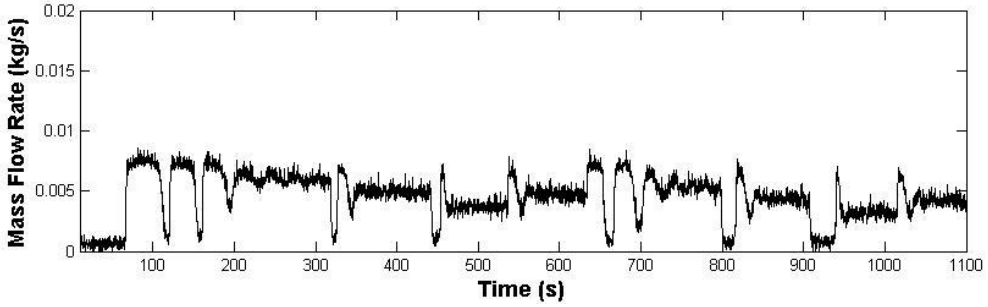

Figure 26: Superheat change test – mass flow rate using EEV on water chiller system

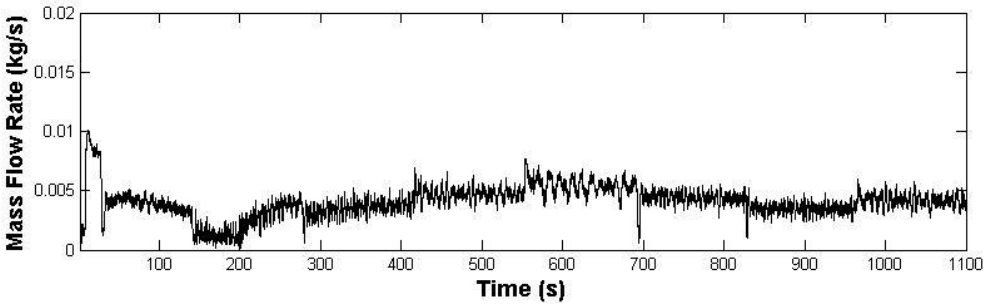

Figure 27: Superheat change test – mass flow rate using PPEV on water chiller system

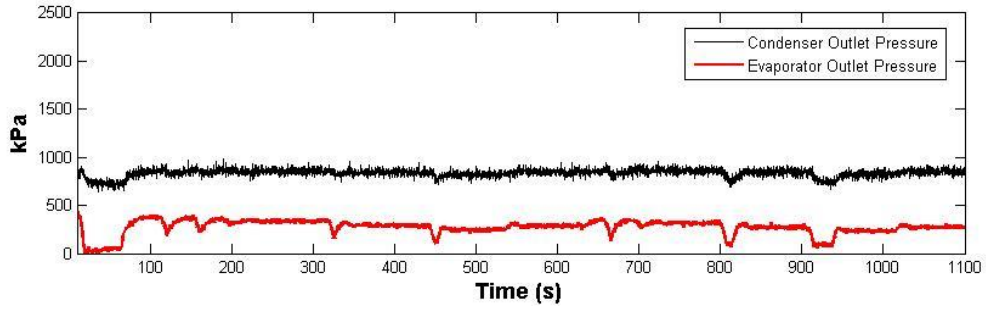

Figure 28: Superheat change test – condenser and evaporator outlet pressures using EEV on water chiller system

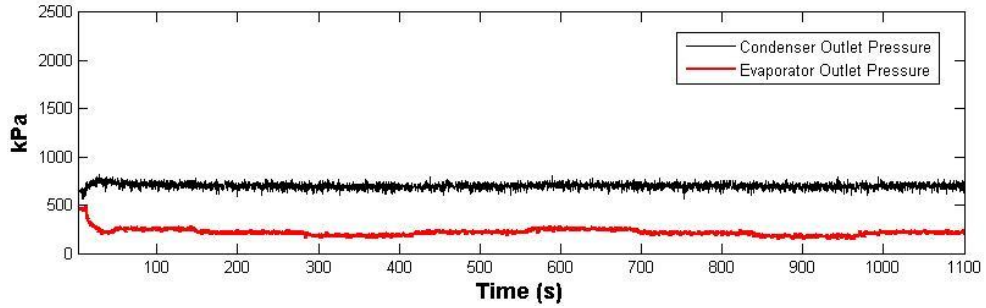

Figure 29: Superheat change test – condenser and evaporator outlet pressures using PPEV on water chiller system

Cooling capacity and COP are the two main factors that are ultimately used to assess the performance of a VCC system. For each of the tests carried out in this project the cooling capacity and COP were calculated. Figure 30 and Figure 31 illustrate the cooling capacity results from the superheat change test on the water chiller system.

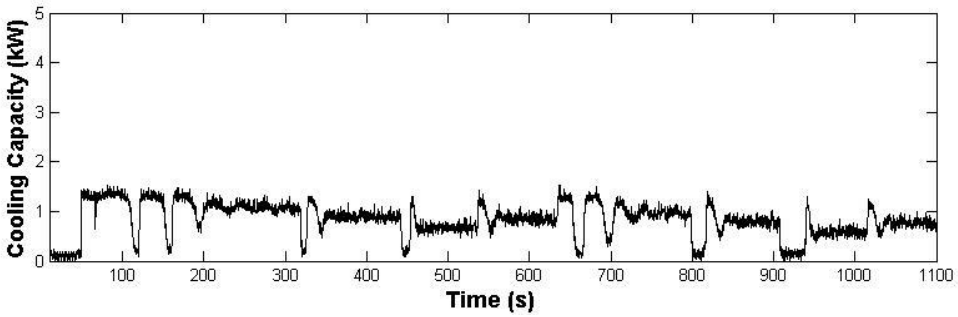

Figure 30: Superheat change test – cooling capacity using EEV on water chiller system

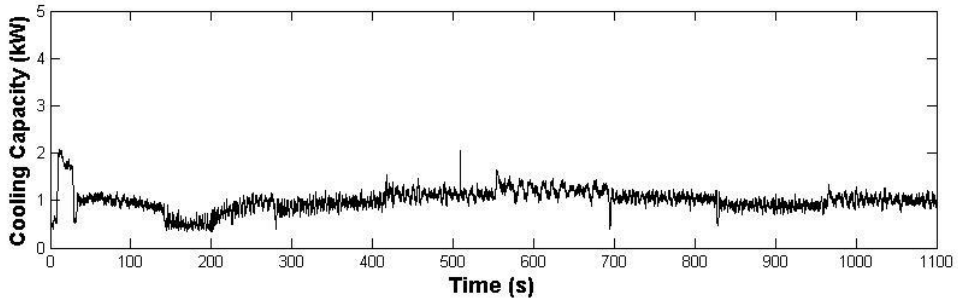

Figure 31: Superheat change test – cooling capacity using EEV on water chiller system

As can be seen, the cooling capacity using the PPEV is more stable and fluctuates less than that using the EEV. Due to its better performance, the PPEV is able to achieve more cooling using less compressor work as shown by the COP values on Table 9. The experiment was broken down into eight sections of 90 seconds and the COP at each of these sections was evaluated independently in order to provide a fair and

accurate evaluation of each valve's performance. Figure 32 and Figure 33 illustrate the breakdown of the sections used to calculate and compare the COP values.

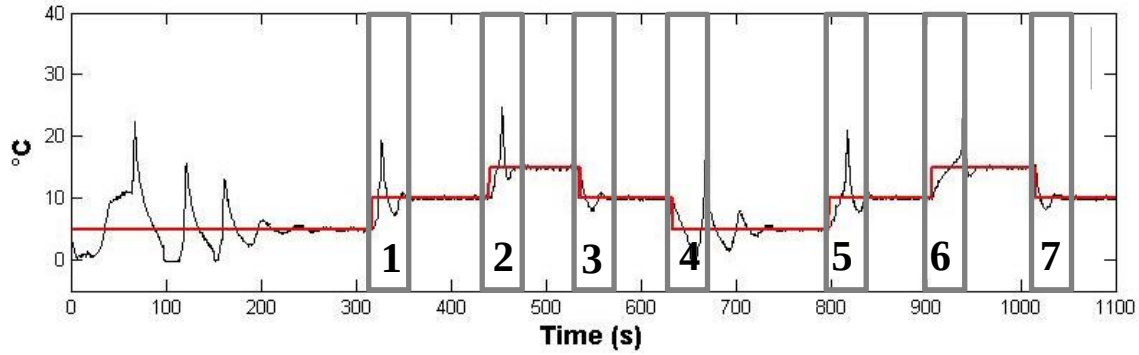

Figure 32: Superheat change test – section breakdown of EEV data for COP analysis on water chiller system

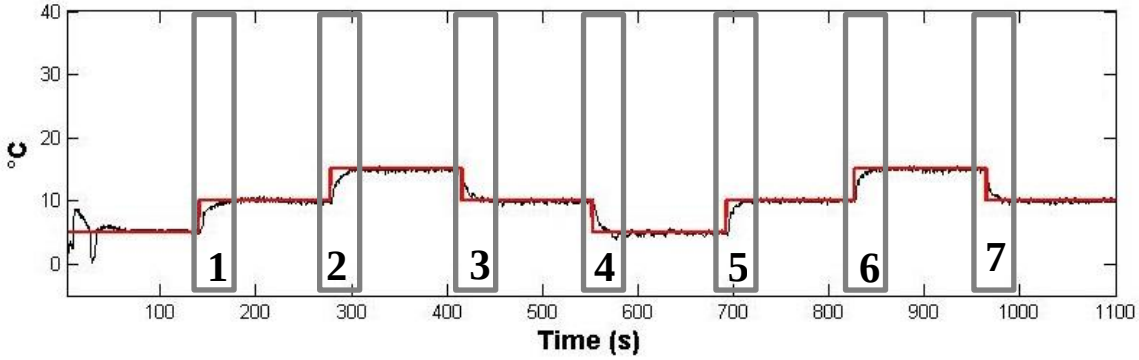

Figure 33: Superheat change test – section breakdown of PPEV data for COP analysis on water chiller system

Table 9: COP values for superheat change test on water chiller system

Section		PPEV	EEV
1	**CC (kW)**	0.79	0.54
	Work (kW)	0.27	0.21
	COP	2.92	2.57
	COP Improvement (%)		**13.6**
2	**CC (kW)**	0.98	0.60
	Work (kW)	0.32	0.24
	COP	3.1	2.50
	COP Improvement (%)		**24**
3	**CC (kW)**	1.17	1.05
	Work (kW)	0.38	0.37
	COP	3.01	2.83
	COP Improvement (%)		**14.8**
4	**CC (kW)**	1.28	0.77
	Work (kW)	0.41	0.29
	COP	3.12	2.65
	COP Improvement (%)		**17.7**
5	**CC (kW)**	1.21	0.41
	Work (kW)	0.39	0.17
	COP	3.10	2.41
	COP Improvement (%)		**28.6**
6	**CC (kW)**	1.18	0.47
	Work (kW)	0.38	0.18
	COP	3.11	2.61
	COP Improvement (%)		**19.2**
7	**CC (kW)**	1.22	1.31
	Work (kW)	0.39	0.49
	COP	3.13	2.67
	COP Improvement (%)		**17.3**
Time (s)		90	90

Direct Exchange Split Heat Pump System

Figure 34 shows how the compressor speed signal changes across the test. The system responses to these changes in superheat setpoint are as shown in Figure 35, Figure 36, Figure 37 and Figure 38 for the direct exchange split heat pump.

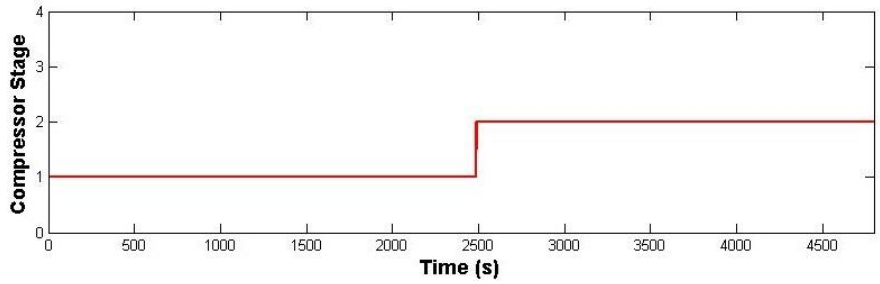

Figure 34: Superheat change test - compressor stage signal

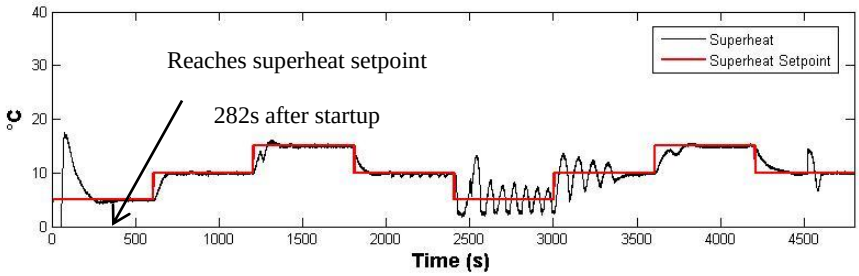

Figure 35: Superheat change test – superheat vs superheat setpoint using EEV on heat pump system

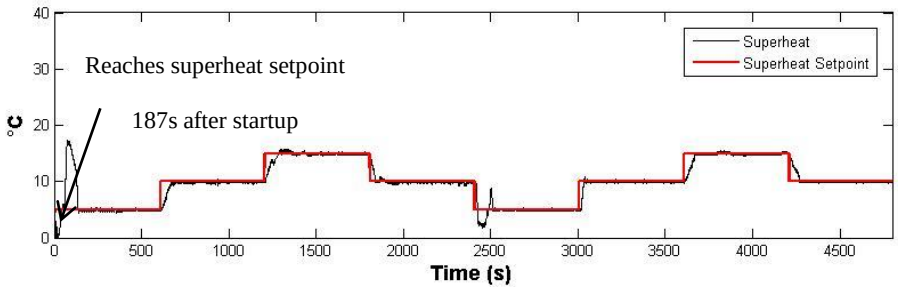

Figure 36: Superheat change test – superheat vs superheat setpoint using PPEV on heat pump system

As shown in Figure 35 and Figure 36, from startup, the PPEV reaches the superheat setpoint 187 seconds after startup while the EEV reaches the superheat setpoint 282 seconds after start-up. Just like on the modulated water chiller system, this indicates quicker response time and ability to reach operating conditions quicker thus minimizing compressor use. Figure 37 and Figure 38 illustrate how changing the compressor speed affects the level of superheat control by the valve. The compressor speed was 2,000 RPM for the first cycle and then it was increased to 4,000 RPM for the second cycle.

When the EEV is used and the compressor speed is increased, the system's superheat becomes disrupted and oscillates briefly starts hunting before finally settling back to the setpoint. The negative impact of hunting on the system's energy efficiency has been extensively discussed [4], [10], [11], including in this thesis. However, when the PPEV is used in the same conditions, it is able to respond fast enough to the change in the compressor speed that there is just a slight disruption in the level of superheat and no hunting behavior is observed in spite of the change in the operational conditions. The mass flow rates associated with these tests are as shown in Figure 39 and Figure 40.

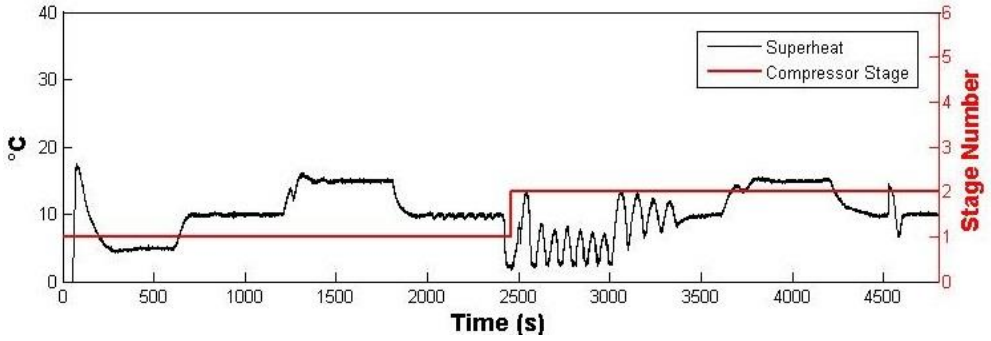

Figure 37: Superheat change test – superheat vs compressor speed using EEV on heat pump system

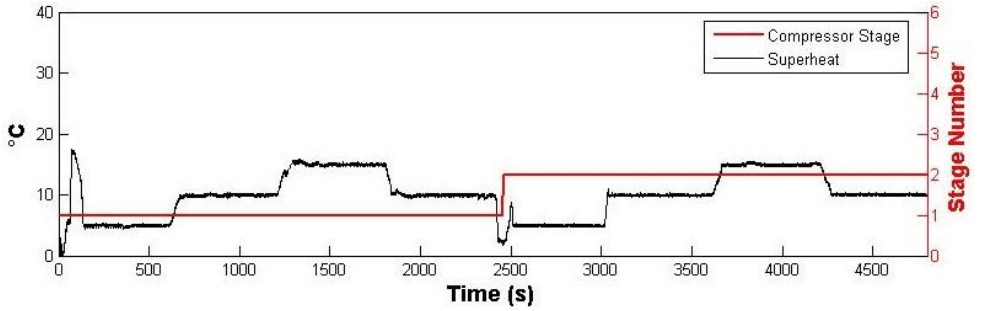

Figure 38: Superheat change test – superheat vs compressor speed using PPEV on heat pump system

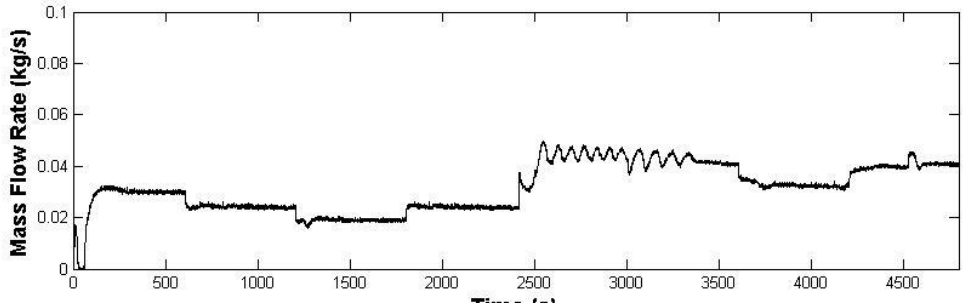

Figure 39: Superheat change test – mass flow rate using EEV on heat pump system

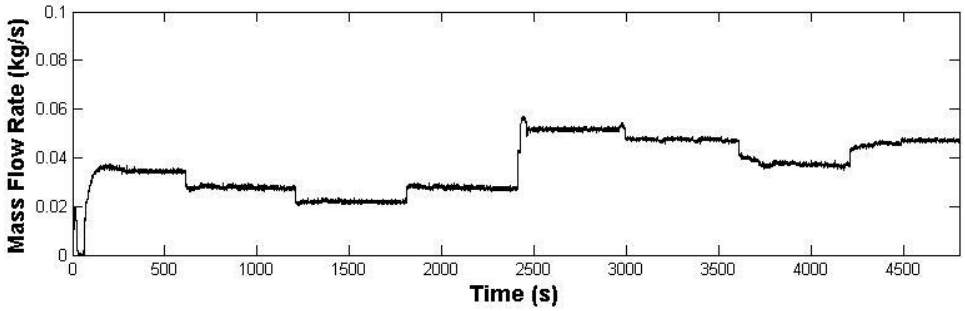

Figure 40: Superheat change test – mass flow rate using PPEV on heat pump system

As seen in these figures, the refrigerant flow across both valves is steady and responds well to changes in the superheat set points. However, when the compressor speed is increased the mass flow rate across the EEV starts fluctuates considerably before settling while the mass flow rate across the PPEV is more stable. This translates into more efficiency and more energy savings as will be demonstrated in the evaluation of the respective COPs. The condenser outlet pressures and evaporator outlet pressures associated with these tests are as shown in Figure 41 and Figure 42.

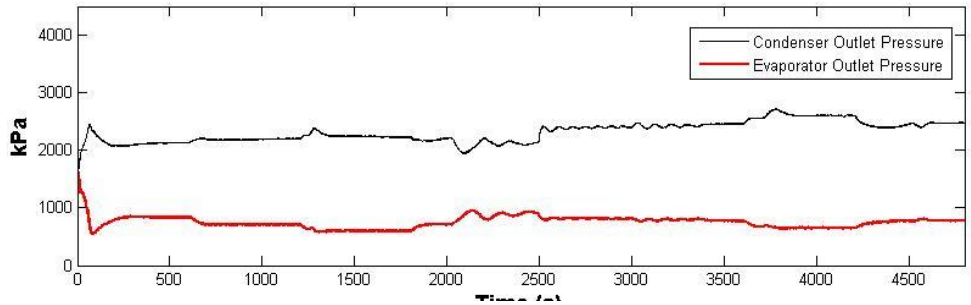

Figure 41: Superheat change test – condenser and evaporator outlet pressures using EEV on heat pump system

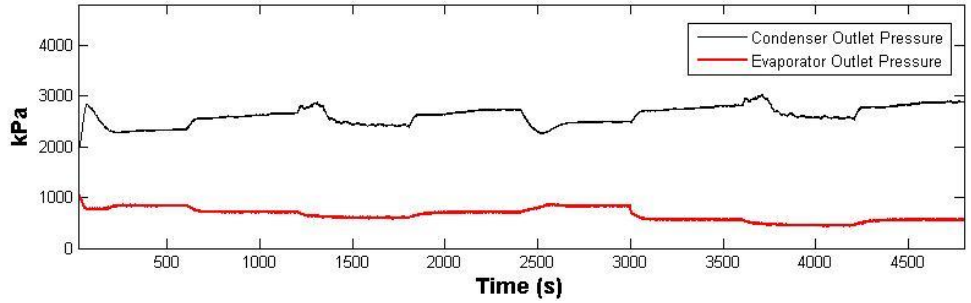

Figure 42: Superheat change test – condenser and evaporator outlet pressures using PPEV on heat pump system

As seen in the aforementioned figures, the flow of refrigerant using the PPEV is more stable and the outlet pressures reach operating conditions more rapidly when the PPEV is used. Figure 43 and Figure 44 illustrate the cooling capacity results from the superheat change test on the water chiller system.

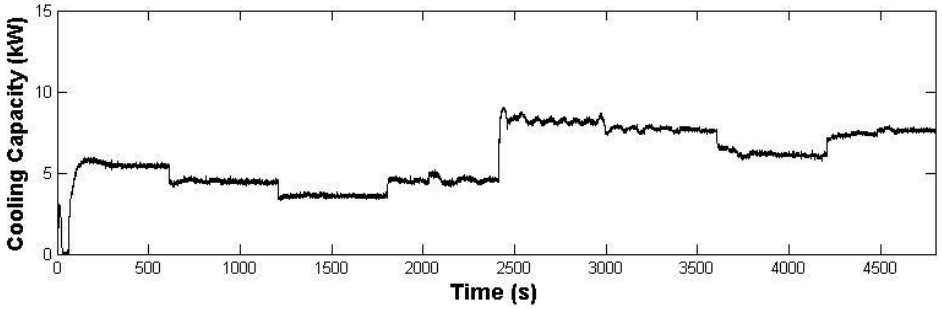

Figure 43: Superheat change test – cooling capacity using EEV on heat pump system

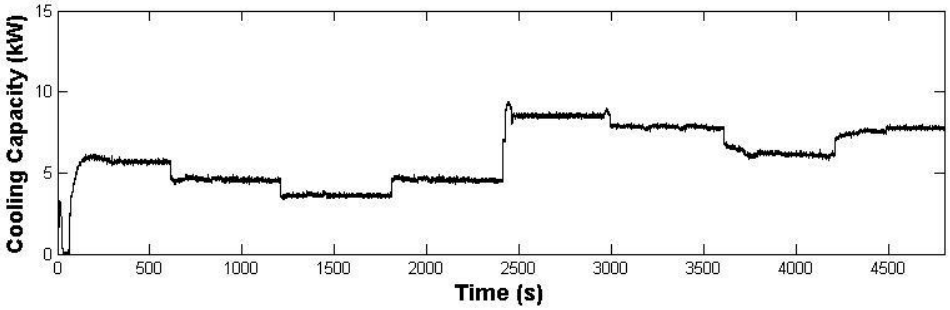

Figure 44: Superheat change test – cooling capacity using EEV on heat pump system

Thus, the cooling capacity using the PPEV is more stable and fluctuates less than that using the EEV especially when the compressor speed is increased.. Due to its better performance, the PPEV is able to achieve more cooling using less compressor work as shown by the COP values in Table 10. The experiment was broken down into seven sections of 300 seconds as shown in Figure 45 and Figure 46. The COP at each of these sections was evaluated independently as shown in Table 10. This was done in order to provide a fair and accurate evaluation of each valve's performance. This COP is based

on the power input to the compressor and is calculated as shown earlier in this Chapter in Equation 18.

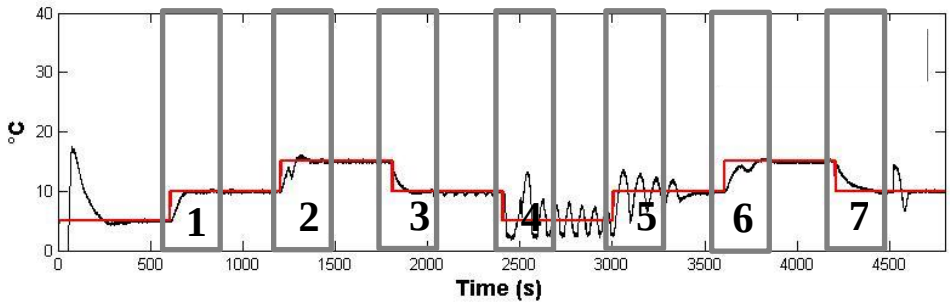

Figure 45: Superheat change test – section breakdown of EEV data for COP analysis on heat pump system

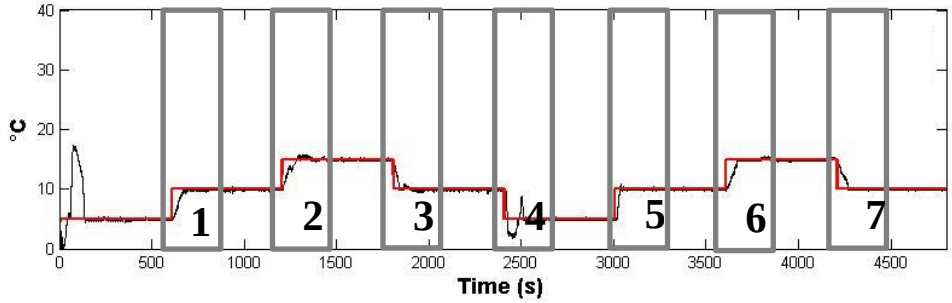

Figure 46: Superheat change test – section breakdown of PPEV data for COP analysis on heat pump system

Table 10: COP values for superheat change test on heat pump system

Section		PPEV	EEV
1	**CC (kW)**	5.51	4.98
	Power (kW)	3.25	3.17
	COP	1.71	1.57
	COP Improvement (%)		**9.1**
2	**CC (kW)**	4.99	4.32
	Power (kW)	2.81	2.7
	COP	1.78	1.60
	COP Improvement (%)		**6.1**
3	**CC (kW)**	5.42	7.89
	Power (kW)	3.12	5.22
	COP	1.74	1.51
	COP Improvement (%)		**10.1**
4	**CC (kW)**	9.48	7.58
	Power (kW)	5.63	4.95
	COP	1.68	1.47
	COP Improvement (%)		**12.4**
5	**CC (kW)**	9.11	7.28
	Power (kW)	5.43	4.95
	COP	1.68	1.47
	COP Improvement (%)		**12.4**
6	**CC (kW)**	7.88	6.38
	Power (kW)	4.57	4.16
	COP	1.72	1.53
	COP Improvement (%)		**11.0**
7	**CC (kW)**	8.74	7.22
	Power (kW)	4.97	4.66
	COP	1.76	1.55
	COP Improvement (%)		**11.8**
Time (s)		300	300

Startup Test Results

This test is designed to assess how quickly the system is able to reach the set operating conditions. From startup, the system was allowed to run for three minutes, then the compressor was shut down for three minutes and the on/off cycle was repeated two more times.

Modulated Water Chiller System

Figure 47, Figure 48 and Figure 49 illustrate the system's superheat in response to a given superheat setpoint for this test. As shown in these figures, from startup, the PPEV reaches the superheat setpoint 82 seconds after startup while the EEV reaches the superheat setpoint 131seconds after start-up and the TEV reaches the setpoint 153 seconds after startup. The mass flow rates associated with these tests are as shown in Figure 50, Figure 51 and Figure 52.

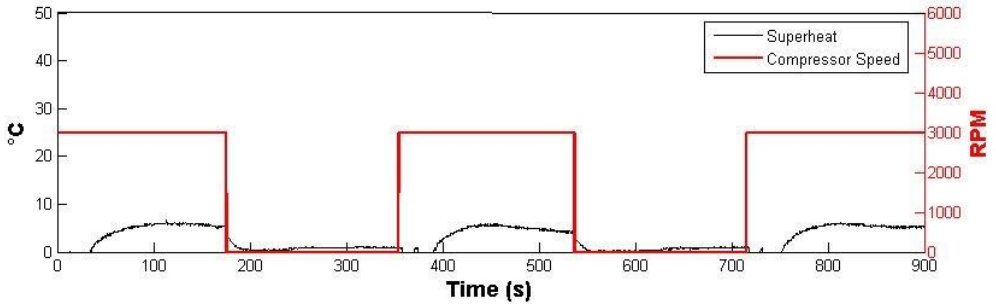

Figure 47: Startup test – superheat vs superheat setpoint using TEV on water chiller system

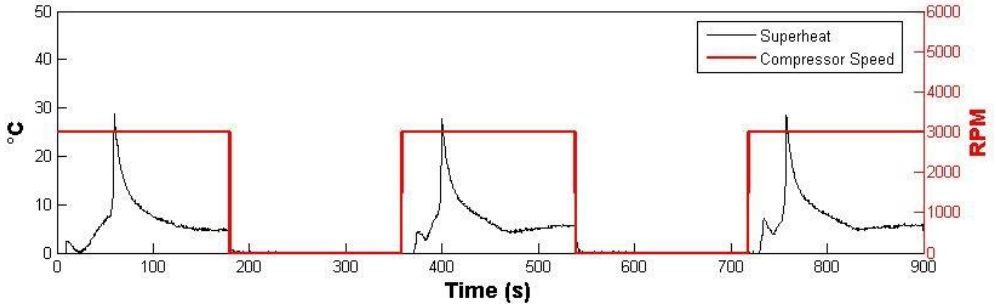

Figure 48: Startup test – superheat vs superheat setpoint using EEV on water chiller system

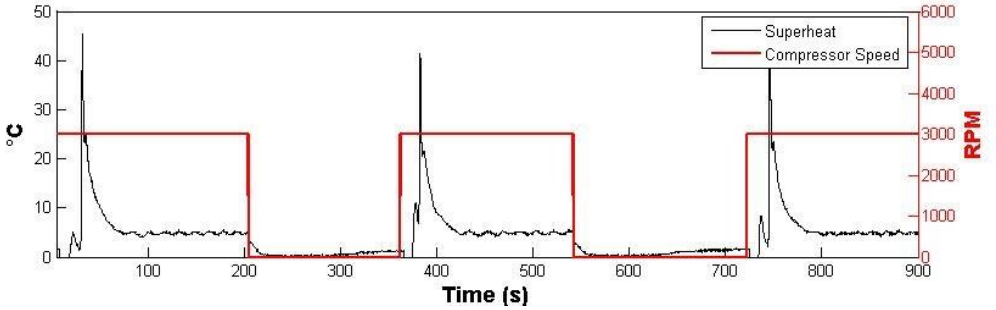

Figure 49: Startup test – superheat vs superheat setpoint using PPEV on water chiller system

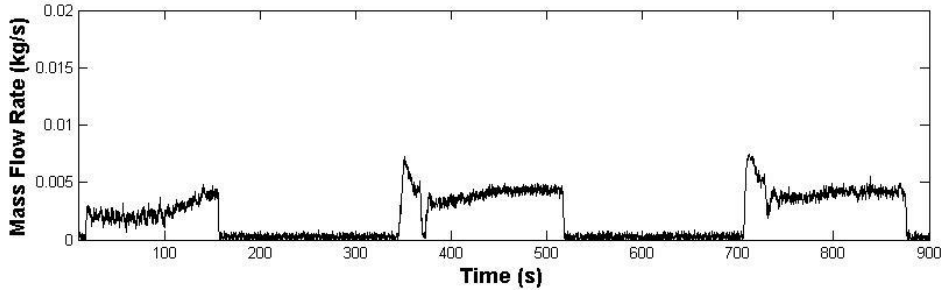

Figure 50: Startup test – mass flow rate using TEV on water chiller system

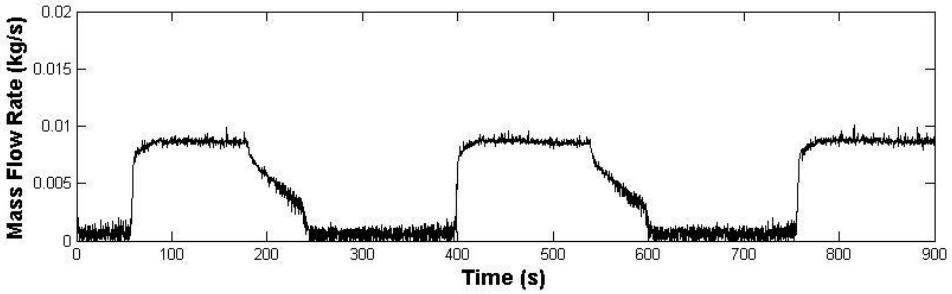

Figure 51: Startup test – mass flow rate using EEV on water chiller system

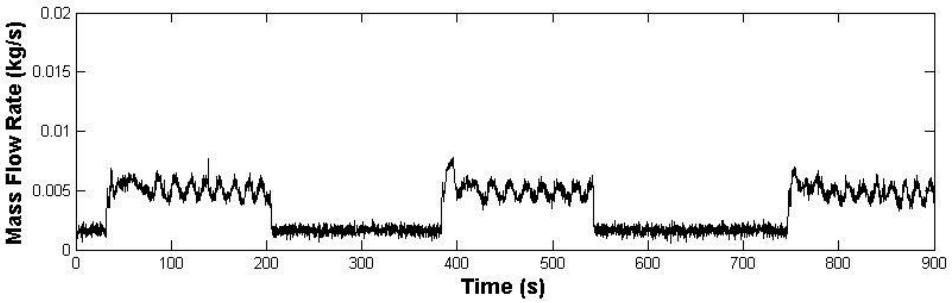

Figure 52: Startup test – mass flow rate using PPEV on water chiller system

Figure 53, Figure 54 and Figure 55 show the pressures associated with these tests.

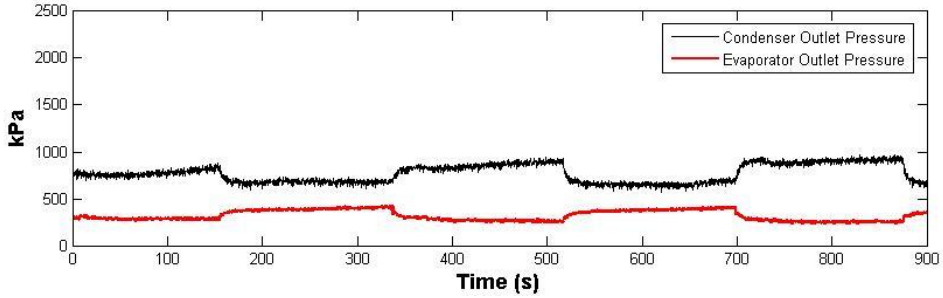

Figure 53: Startup test – condenser and evaporator outlet pressures using TEV on water chiller system

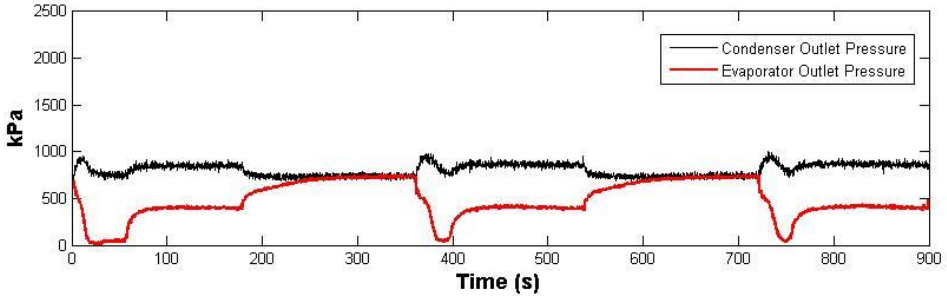

Figure 54: Startup test – condenser and evaporator outlet pressures using EEV on water chiller system

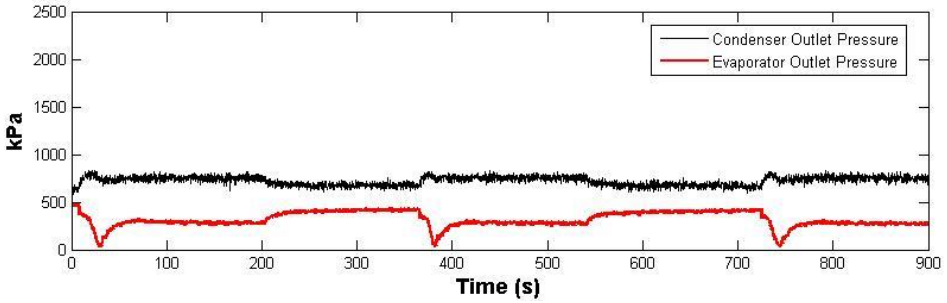

Figure 55: Startup test – condenser and evaporator outlet pressures using PPEV on water chiller system

Figure 56, Figure 57 and Figure 58 illustrate the cooling capacity results from the superheat change test on the water chiller system.

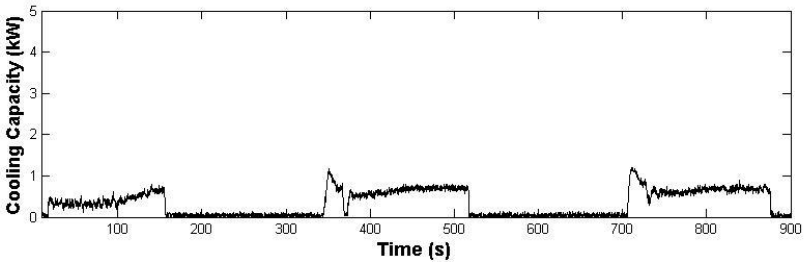

Figure 56: Startup test – cooling capacity using TEV on water chiller system

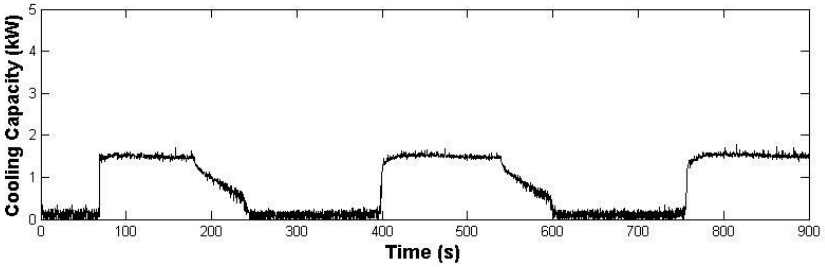

Figure 57: Startup test – cooling capacity using EEV on water chiller system

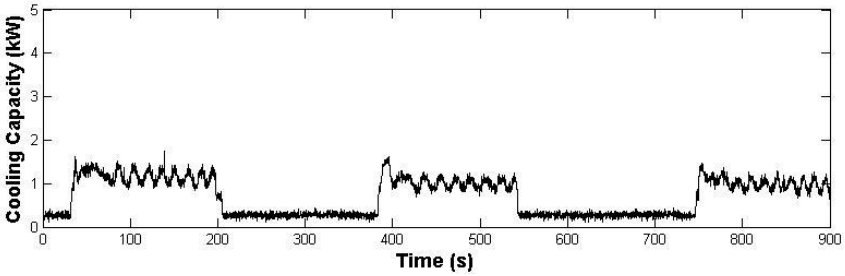

Figure 58: Startup test – cooling capacity using PPEV on water chiller system

As shown in the figures, the PPEV is able to reach operating conditions much faster than the EEV and TEV and so it is able to provide the required cooling using less energy than the EEV and the TEV as shown by the calculated COP values in Table 11. When the PPEV is used the overall cooling obtained during these startup cycles is higher. The experimental data was broken down into three sections of 180 seconds as shown in Figure 59, Figure 60 and Figure 61. The cooling capacity, electrical energy input and COP at each of these sections were evaluated independently in order to provide a fair and accurate evaluation of each valve's performance.

As can be seen in Table 11, in all three sections, the system produces the most cooling when it is equipped with the PPEV. It is also when it is equipped with the most cooling that it consumes the most energy. However the ratio for the amount of cooling produced to the amount of energy consumed is evaluated, the PPEV comes ahead of the EEV and the TEV. For the various sections considered when the compressor was running at first stage, the PPEV's COP is about 17% higher than that of the EEV about 35% higher than that of the TEV.

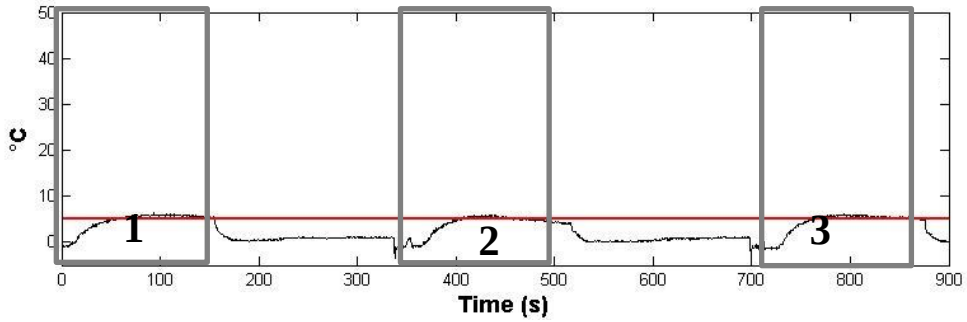

Figure 59: Startup test – section breakdown of TEV data for COP analysis on water chiller system

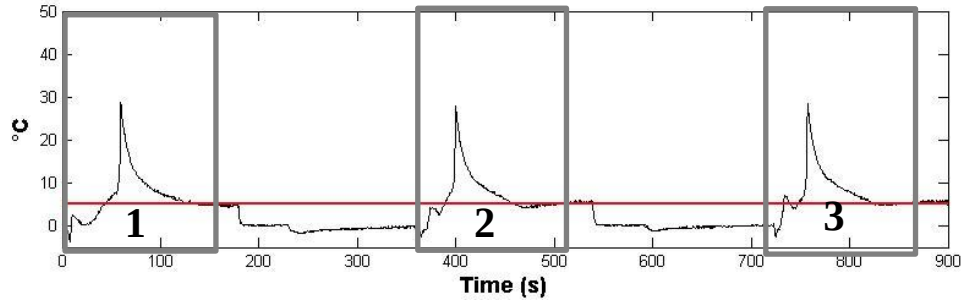

Figure 60: Startup test – section breakdown of EEV data for COP analysis on water chiller system

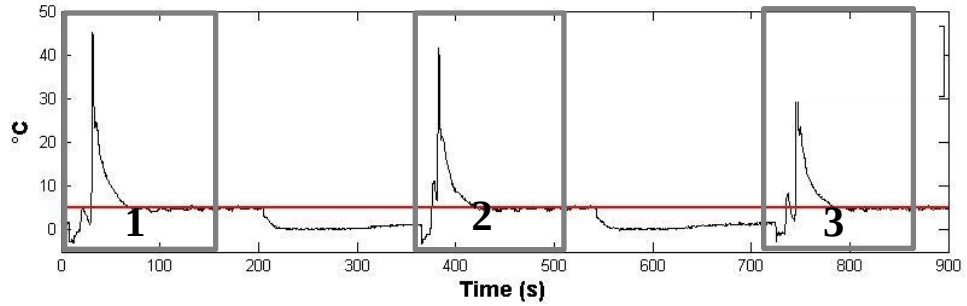

Figure 61: Startup test – section breakdown of PPEV data for COP analysis on water chiller system

Table 11: COP values for startup test on water chiller system

Section		PPEV	EEV	TEV
1	**CC (kW)**	1.17	0.87	0.31
	Work (kW)	0.54	0.47	0.22
	COP	2.17	1.85	1.40
	COP Improvement (%)		**17.3**	**55**
2	**CC (kW)**	1.16	0.91	0.47
	Work (kW)	0.53	0.49	0.29
	COP	2.19	1.86	1.62
	COP Improvement (%)		**17.7**	**35.2**
3	**CC (kW)**	1.13	0..88	0.45
	Work (kW)	0.51	0.48	0.27
	COP	2.22	1.83	1.67
	COP Improvement (%)		**21.3**	**32.9**
Time (s)		180	180	180

Direct Exchange Split Heat Pump System

Figure 62, Figure 63 and Figure 64 illustrate how the system's superheat responds to three cycles of startup for compressor startup for nine minutes and compressor shutdown for one minute when it is equipped with the TEV, EEV and PPEV respectively.

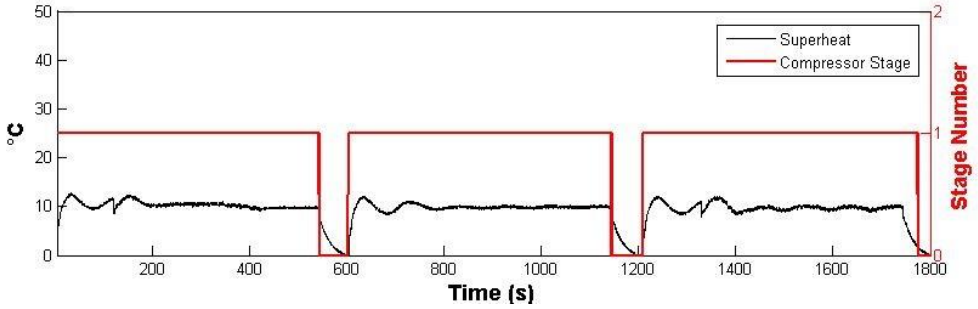

Figure 62: Startup test – superheat vs superheat setpoint using TEV on heat pump system

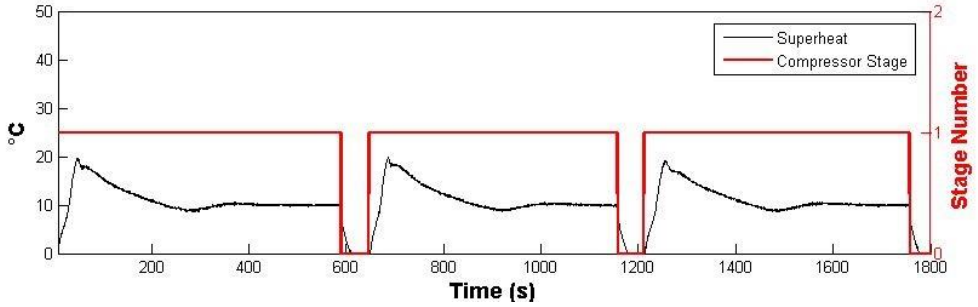

Figure 63: Startup test – superheat vs superheat setpoint using EEV on heat pump system

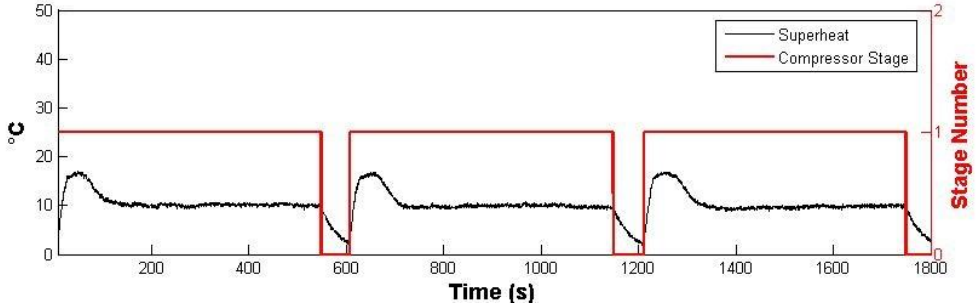

Figure 64: Startup test – superheat vs superheat setpoint using PPEV on heat pump system

As shown in these figures, from startup, the PPEV reaches the superheat setpoint 179 seconds after startup while the EEV reaches the superheat setpoint 334 seconds after start-up and the TEV reaches the setpoint 204 seconds after startup. The mass flow rates and pressures associated with these tests are as shown in Figure 68, Figure 69 and Figure 70.

Similar to the results obtained from the test on the water chiller system, at startup for both the EEV and the PPEV, the superheat first spikes and goes beyond the superheat setpoint before eventually coming back down and settling at the setpoint of 10°C. However in the case of the TEV, this does not occur. The superheat gradually increases till it reaches the superheat setpoint and then it settles there. In spite of their initial overshoot, the EEV and the PPEV are able to produce much more cooling than the TEV in at startup. The mass flow rates associated with these tests are as shown in Figure 65, Figure 66, and Figure 67. Similarly, Figure 68, Figure 69 and Figure 70 illustrate how the condenser outlet pressures and the evaporator outlet pressures react in these startup cycles.

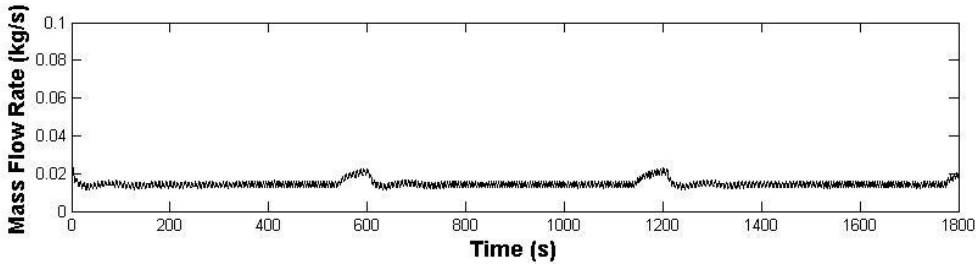

Figure 65: Startup test – mass flow rate using TEV on heat pump system

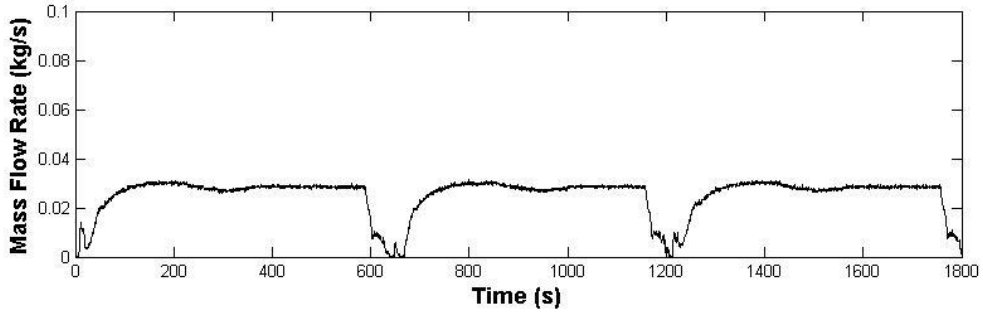

Figure 66: Startup test – mass flow rate using EEV on heat pump system

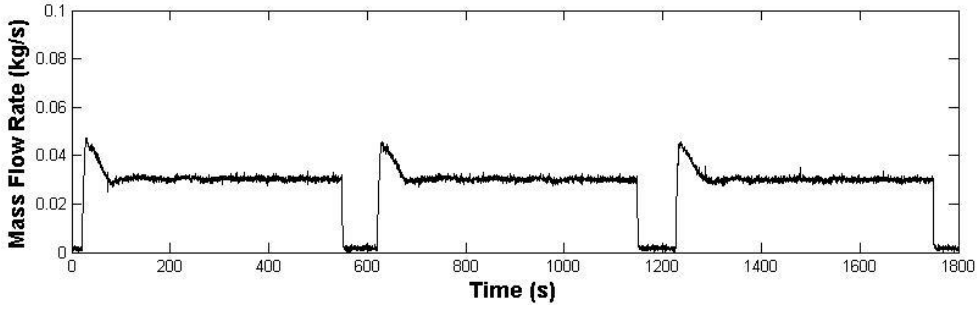

Figure 67: Startup test – mass flow rate using PPEV on heat pump system

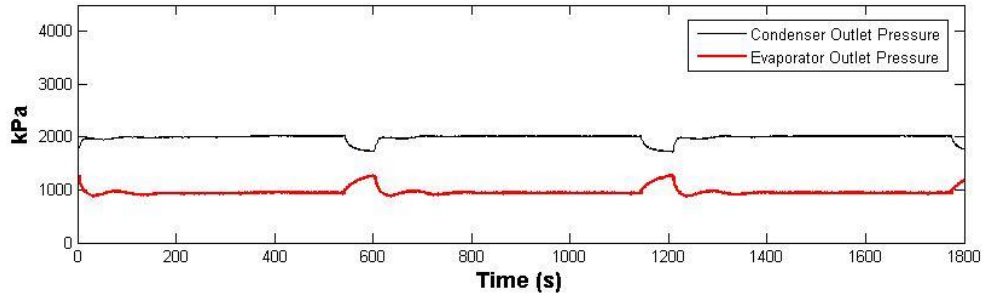

Figure 68: Startup test – condenser and evaporator outlet pressures using TEV on heat pump system

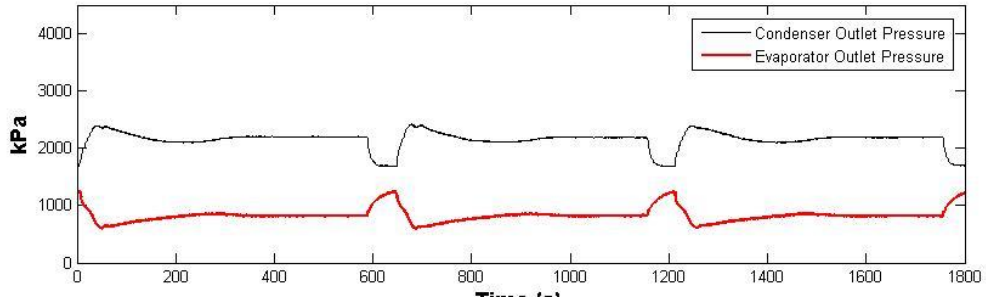

Figure 69: Startup test – condenser and evaporator outlet pressures using EEV on heat pump system

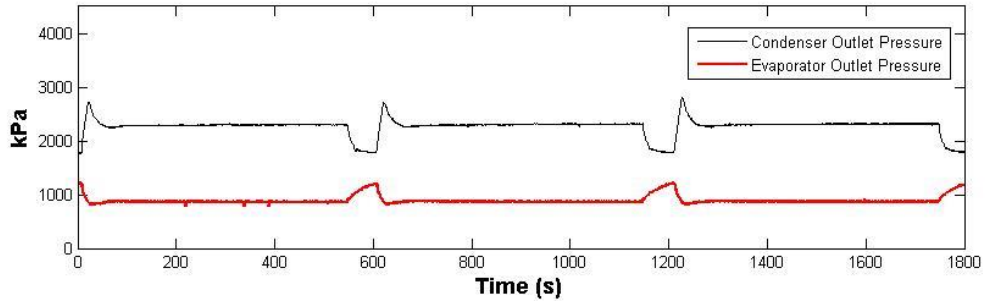

Figure 70: Startup test – condenser and evaporator outlet pressures using PPEV on heat pump system

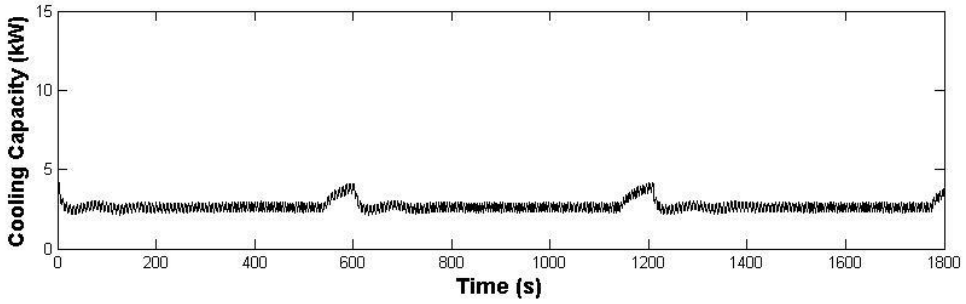

Figure 71: Startup test – cooling capacity using TEV on heat pump system

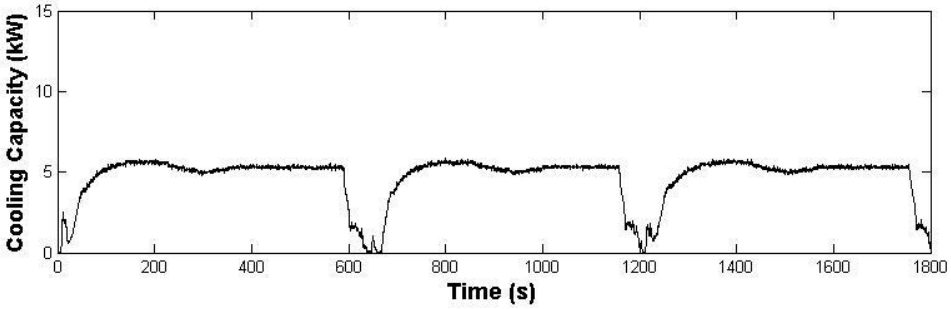

Figure 72: Startup test – cooling capacity using EEV on heat pump system

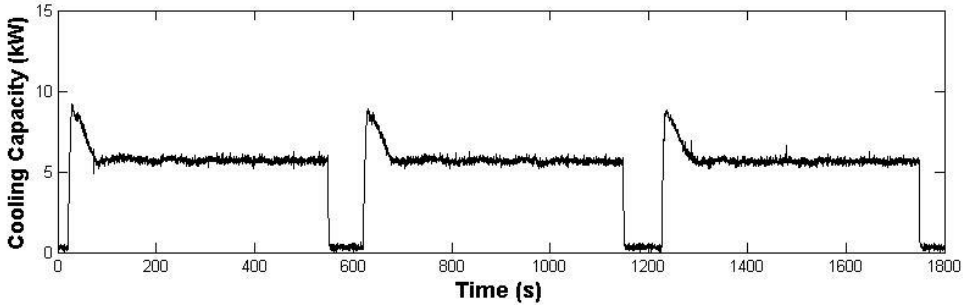

Figure 73: Startup test – cooling capacity using PPEV on heat pump system

Figure 71, Figure 72 and Figure 73 illustrate the cooling capacity results from the superheat change test on the water chiller system. The PPEV is able to reach operating conditions much faster than the EEV and TEV and so it is able to provide the required cooling using less energy than the EEV and the TEV as shown by the calculated COP values in Table 12. When the PPEV is used the overall cooling obtained during these startup cycles is higher. The experimental data was broken down into three sections of 300 seconds as shown in Figure 74, Figure 75 and Figure 76. The cooling capacity, electrical energy input and COP at each of these sections were evaluated independently in order to provide a fair and accurate evaluation of each valve's performance.

As can be seen in Table 12, in all three sections, the system produces the most cooling when it is equipped with the PPEV. It is also when it is equipped with the most cooling that it consumes the most energy. However the ratio for the amount of cooling produced to the amount of energy consumed is evaluated, the PPEV comes ahead of the EEV and the TEV. For the various sections considered when the compressor was running at first stage, the PPEV's COP is about 13% higher than that of the EEV about 22% higher than that of the TEV.

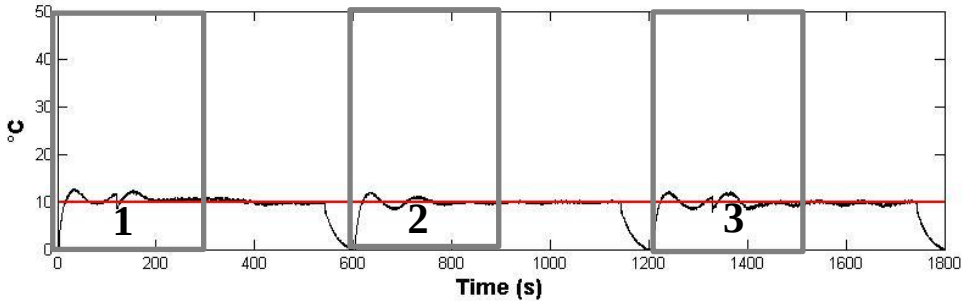

Figure 74: Startup test – section breakdown of TEV data for COP analysis on heat pump system

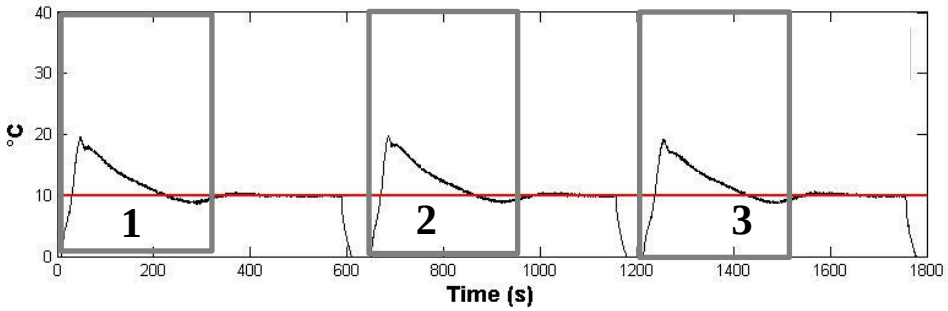

Figure 75: Startup test – section breakdown of EEV data for COP analysis on heat pump system

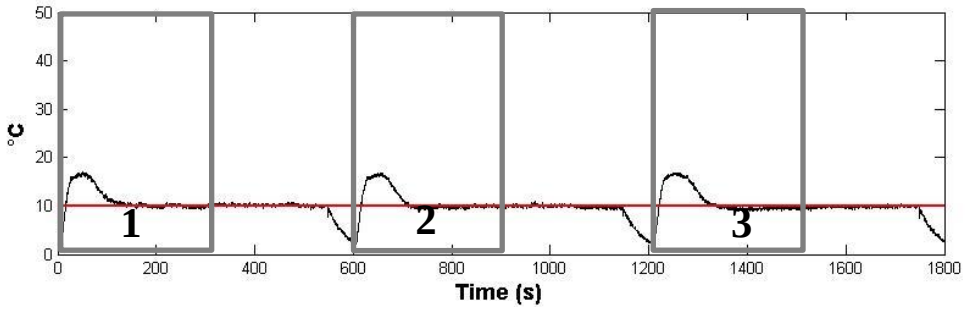

Figure 76: Startup test – section breakdown of PPEV data for COP analysis on heat pump system

Table 12: COP values for startup test on heat pump system

Section		PPEV	EEV	TEV
1	**CC (kW)**	5.81	4.82	2.50
	Power (kW)	3.74	3.47	1.94
	COP	1.55	1.39	1.28
	COP Improvement (%)		**11.5**	**21.1**
2	**CC (kW)**	5.56	4.78	2.58
	Power (kW)	3.45	3.39	1.97
	COP	1.61	1.41	1.31
	COP Improvement (%)		**14.1**	**22.9**
3	**CC (kW)**	5.54	4.77	2.56
	Power (kW)	3.46	3.43	1.97
	COP	1.60	1.39	1.30
	COP Improvement (%)		**15.1**	**23.1**
Time (s)		300	300	300

External Fluid Flow Rate Change Test Results

This test is designed to assess how the system responds to sudden changes in load during operation. The change in the flow rate of the external fluid is a good representation of the load changes that can occur to a VCC system in practical application such as the door of a refrigerator being opened. The water flow rate is progressively increased from 23 GPH to 115 GPH at 2,000 RPM and the same was done at 4,000 RPM.

Modulated Water Chiller System

Figure 77, Figure 78 and Figure 79 illustrate how the system's superheat responds to changes in the flow rate of the external fluid (water) across the evaporator when it is equipped with a TEV, EEV and PPEV respectively. As shown in these figures, from startup, the PPEV reaches the superheat setpoint 218 seconds after startup while the EEV reaches the superheat setpoint 448 seconds after start-up and the TEV reaches the setpoint 424 seconds after startup. Furthermore as the compressor speed is increased the TEV starts hunting and the EEV is quite disturbed but is eventually able to restore operational conditions. Meanwhile the PPEV remains relatively undisturbed. This is due to the quick action of the PPEV's PDAVs which enable to quick adapt to the change in compressor speed. These observations are as shown in Figure 80, Figure 81 and Figure 82.

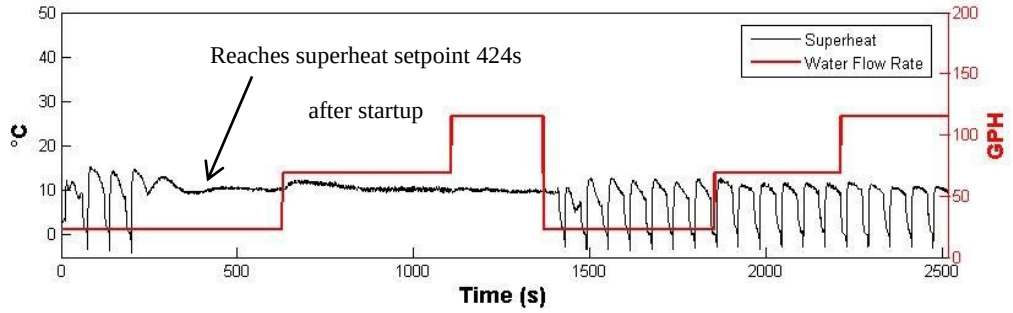

Figure 77: External fluid flow rate change test – superheat vs superheat setpoint using TEV on water chiller system

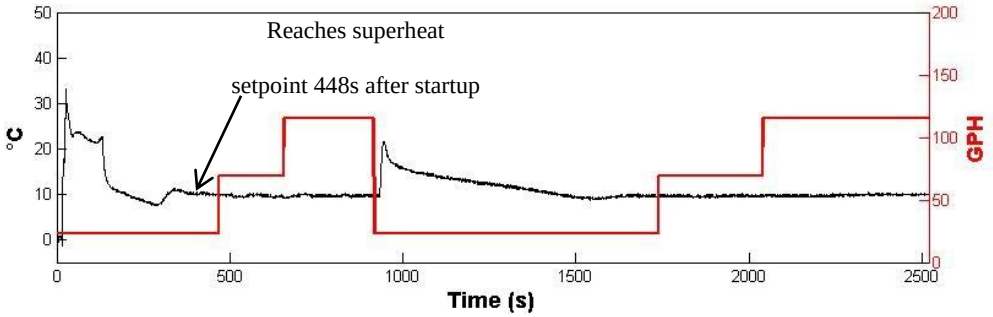

Figure 78: External fluid flow rate change test – superheat vs superheat setpoint using EEV on water chiller system

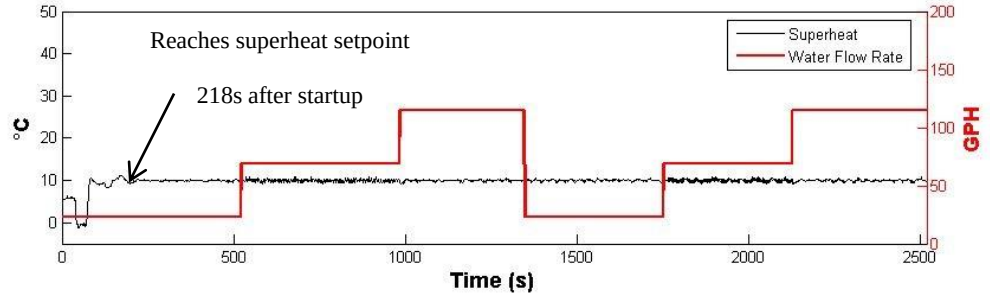

Figure 79: External fluid flow rate change test – superheat vs superheat setpoint using PPEV on water chiller system

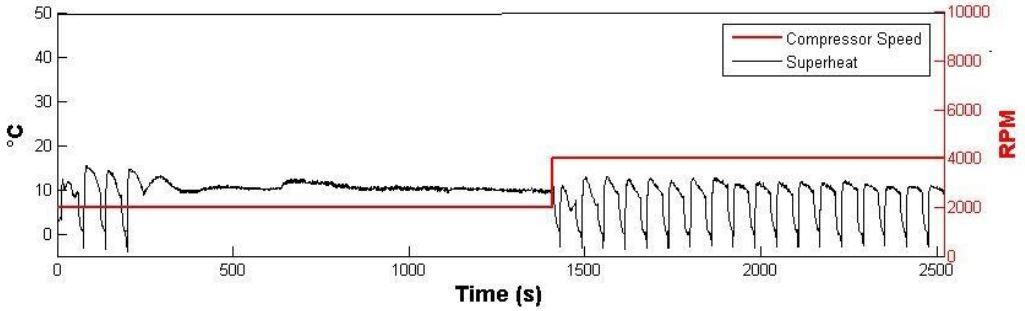

Figure 80: External fluid flow rate change test – superheat vs compressor speed using TEV on water chiller system

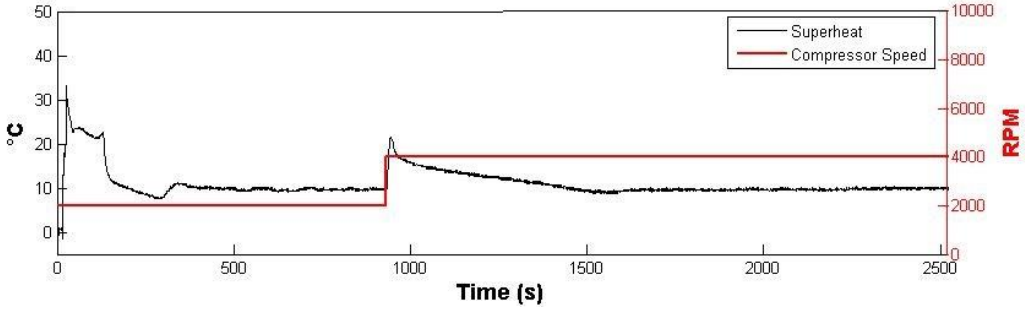

Figure 81: External fluid flow rate change test – superheat vs compressor speed using TEV on water chiller system

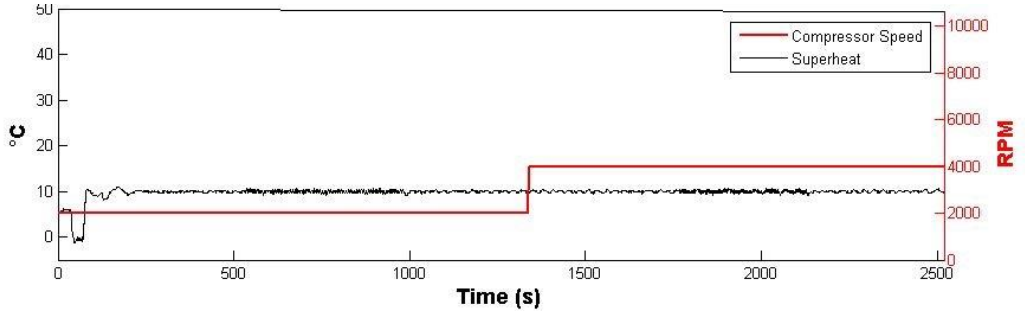

Figure 82: External fluid flow rate change test – superheat vs compressor speed using TEV on water chiller system

The next figures illustrate how much trouble the TEV has after the compressor speed is increased. The TEV hunts a little bit after start up but is eventually able to reach the operating conditions. However, once the compressor speed is increased, the TEV starts hunting. This causes big fluctuations in refrigerant mass flow rates as shown in Figure 83 as well as condenser outlet pressure as shown in Figure 86. This negatively impacts the system's energy consumption.

The EEV takes a little while to reach the superheat setpoint and finally does so after 448 seconds. From then, it is able to easily maintain the operating conditions. However, when the compressor speed is increased, the system experiences a considerable amount of disruption but the EEV is slowly able to get back on track and restore the superheat to its setpoint. These are as shown in Figure 84 and Figure 87.

The PPEV on the other hand reaches the superheat setpoint in about half the time that the two other valves take to reach it. Once it does, it maintains the superheat at its setpoint. When the compressor speed is increased, it is able to react so quickly that the mass flow rate, condenser pressure and evaporator outlet pressure do not start to oscillate. These are as shown in Figure 85 and Figure 88.

.

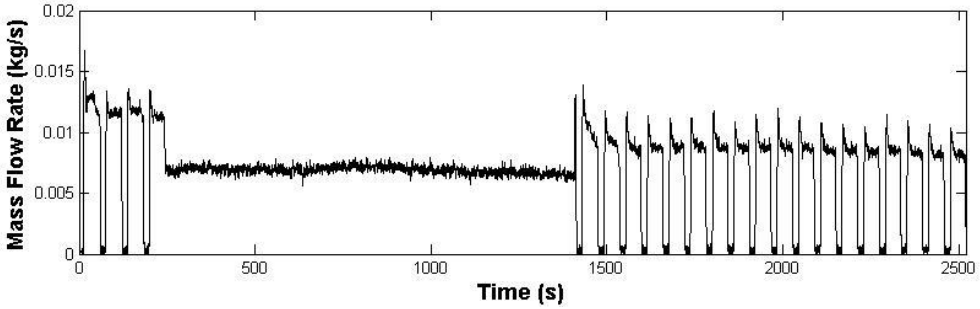

Figure 83: External fluid flow rate change test – mass flow rate using TEV on water chiller system

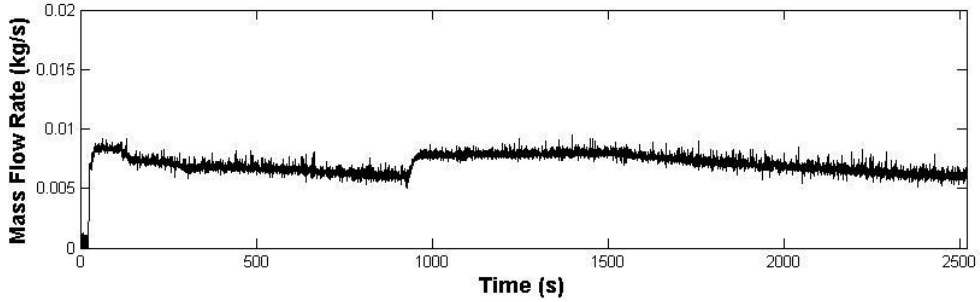

Figure 84: External fluid flow rate change test – mass flow rate using EEV on water chiller system

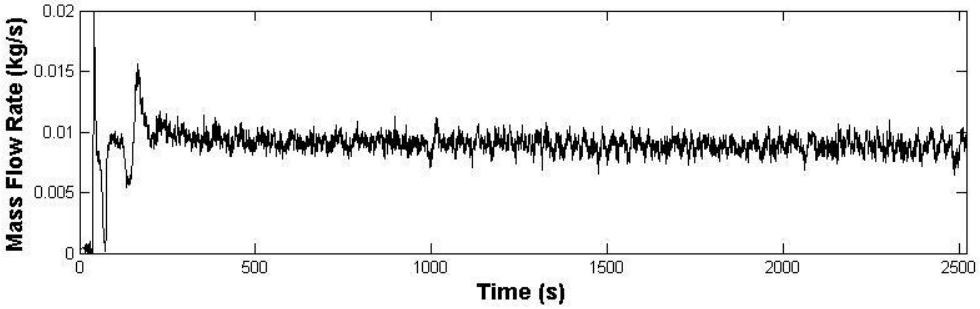

Figure 85: External fluid flow rate change test – mass flow rate using PPEV on water chiller system

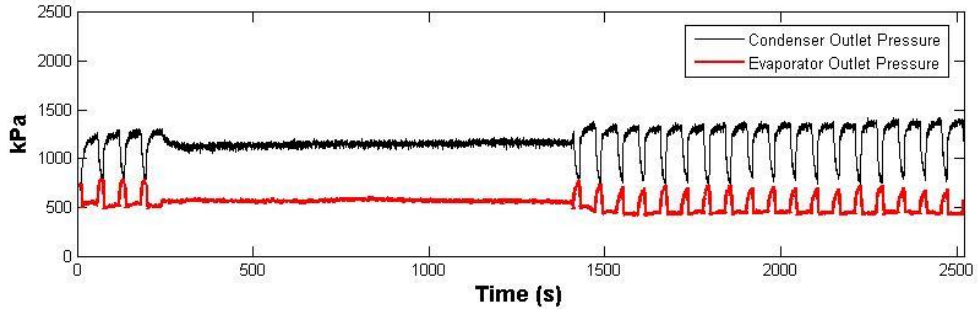

Figure 86: External fluid flow rate change test – condenser and evaporator outlet pressures using TEV on water chiller system

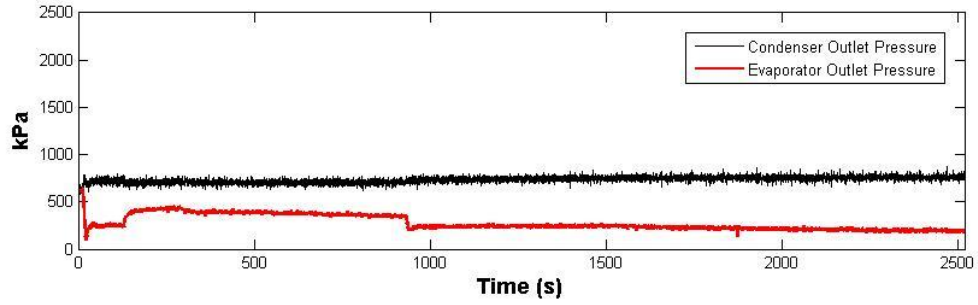

Figure 87: External fluid flow rate change test – condenser and evaporator outlet pressures using EEV on water chiller system

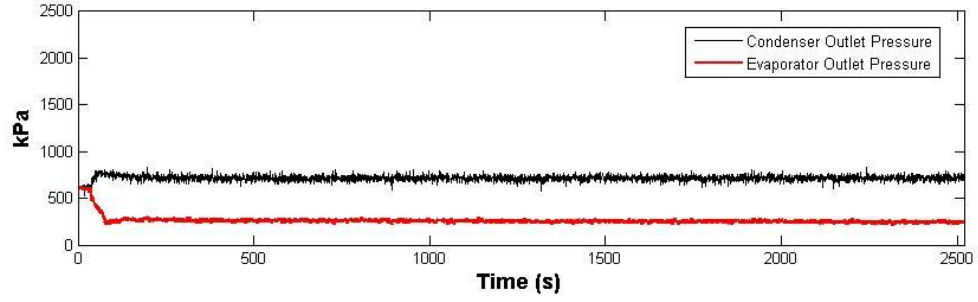

Figure 88: External fluid flow rate change test – condenser and evaporator outlet pressures using PPEV on water chiller system

The superior performance of the PPEV when compared to the TEV and EEV is best illustrated in terms of the amount of cooling it is able to achieve. Figure 89, Figure 90 and Figure 91 show that the PPEV consistently produces more cooling than the TEV and the EEV. Here we see that when the TEV is used at a compressor speed of 2000 RPM and the water flow rate is gradually increased, it has a little bit of trouble at startup and after that it is able to provide fairly stable and constant cooling of about 1.2 kW. However, when the compressor speed is increased, the valve starts hunting and consequently the refrigerant mass flow rate and cooling capacity start oscillating. This is bad for the system as it leads to increased compressor use and loss of efficiency. The EEV deals well with those changes as the increase in compressor leads to an increase in cooling and energy use but the valve is able to avoid hunting. Through the quick action of its microvalves, the PPEV is able to quickly adjust to the increase in compressor speed and so it able to maintain a good amount of cooling without compromising energy efficiency.

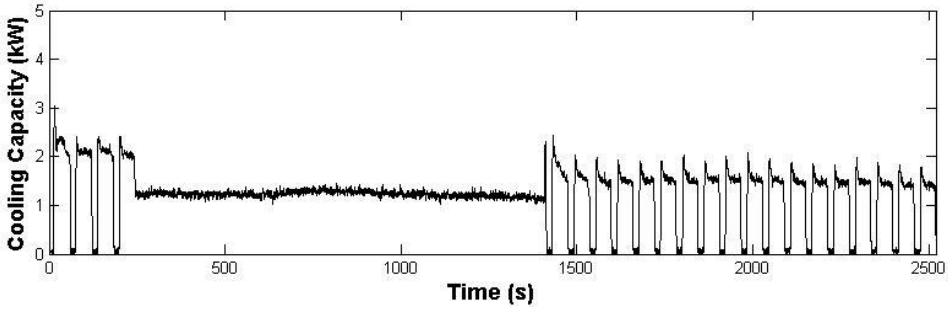

Figure 89: External fluid flow rate change test – cooling capacity using TEV on water chiller system

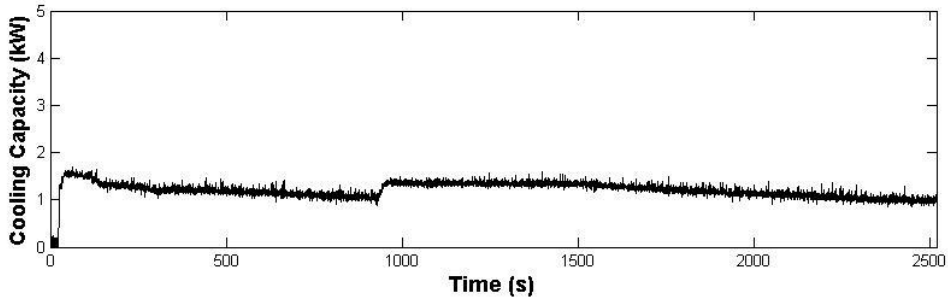

Figure 90: External fluid flow rate change test – cooling capacity using EEV on water chiller system

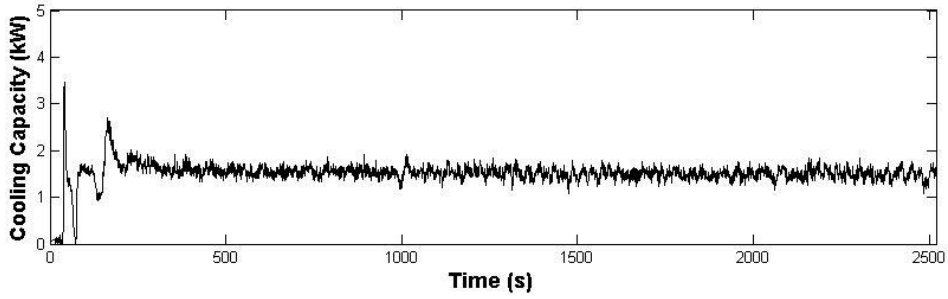

Figure 91: External fluid flow rate change test – cooling capacity using PPEV on water chiller system

The cooling capacity using the PPEV is more stable and fluctuates less than that using the EEV. Due to its better performance, the PPEV is able to achieve more cooling using less compressor work as shown by the COP values in Table 13. The experimental data was broken down into five sections of 180 seconds as shown in Figure 92, Figure 93 and Figure 94. The cooling capacity, electrical energy input and COP at each of these sections were evaluated independently in order to provide a fair and accurate evaluation of each valve's performance.

As can be seen in Table 13., in all five sections, the system produces the most cooling when it is equipped with the PPEV. It is also when it is equipped with the most cooling that it consumes the most energy. However ratio for the amount of cooling produced to the amount of energy consumed is evaluated, the PPEV comes ahead of the EEV and the TEV. For the various sections considered when the compressor was running at first stage, the PPEV's COP is about 12% higher than that of the EEV about 20% higher than that of the TEV. However, when the compressor speed is increased to second stage, the PPEV's COP is about 16% higher than that of the EEV while it is about 25% higher than the COP of the TEV.

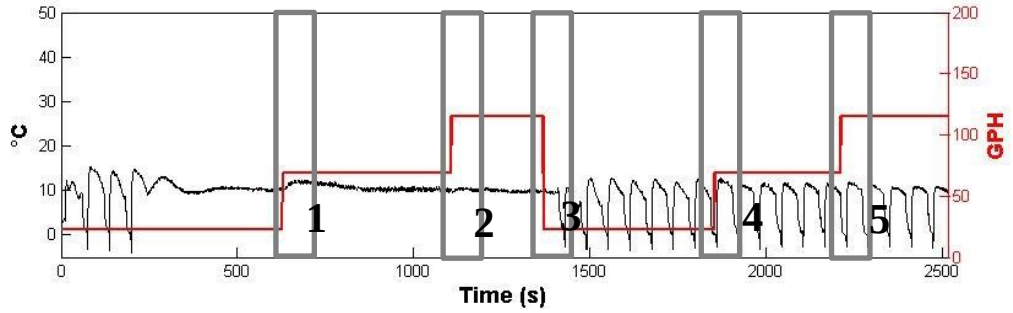

Figure 92: External fluid flow rate change test - section breakdown of EEV data for COP analysis on water chiller system

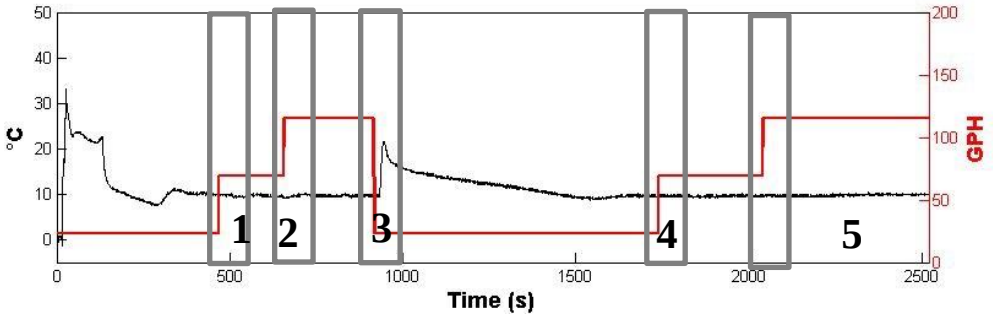

Figure 93: External fluid flow rate change test - section breakdown of EEV data for COP analysis on water chiller system

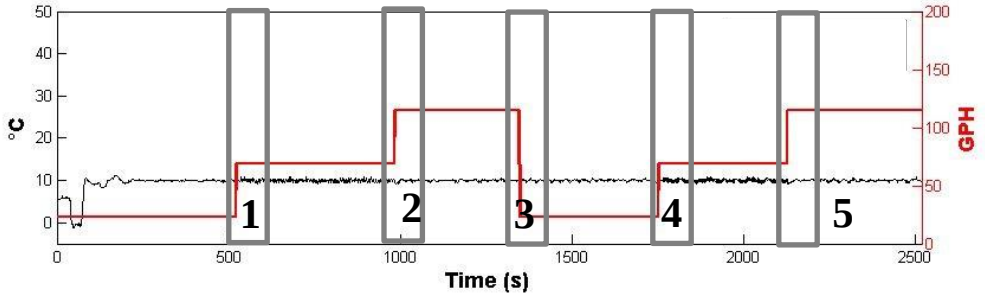

Figure 94: External fluid flow rate change test - section breakdown of PPEV data for COP analysis on water chiller system

Table 13: COP values for external fluid flow rate change test on water chiller system

Section		PPEV	EEV	TEV
1	**CC (kW)**	1.47	1.08	0.99
	Work (kW)	0.46	0.38	0.37
	COP	3.20	2.84	2.66
	COP Improvement (%)		**12**	**20.3**
2	**CC (kW)**	1.45	1.10	1.04
	Work (kW)	0.44	0.39	0.39
	COP	3.29	2.82	2.67
	COP Improvement (%)		**16.7**	**23.2**
3	**CC (kW)**	1.59	1.31	1.10
	Work (kW)	0.48	0.44	0.38
	COP	3.31	2.97	2.89
	COP Improvement (%)		**11.5**	**14.5**
4	**CC (kW)**	1.50	1.29	1.15
	Work (kW)	0.47	0.47	0.45
	COP	3.19	2.74	2.55
	COP Improvement (%)		**16.4**	**25.1**
5	**CC (kW)**	1.53	1.27	1.13
	Work (kW)	0.48	0.47	0.44
	COP	3.19	2.70	2.57
	COP Improvement (%)		**18.2**	**24.1**
Time (s)		180	180	180

Direct Exchange Split Heat Pump System

Figure 95, Figure 96 and Figure 97 illustrate how the system's superheat responds to changes in the flow rate of the external fluid (air) across the evaporator when it is equipped with a TEV, EEV and PPEV respectively.

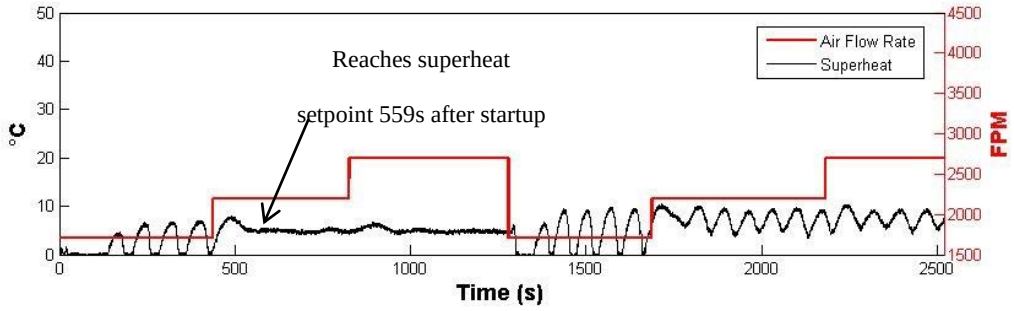

Figure 95: External fluid flow rate change test Test – superheat vs superheat setpoint using TEV on heat pump system

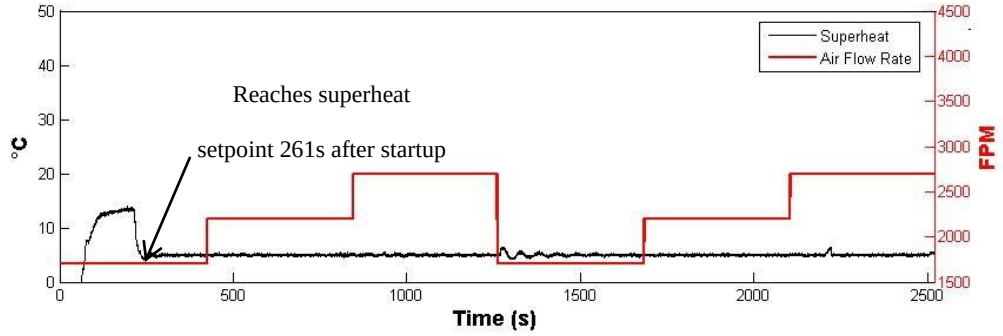

Figure 96: External fluid flow rate change test – superheat vs superheat setpoint using EEV on heat pump system

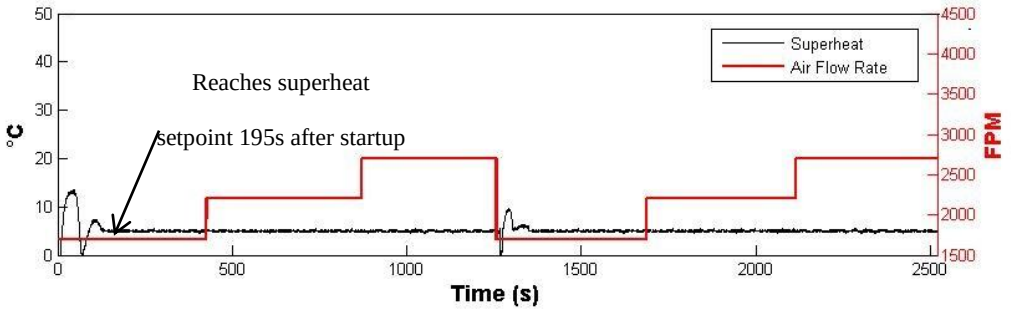

Figure 97: External fluid flow rate change test – superheat vs superheat setpoint using PPEV on heat pump system

As shown in these figures, from startup, the PPEV reaches the superheat setpoint 195 seconds after startup while the EEV reaches the superheat setpoint 261 seconds after start-up and the TEV reaches the superheat setpoint 559 seconds after startup. Similar to the results obtained from the test on the water chiller system, as the compressor speed is increased from first stage to second stage, the TEV starts hunting. It is never able to regain stable superheat control. The EEV is able to deal better with the change in compressor speed and is not very disturbed. It is able to maintain stable superheat control throughout these changes in operational conditions. Meanwhile the PPEV experiences a little disruption in superheat but is able to quickly adjust. This is due to the quick action of the PPEV's PDAVs which enable to quick adapt to the change in compressor speed. These observations are as shown in Figure 98, Figure 99 and Figure 100. Mass flow rate, evaporator pressure and condenser pressure are also observed for this test.

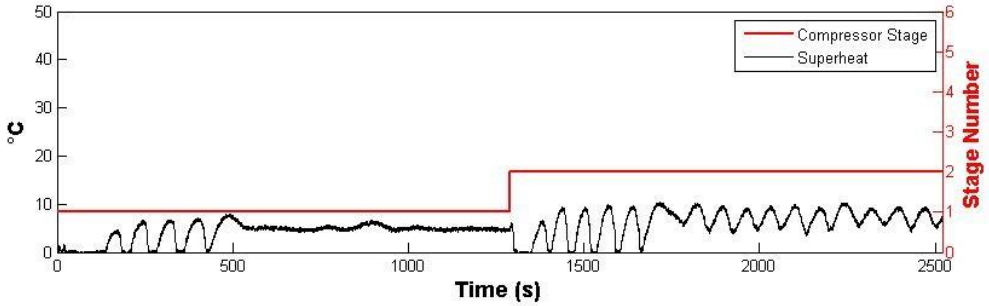

Figure 98: External fluid flow rate change test – superheat vs compressor stage using TEV on heat pump system

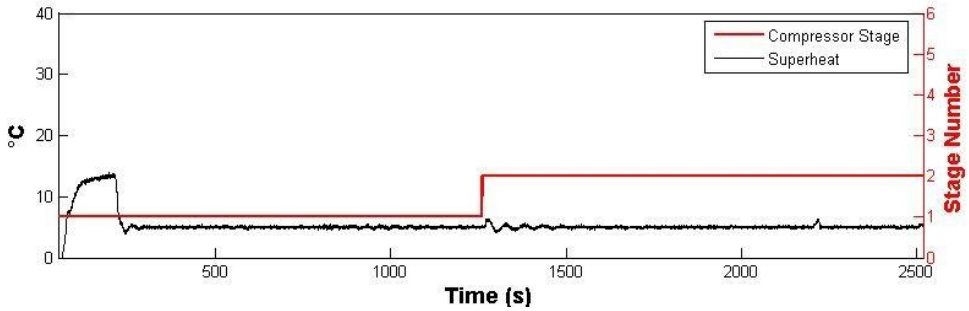

Figure 99: External fluid flow rate change test – superheat vs compressor stage using EEV on heat pump system

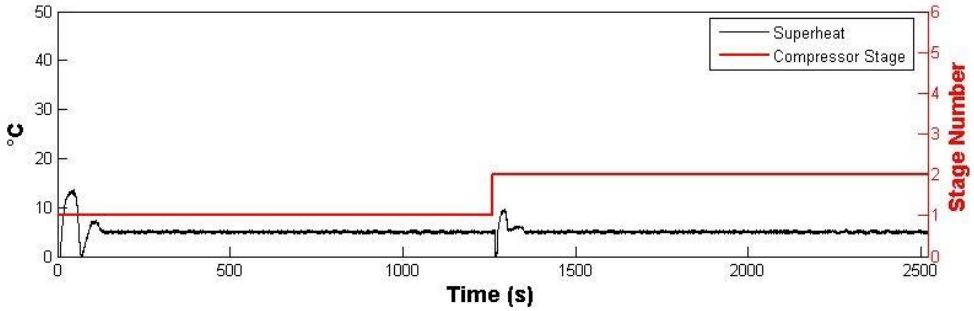

Figure 100: External fluid flow rate change test – superheat vs compressor stage using PPEV on heat pump system

Figure 101, Figure 102 and Figure 103 illustrate how the system's mass flow rate changes as the external fluid flow rate and compressor speed

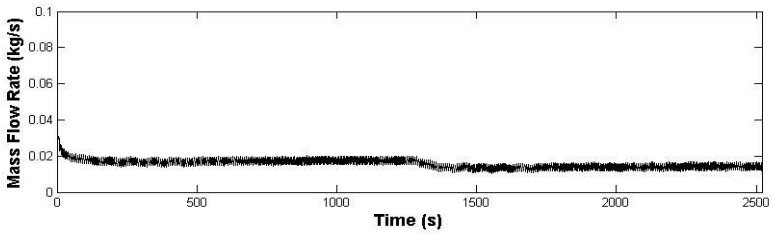

Figure 101: External fluid flow rate change test – refrigerant mass flow rate using TEV on heat pump system

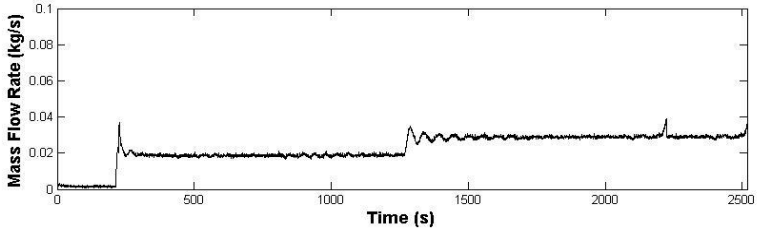

Figure 102: External fluid flow rate change test – refrigerant mass flow rate using EEV on heat pump system

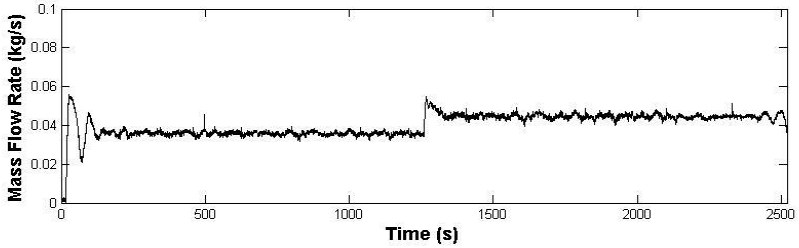

Figure 103: External fluid flow rate change test – refrigerant mass flow rate using PPEV on heat pump system

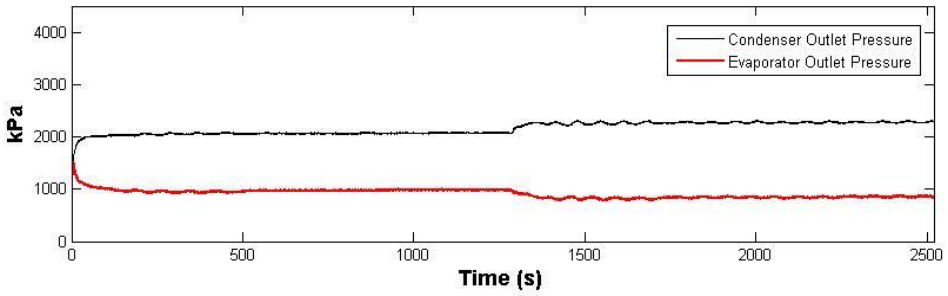

Figure 104: External fluid flow rate change test – condenser and evaporator outlet pressures using TEV on heat pump system

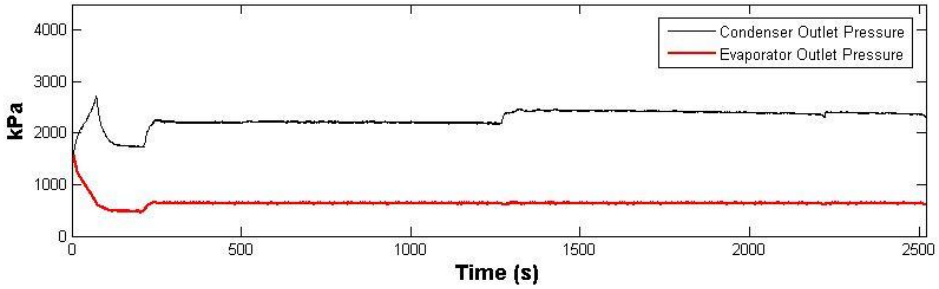

Figure 105: External fluid flow rate change test – condenser and evaporator outlet pressures using EEV on heat pump system

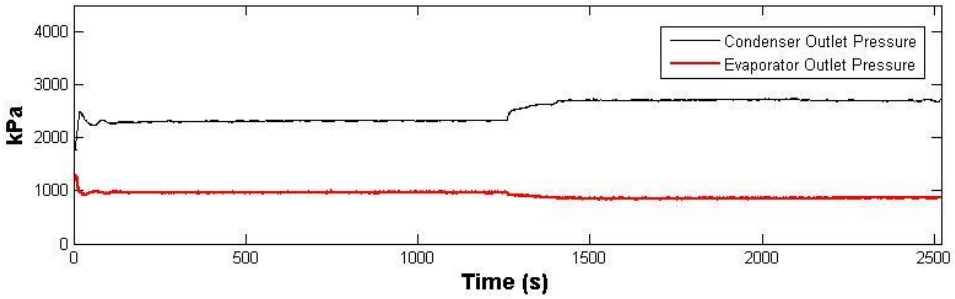

Figure 106: External fluid flow rate change test – condenser and evaporator outlet pressures using PPEV on heat pump system

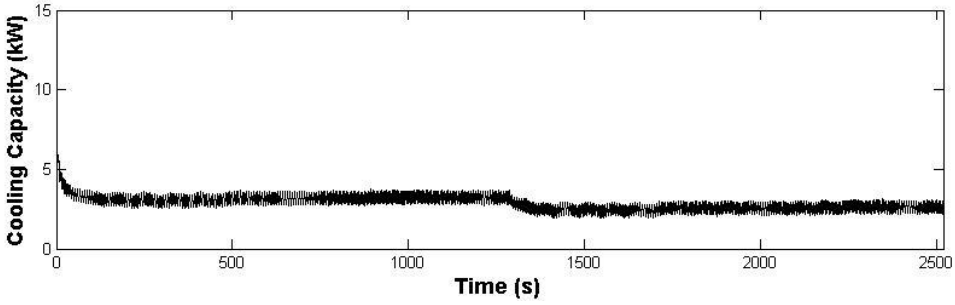

Figure 107: External fluid flow rate change test – cooling capacity using TEV on heat pump system

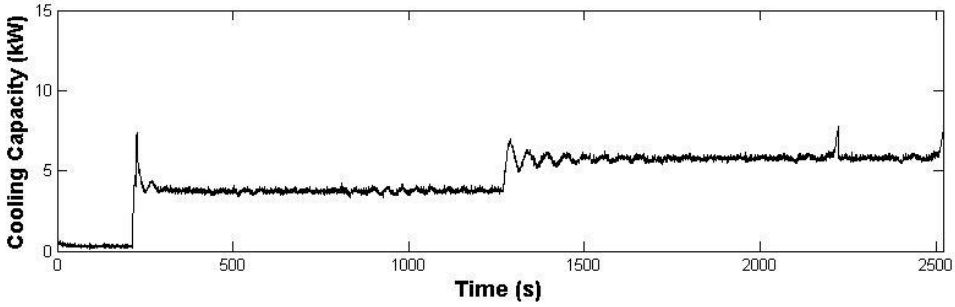

Figure 108: External fluid flow rate change test – cooling capacity using EEV on heat pump system

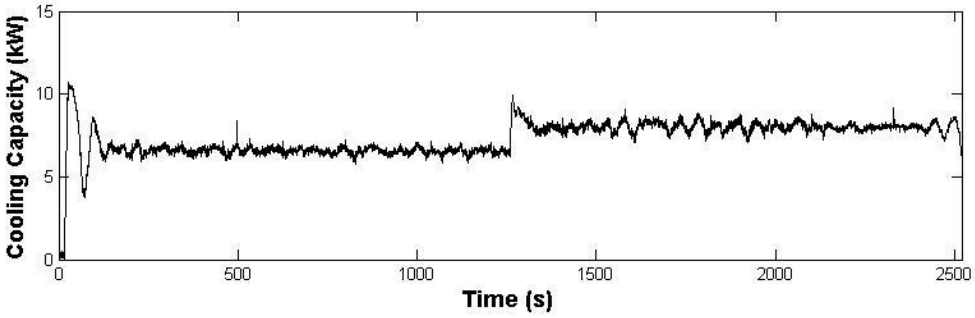

Figure 109: External fluid flow rate change test – cooling capacity using PPEV on heat pump system

Figure 104, Figure 105 and Figure 106 show how the condenser outlet pressure and the evaporator outlet pressure react to the aforementioned changes. Similarly, Figure 107, Figure 108 and Figure 109 illustrate the cooling capacity results from the superheat change test on the water chiller system. The cooling capacity using the PPEV is more stable and fluctuates less than that using the EEV. Due to its better performance, the PPEV is able to achieve more cooling using less compressor work as shown by the COP values in Table 14. The experimental data was broken down into five sections of 180 seconds as shown in Figure 110, Figure 111 and Figure 112. The cooling capacity, electrical energy input and COP at each of these sections were evaluated independently in order to provide a fair and accurate evaluation of each valve's performance.

As can be seen in Table 14, in all five sections, the system produces the most cooling when it is equipped with the PPEV. It is also when it is equipped with the most cooling that it consumes the most energy. However ratio for the amount of cooling produced to the amount of energy consumed is evaluated, the PPEV comes ahead of the EEV and the TEV. For the various sections considered when the compressor was running at first stage, the PPEV's COP is about 8% higher than that of the EEV about 10% higher than that of the TEV. However, when the compressor speed is increased to second stage, the PPEV's COP is only slightly higher than that of the EEV while it is about 30% higher than the COP of the TEV.

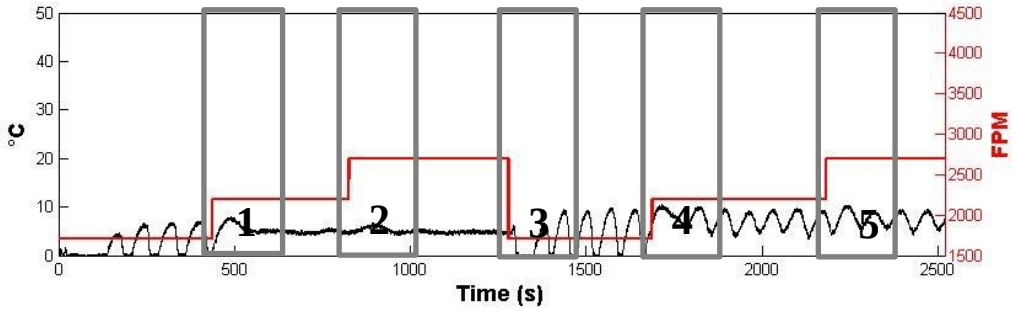

Figure 110: External fluid flow rate change test - section breakdown of EEV data for COP analysis on heat pump system

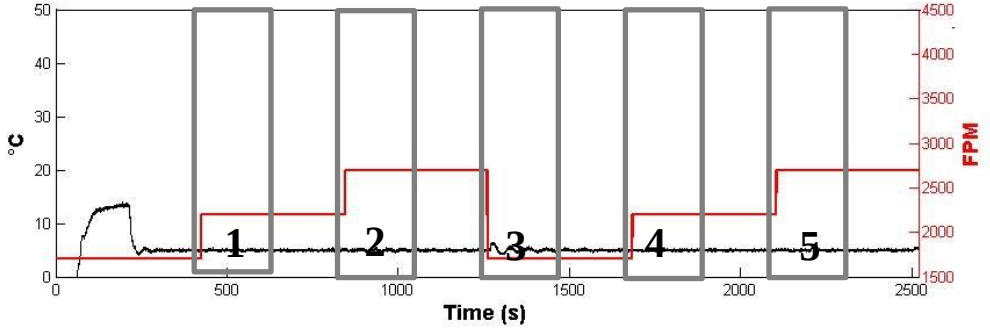

Figure 111: External fluid flow rate change test - section breakdown of EEV data for COP analysis on heat pump system

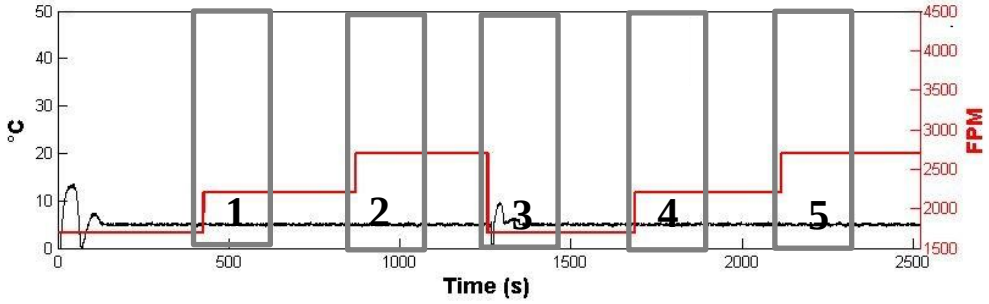

Figure 112: External fluid flow rate change test - section breakdown of PPEV data for COP analysis on heat pump system

Table 14: COP values for external fluid flow rate change test on heat pump system

Section		PPEV	EEV	TEV
1	**CC (kW)**	6.75	3.71	3.39
	Power (kW)	4.02	2.39	2.29
	COP	1.68	1.55	1.48
	COP Improvement (%)		**8.4**	**13.5**
2	**CC (kW)**	6.64	3.73	3.47
	Power (kW)	3.95	2.39	2.24
	COP	1.68	1.56	1.55
	COP Improvement (%)		**7.7**	**8.3**
3	**CC (kW)**	6.57	5.61	2.81
	Power (kW)	3.96	3.42	2.15
	COP	1.66	1.60	1.31
	COP Improvement (%)		**3.8**	**26.7**
4	**CC (kW)**	6.54	5.74	2.78
	Power (kW)	3.96	3.63	2.42
	COP	1.65	1.58	1.24
	COP Improvement (%)		**4.4**	**33.0**
5	**CC (kW)**	7.99	5.90	2.82
	Power (kW)	4.81	3.66	2.22
	COP	1.66	1.61	1.27
	COP Improvement (%)		**3.1**	**30.7**
Time (s)		180	180	180

Integrated Design Tests

The superheat change test, startup tests and external fluid change test results that have been discussed are good indicators of the ability to the expansion valve to perform efficiently at varying conditions. As shown by the results obtained, the PPEV consistently outperforms the other valves. However it is important to note that the

pressure source used to operate the PPEV in these tests is a nitrogen tank. This nitrogen tank provided a constant, steady flow of nitrogen at 150psi that was used to operate the PPEV. Considering the fact that it would not be practical for the use of the PPEV to be dependent on the availability of a nitrogen tank, this project proposes a design whereby the PPEV would be an integral part of the VCC. The proposed design frees the PPEV of dependence on any external component for its operation. The schematic of the proposed integrated design is illustrated in Figure 113.

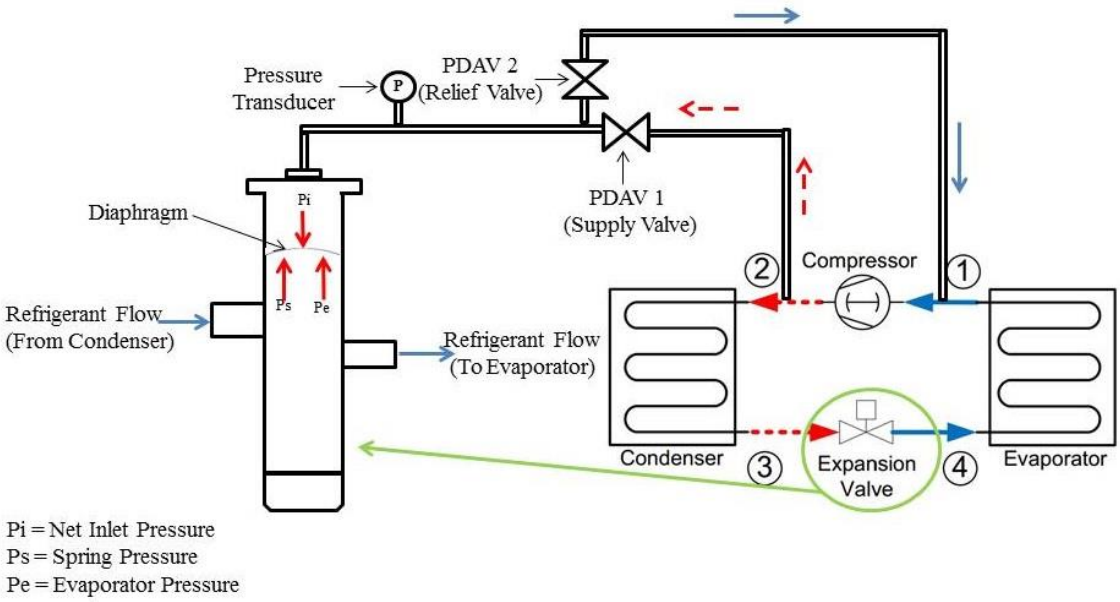

Figure 113: Schematic of proposed integrated design

The proposed design makes use of connections between the PDAVs and the compressor's inlet and outlet. Thus instead of a nitrogen tank, the supply pressure is

tapped directly from the outlet of the compressor and instead of venting the nitrogen which is surplus to requirements into the atmosphere, the extra refrigerant would be vented back into the compressor inlet.

One of the main concerns expressed with this proposed design is the ability of the compressor outlet to produce enough pressure to generate flow across the PPEV. Another concern was the ability to the system to provide enough stable pressure to enable the valve to operate efficiently. These tests are therefore designed to see if effectively at start up, there is enough pressure to generate flow across the PPEV and to see if the pressure supplied would be stable enough to ensure that the valve does not start hunting. They were carried out only on the direct exchange split heat pump system. The schematic shown in Figure 83 was implemented as shown in Figure 114 and Figure 115.

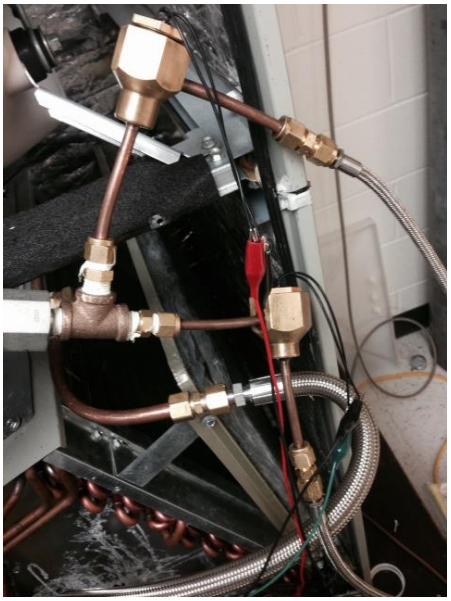

Figure 114: PDAV1 (supply) and PDAV2 (relief) connections

Figure 115: Compressor inlet and outlet connections

Superheat Change Test

After the connections were properly installed, the system was started. The supply valve of the PPEV was progressively closed while the relief valve was progressively opened. Figure 116, Figure 117, Figure 118 and Figure 119 illustrate the results obtained for superheat, mass flow rate, condenser outlet pressure, evaporator outlet pressure and cooling capacity after a 1080 seconds run.

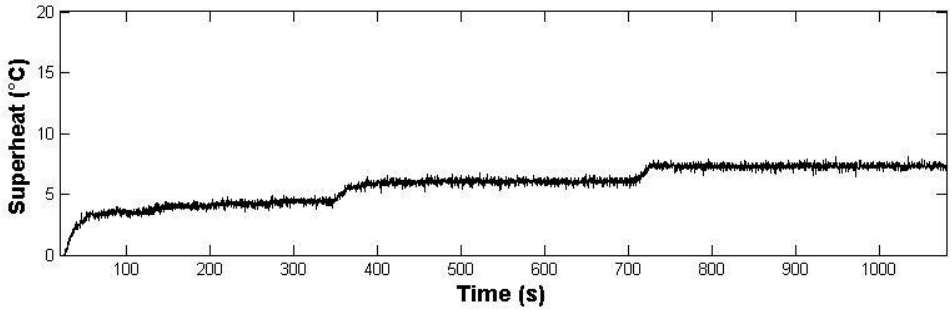

Figure 116: Superheat change test - superheat using integrated design

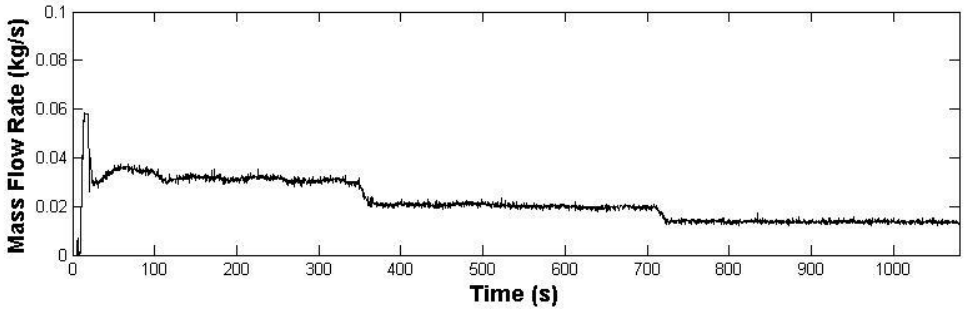

Figure 117: Superheat change test – mass flow rate using integrated design

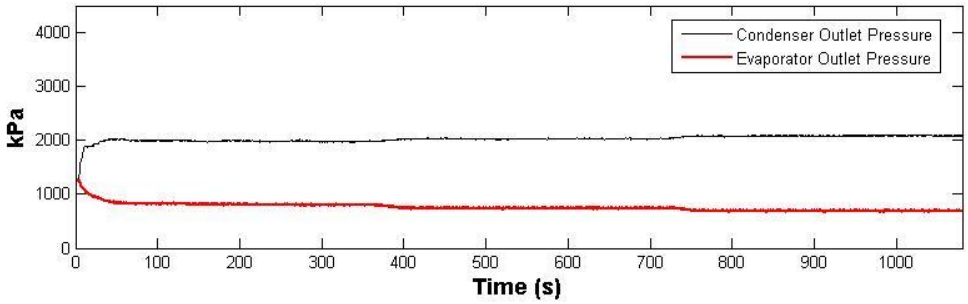

Figure 118: Superheat change test – condenser and evaporator outlet pressures using integrated design

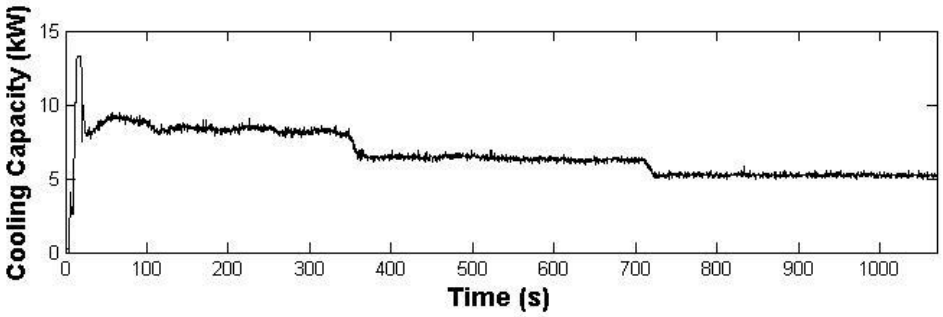

Figure 119: Superheat change test - cooling capacity using integrated design

As can be seen in these results, the compressor provides enough pressure to generate flow with relative ease. The first six minutes of the test were with the supply valve fully open and the relief valve fully closed. Both valves were then each half opened for 6 minutes and then the supply valve was closed while the relief valve was fully open. These results show that the flow and indeed the superheat can be controlled with this set up. The valve is also able to operable rather steadily. The PDAVs used in the PPEV tested here are designed to leak. That combined with the high condenser outlet pressure account for the residual flow of refrigerant even after the valve is closed. Furthermore, the PDAVs are microvalves and hence there is a limit to how much flow they can allow. Complete superheat control can be achieved by regulation the diaphragm and spring constants and by adjusting the openings and the leak rates of the PDAVs.

As with the other tests, this test was broken down into three sections and an analysis of the cooling capacity, electrical energy input and COP at each of these sections carried out. The section breakdown is as shown in Figure 120.

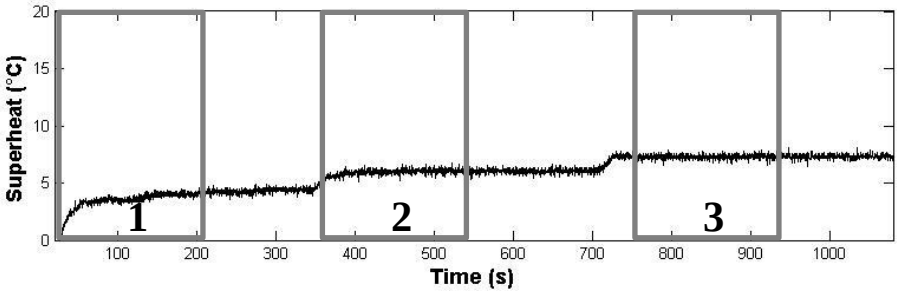

Figure 120: Superheat change test - section breakdown using integrated design for COP analysis

Table 15 shows how the cooling capacity, electrical energy input and Coefficient Of Performance vary for each of the three test sections considered for this analysis. As can be seen in this table, the system is able to achieve levels of cooling and COP which are on par with those obtained when a similar test was carried out with the PPEV being operated using pressure from a nitrogen tank. This again confirms the feasibility of the integrated design.

Table 15: COP values for superheat change when using integrated design

Section		**PPEV**
1	**CC (kW)**	8.92
	Power (kW)	5.31
	COP	**1.68**
2	**CC (kW)**	6.37
	Power (kW)	3.74
	COP	**1.70**
3	**CC (kW)**	5.19
	Power (kW)	2.93
	COP	**1.77**
Time (s)		180

Startup Test

The next test to be carried out on the integrated PPEV was a startup test. Figure 121, Figure 122, Figure 123 and Figure 124 illustrate the results obtained for superheat, refrigerant mass flow rate, condenser outlet pressure, evaporator outlet pressure and cooling capacity for this test. The compressor was turned on for five minutes and then shut down for one minute. This makes up one startup cycle and three startup cycles were performed for a total test duration of 1080 seconds.

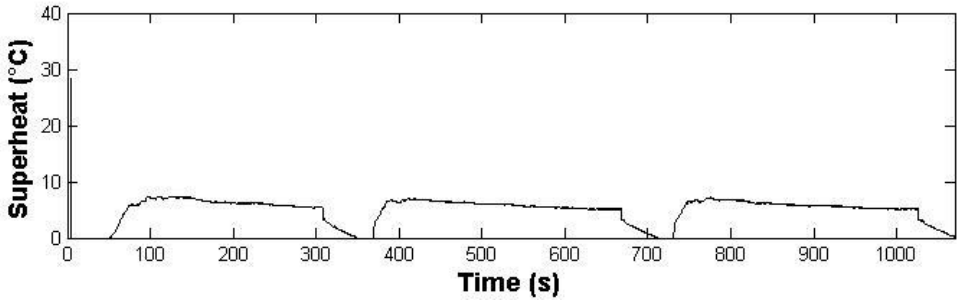

Figure 121: Startup test - superheat using integrated design

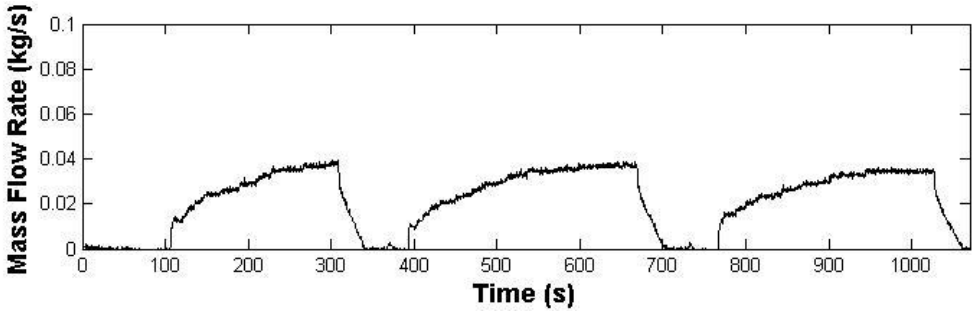

Figure 122: Startup test - mass flow rate using integrated design

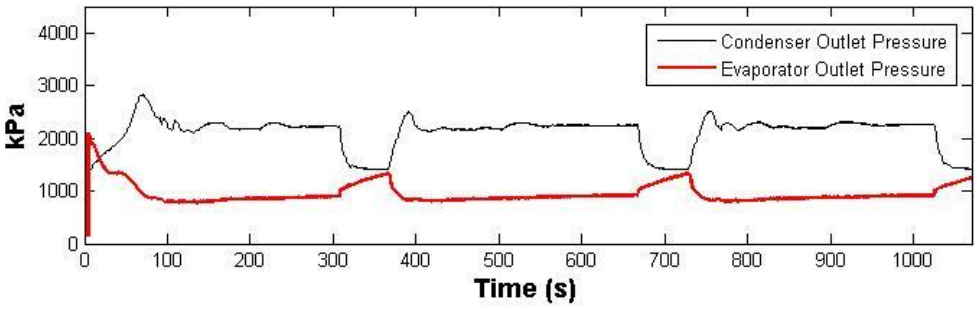

Figure 123: Startup test - condenser and evaporator outlet pressures using integrated design

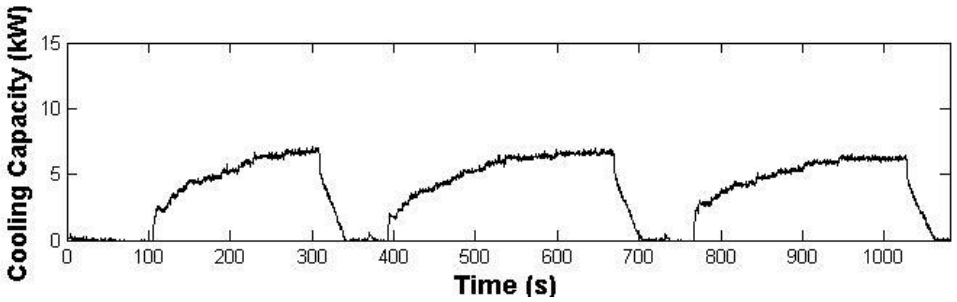

Figure 124: Startup test - cooling capacity using integrated design

As can be seen in these results, again the compressor provides enough pressure to generate flow and make the system operational at every attempt. These results show that the flow and indeed the superheat can be controlled with the integrated set up. The valve is also able to operable steadily. The PDAVs used in the PPEV tested here are also designed to leak. Complete superheat control and time to reach operating conditions from startup can be achieved by regulation the diaphragm and spring constants and by adjusting the leak rates of the PDAVs.

This test was broken down into three sections of 180 seconds each and an analysis of the cooling capacity, electrical energy input and COP at each of these sections carried out. The section breakdown is as shown in Figure 125.

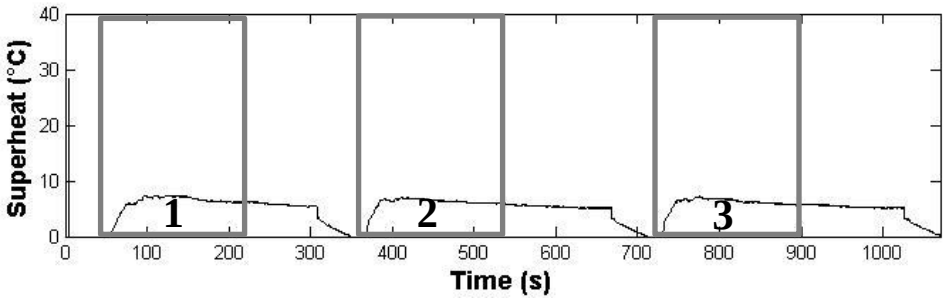

Figure 125: Startup test - section breakdown using integrated design for COP analysis

Table 16 shows how the cooling capacity, electrical energy input and COP vary for each of the three test sections considered for this analysis. Like with the superheat change test using the integrated design, this table shows that the system is able to achieve levels of cooling and COP which are not far off from those obtained when a similar test was carried out with the PPEV being operated by the nitrogen tank. Section one also indicates an unusually low COP, this is probably due to the fact that this experiment was carried out from a cold start and so the system was still adjusting as shown by the fact that the COP values obtained in sections 2 and 3 are much higher.

Table 16: COP values for startup test when using integrated design

Section		PPEV	EEV	TEV	Integrated
1	**CC (kW)**	5.81	4.82	2.50	3.92
	Power (kW)	3.74	3.47	1.94	3.08
	COP	1.55	1.39	1.28	1.27
	COP Improvement (%)		**11.5**	**21.1**	**22**
2	**CC (kW)**	5.56	4.78	2.58	4.63
	Power (kW)	3.45	3.39	1.97	2.79
	COP	1.61	1.41	1.31	1.68
	COP Improvement (%)		**14.1**	**22.9**	**-4.1**
3	**CC (kW)**	5.54	4.77	2.56	4.17
	Power (kW)	3.46	3.43	1.97	2.62
	COP	1.60	1.39	1.30	1.59
	COP Improvement (%)		**15.1**	**23.1**	**0.6**
Time (s)		300	300	300	300

External Fluid Flow Rate Change Test

For the scope of this thesis project, the final test to be carried out on the integrated PPEV was an external fluid flow rate change test. The external fluid on this system is air. This test was carried out in two phases. The first phase was carried out a first stage compressor speed and the second phase was carried out at second stage compressor speed. After startup, the system reaches a superheat of 5 °C in 45 seconds. The airflow rate at startup was set at 1,700 fpm, after 100 seconds it was increased to 2,200 fpm and after another 100 seconds it was further increased 2,700 fpm. This concluded the first phase of this test. The second stage was then immediately initiated by increasing the compressor speed from first stage to second stage. Once again the airflow

rate was progressively increased from 1,700 fpm to 2,200 fpm and then 2,700 fpm. Again, the time between the airflow rates increments is 100 seconds. Figure 126, Figure 127, Figure 128 and Figure 129 illustrate the results obtained for superheat, mass flow rate, condenser outlet pressure, evaporator outlet pressure and cooling capacity for the external fluid low rate change test.

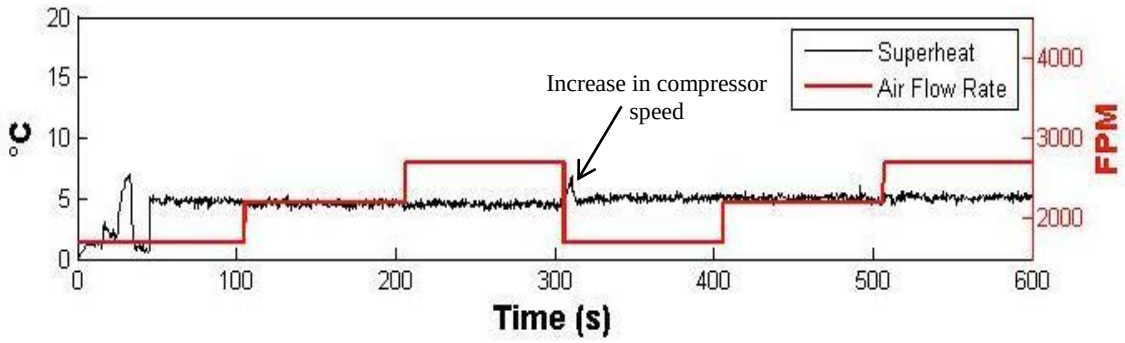

Figure 126: External fluid flow rate change test - superheat using integrated design

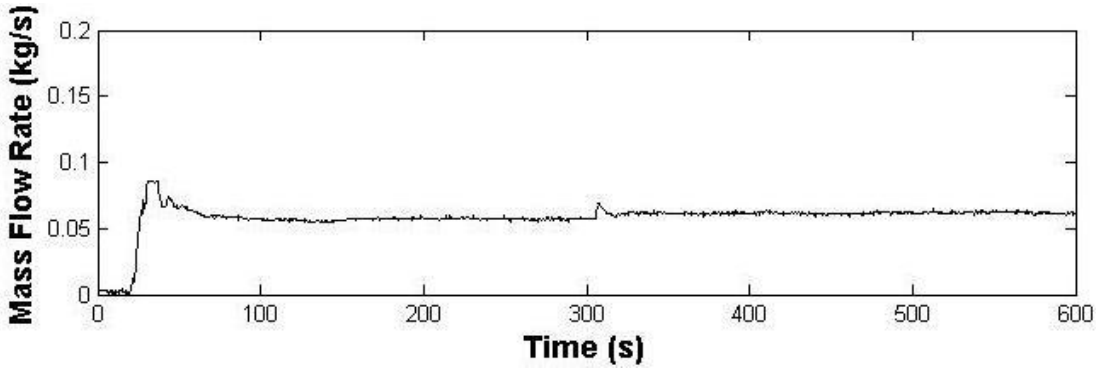

Figure 127: External fluid flow rate change test - mass flow rate using integrated design

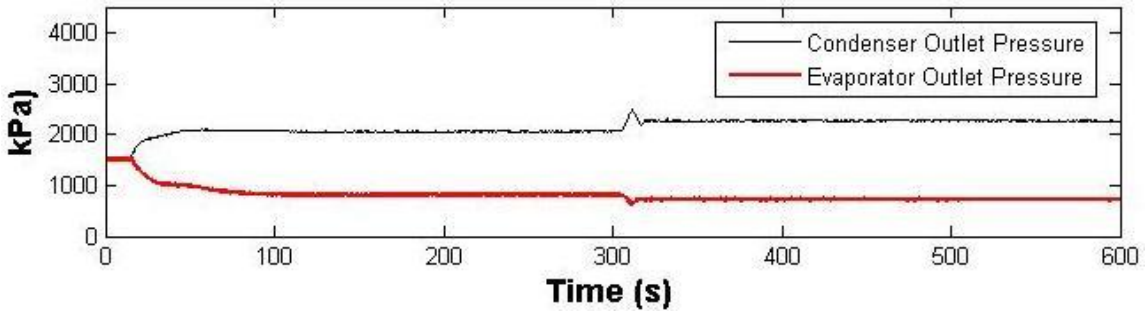

Figure 128: External fluid flow rate change test - condenser and evaporator outlet pressures using integrated design

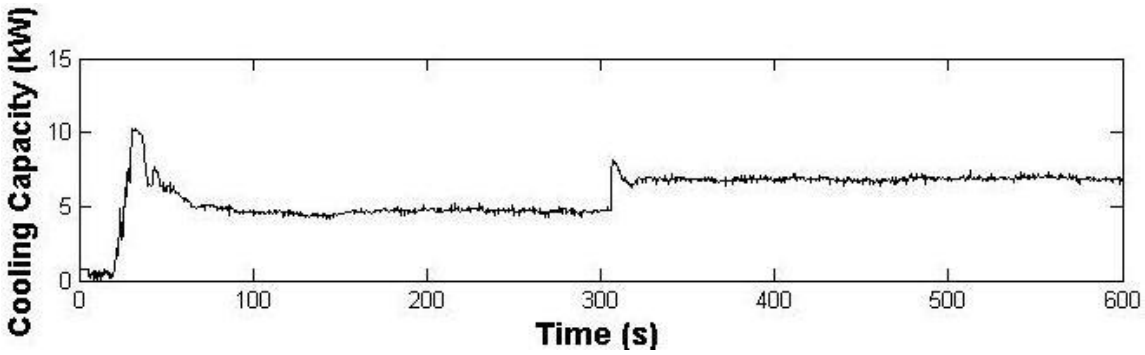

Figure 129: External fluid flow rate change test - cooling capacity using integrated design

As shown in the figures, the system's superheat reaches operating conditions 45 seconds after startup. Through the quick actions of its PDAVs, the PPEV is able to maintain operating conditions and avoid disruption even as the airflow rate is increased. At the second phase of the test, when the compressor speed is increased, the superheat increase and condenser outlet pressure increase as well but unlike was the case with the EEV and the TEV; the PPEV does not start hunting. It is able to maintain operational

conditions. Like the other two tests performed with this design, these results confirm the compressor's ability to generate flow and the PPEV's ability to operate normally in an integrated design. It also proves that the superheat can be controlled with this set up.

Furthermore, the test was broken down into five sections of 90 seconds each and an analysis of the cooling capacity, electrical energy input and COP at each of these sections carried out. The section breakdown is as shown in Figure 130.

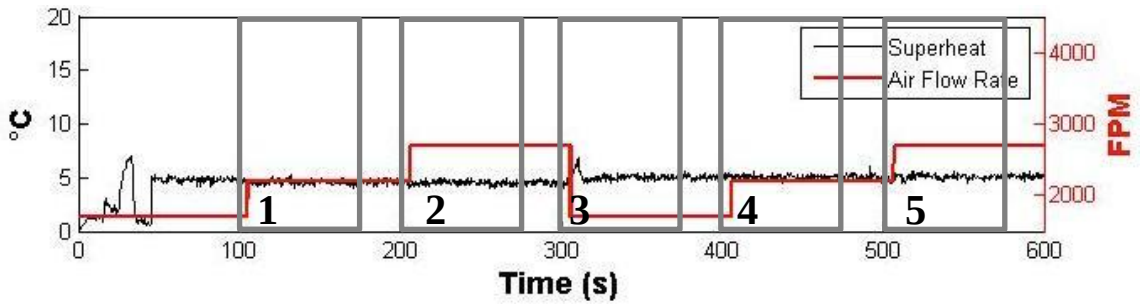

Figure 130: External fluid flow rate change test - section breakdown using integrated design for COP analysis

Table 17 shows how the cooling capacity, electrical energy input and COP vary for each of the five test sections considered for this analysis. Like with the other two tests using the integrated design which have been discussed, this table shows that the system is able to achieve levels of cooling and COP which seem reasonable when compared to the results obtained with the PPEV connected to the nitrogen tank during operation on the residential heat pump system. Thus all three tests indicate that the PPEV can operate well using the suggested integrated design.

Table 17: COP values for external fluid flow rate change using integrated design

Section		PPEV	EEV	TEV	Integrated
1	CC (kW)	6.75	3.71	3.39	4.41
	Power (kW)	4.02	2.39	2.29	2.69
	COP	1.68	1.55	1.48	1.64
	COP Improvement (%)		**8.4**	**13.5**	**2.4**
2	CC (kW)	6.64	3.73	3.47	4.88
	Power (kW)	3.95	2.39	2.24	2.91
	COP	1.68	1.56	1.55	1.68
	COP Improvement (%)		**7.7**	**8.3**	**0.0**
3	CC (kW)	6.57	5.61	2.81	6.94
	Power (kW)	3.96	3.42	2.15	4.31
	COP	1.66	1.60	1.31	1.61
	COP Improvement (%)		**3.8**	**26.7**	**3.1**
4	CC (kW)	6.54	5.74	2.78	6.73
	Power (kW)	3.96	3.63	2.42	4.08
	COP	1.65	1.58	1.24	1.65
	COP Improvement (%)		**4.4**	**33.0**	**0.0**
5	CC (kW)	7.99	5.90	2.82	6.81
	Power (kW)	4.81	3.66	2.22	4.19
	COP	1.66	1.61	1.27	1.63
	COP Improvement (%)		**3.1**	**30.7**	**1.8**
Time (s)		180	180	180	180

Moreover, with help from Erik Rodriguez at the Texas A&M Thermofluids Controls Laboratory, a dynamic model of the heat pump system was constructed in Simulink to test the effects of the PPEV diaphragm pressure and spring constant on the valve's ability to control superheat when using the compressor outlet pressure as the diaphragm pressure source. This model was created using the PPEV model derived in

Chapter IV of this thesis. The remaining model components, i.e. compressor, evaporator, and condenser, used are from the Texas A&M Thermofluids Controls Laboratory Modeling Library. These models have previously been validated against experimental data as both individual components and system level integrated components [26]. A schematic of the Simulink model is illustrated in Figure 131.

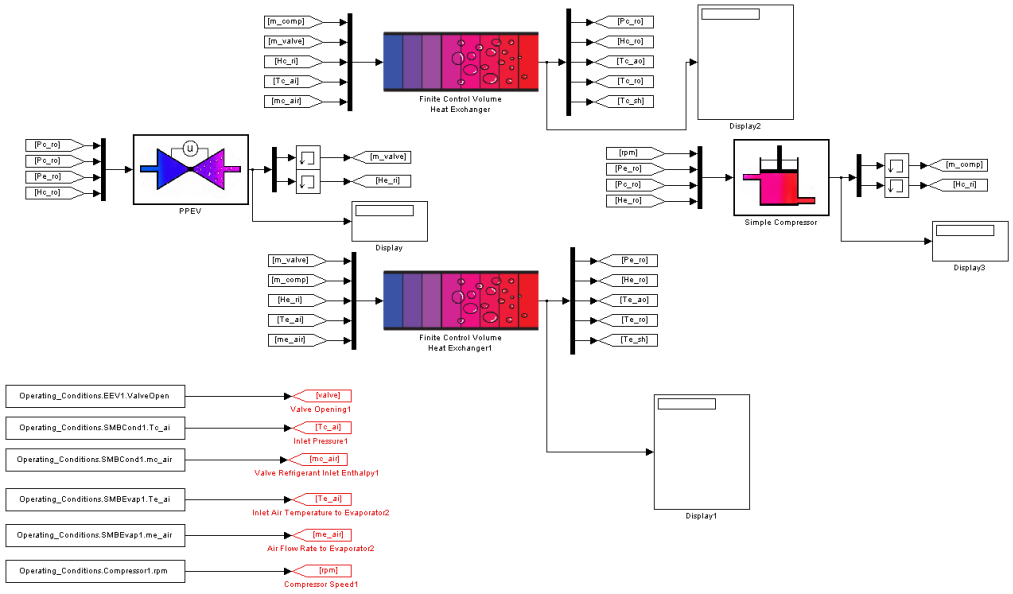

Figure 131: Schematic of complete model

After calibrating this model to the heat pump system's physical parameters, two sets of simulations were run. The first set of simulations tested the effects of the PPEV spring constant by varying this parameter in the individual PPEV model component.

This test was conducted with 90% of the compressor outlet pressure applied to the PPEV diaphragm (i.e. 10% pressure vented through relief valve). The second set of simulations were run to test the effects of decreasing the PPEV supplied diaphragm pressure by increasing the amount of refrigerant vented by the pressure relief valve. Results for both of these simulation sets are shown in respectively.

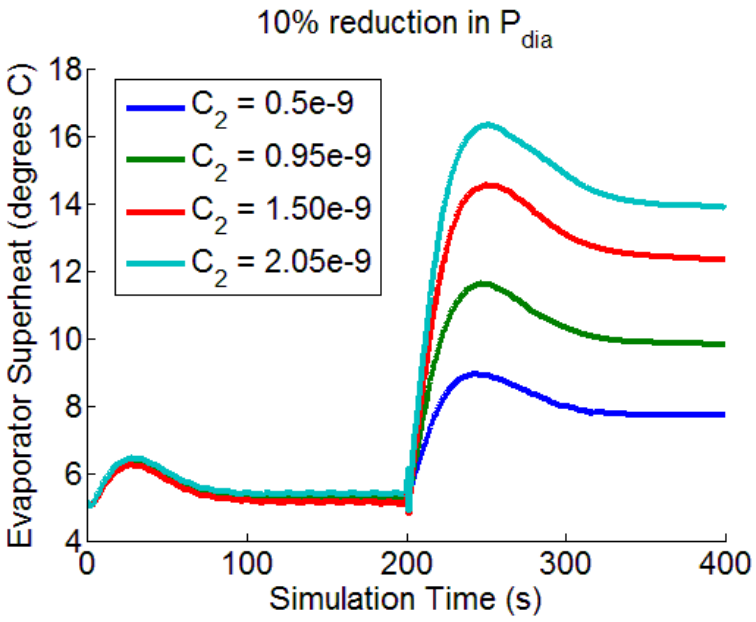

Figure 132: Effects of variation of diaphragm pressure

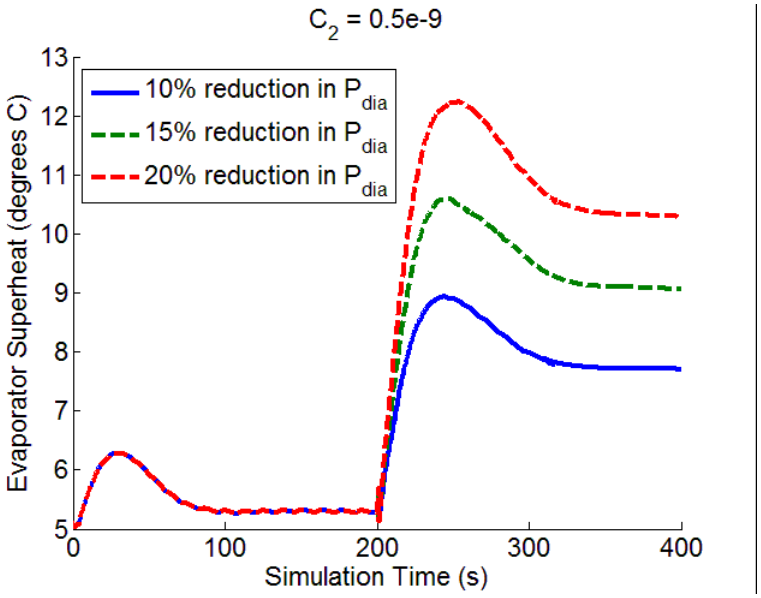

Figure 133: Effects of variation of valve parameter

Results from Figure 132 show that a higher PPEV diaphragm stiffness requires a much larger drop in supplied diaphragm pressure to induce the a significant change in evaporator superheat. This suggests that the PPEV was unable to regulate superheat in the experimental system because the maximum amount of refrigerant vented through the relief valve is not enough to cause sufficient movement in the PPEV diaphragm. This is a physical limitation of the micro-valves; therefore adjusting the diaphragm spring stiffness and/or area would most likely be the preferred approach to improving the valve's superheat control capabilities. Results from Figure 133 show that increasing the valve parameter, C_2, greatly increases the valve's ability to affect evaporator superheat for the same change in diaphragm pressure. This change can be implemented by decreasing the PPEV diaphragm stiffness or increasing the total diaphragm area.

CHAPTER VI

CONCLUSION AND FUTURE WORK

The research presented in this thesis makes a contribution towards the collective objective of improving the energy efficiency of vapor compression systems. This contribution is done through the proposal of a hybrid-type expansion device called a Prototype Pilot Expansion Valve (PPEV). The PPEV presented in this thesis is a combination of a conventional Thermal Expansion Valve (TEV) and two Pilot Direct Acting Valves (PDAVs). It is simple to operate, efficient, robust, responds very quickly to changes in operating conditions and is not a victim of hunting unlike that expansion valves used in most VCC systems.

This work presents the design specifications of the PPEV, presents both the simulation and physical models of the PPEV, and discusses the various performance tests which were determined and carried out to evaluate the performance of the PPEV and compare it to that of a conventional Thermal Expansion Valve (TEV) and a conventional Electronic Expansion Valve (EEV). These tests involve a superheat change test to assess the level of superheat control that each of the valves provides a startup test to determine how long the system takes to reach operating conditions when equipped with each of the valves and an external flow rate change test to evaluate the system's ability to respond to changes in operating conditions.

These tests were carried out on two experimental systems; A modulated water chiller operating using R-134a refrigerant and a residential direct exchange split heat

pump system operating using R-410a. The results of these tests indicate that the PPEV outperforms the EEV and TEV in each of the tests. It is able to provide better superheat control, it reaches operating conditions faster from startup and it deals with changes in operating conditions much better than the EEV and the TEV.

This thesis also proposes an integrated design for the PPEV and goes ahead to address the concern that the system pressure at startup might not be enough to generate flow. The PPEV was disconnected from any external pressure source and connected entirely to the system. A startup test was then performed which indicated that there is enough pressure to generate flow across the valve thus paving the way for a compact and efficient design to be implemented.

Future research and tests involving the PPEV may include testing it on other VCC systems such as commercial refrigeration systems and testing it on systems which operate on refrigerants other than R-134A and R-410A. The work presented in this thesis is intended to serve mainly as a proof-of-concept and so future work may also involve improving the PPEV design by making it more compact, robust and efficient. This would serve the goal of ultimately making this valve commercially viable so that it can help improve the energy efficiency of the many HVACR systems across the world.

REFERENCES

[1] Energy Information Administration, "International Energy Outlook 2013," Report # DOE/EIA-0484(2013), 2013. Available at: http://www.eia.doe.gov/oiaf/ieo/world.html/.

[2] M.S. Elliott, B. Shenoy and B.P.Rasmussen, "A control architecture solution to superheat nonlinearity," *Proceedings of the American Control Conference*, pp. 5898-5903, July 2010.

[3] Lennox Industries Inc, "Thermal Expansion Valves," Available at: http://www.centralcityair.com/news.html?n_id=147.

[4] P.M.T. Broersen and M.F.G. van der Jagt, "Hunting of evaporators controlled by a thermostatic expansion valve," *Journal of Dynamic Systems, Measurement, and Control*, vol. 102, no. 2, pp. 130-135, June 1980.

[5] W.D. Gruhle and R. Isermann. "Modeling and control of a refrigerant evaporator," *Journal of Dynamic Systems, Measurement, and Control*, vol. 107, no. 4, pp. 235-240, December 1985.

[6] Parker Hannifin Corporation, "12 Solutions for Fixing Common TEV Problems," Form # 10-143, 2012. Available at: http://sporlanonline.com/literature/10/10-143.pdf.

[7] J. Kuhnl-Kinel, "The history of ventilation and air conditioning: is CERN up to date with the latest technological developments?," *Proceedings of the Third ST*

Workshop-CERN, February 2000. Available at: http://st-div.web.cern.ch/st-div/workshop/ST2000WS/Proceedings/techno2/jkk.pdf.

[8] J. Varrasi, "Global Cooling: The History of Air Conditioning." *Proceedings of the American Society of Mechanical Engineers*, June 2011. Available at: https://www.asme.org/engineering-topics/articles/technology-and-society/global-cooling-the-history-of-air-conditioning.

[9] U.S. Energy Information Administration. "Air conditioning in nearly 100 million U.S. homes". RECS 2009, 2011. Available at: http://www.eia.gov/consumption/residential/reports/2009/air-conditioning.cfm.

[10] K. James and R. James, "Transient analysis of thermostatic expansion valves for refrigeration system evaporators using mathematical models," *Transactions of the Institute of Measurements and Control*, vol. 9, pp. 198-205, 1987.

[11] G.A. Ibrahim, "Effect of sudden changes in evaporator external parameters on a refrigeration system with an evaporator controlled by a thermostatic expansion valve," *International Journal of Refrigeration*, vol. 24, pp. 566-576, 2001.

[12] A. Outtagarts, P. Haberschill, and M. Lallemand, "The transient response of an evaporator fed through an electronic expansion valve," *International Journal of Refrigeration*, vol. 25, pp. 793-807, 1997.

[13] R. Lazzarin, D. Nardotto and M. Noro, "Electronic Expansion Valves Vs. Thermal Expansion Valves," *ASHRAE Journal*, vol. 51, no. 2, pp. 34-38, February 2009.

[14] J. Holloway, "Stepper motor vs. pulse width modulation," *RSES Journal*, no. 13, pp. 10-13, November 2012.

[15] J. Kim, J.E. Braun and E.A. Groll, "Analysis of Refrigerant Flow Distribution in Evaporators," *Proceedings of the International Refrigeration and Air Conditioning Conference*, July 2008. Available at: http://docs.lib.purdue.edu/cgi/viewcontent.cgi?article=1965&context=iracc.

[16] M.S.Elliott, B.P.Rasmussen, Z. Walton and B. Bolding, "Superheat control: A hybrid approach", *HVAC&R Research*, vol. 15, no. 6, pp. 1021-1043, 2009.

[17] T.A. Ameel, R.O. Warrington, R.S. Wegeng and M.K. Drost, "Miniaturization technologies applied to energy systems," *Energy Conversion and Management*, vol. 38, no. 10-13, pp. 969-982, July-September 1997.

[18] A.K. Henning, "Microfluidic MEMS," *Proceedings of the Aerospace Conference*, vol. 1, pp. 471-486, March 1998.

[19] MEMS Journal. "MEMS based valves for flow control." 2009. Available at: http://www.memsjournal.com/2009/04/mems-applications-for-flow-control-.html.

[20] DunAn Microstaq. "Modular silicon expansion valve and universal superheat controller/sensor hardware installation manual." Rev 1.3, 2014. Available at: http://dmq-us.com/wp-content/uploads/2014/09/HW-MSEVUSHX-080114-R1.3.pdf.

[21] Parker Hannifin Corporation, "Sporlan Electric Expansion Valves," Bulletin 100-20, 2008. Available at: http://sporlanonline.com/literature/10/10-143.pdf.

[22] DunAn Microstaq. “DunAn Microstaq’s Disruptive Technology.” Available: http://www.dmq-us.com/technology.

[23] Parker Hannifin Corporation. “Thermostatic Expansion Valves.” Bulletin 10-9, 2011. Available at: http://sporlanonline.com/literature/education/10-9.pdf.

[24] M.S. Elliott, “Decentralized model predictive control of a multiple evaporator HVAC system,” *Master’s Thesis*, Department of Mechanical Engineering, Texas A&M University, 2008.

[25] M.J. Moran, H.N. Shapiro, B.R. Munson, D.P. DeWitt, *Introduction to thermal systems engineering: Thermodynamics, fluid mechanics and heat transfer,* 1st ed. John Wiley & Sons: New York, NY, 1996.

[26] B.P. Rasmussen, “Dynamic modeling and advanced control of air conditioning and refrigeration systems”, *PhD Dissertation,* Department of Mechanical Engineering, University of Illinois at Urbana Champaign, 2005.

[27] B. Shenoy, “Single Stage Compressor”, *Thermofluids Control Laboratory*, Department of Mechanical Engineering, Texas A&M University, 2010.

[28] B. Shenoy and E. Rodriguez, “Finite Control Volume Heat Exchanger”, *Thermofluids Control Laboratory*, Department of Mechanical Engineering, Texas A&M University, 2011.

APPENDIX A

A complete derivation of the mathematical equation for the compressor modeling is given here. This work was done by Baskar Shenoy from the Texas A&M Thermofluids Control Lab [27]. The governing equations for the compressor model described in this section are essentially algebraic in nature. The model requires the refrigerant pressures at its inlet and outlet to calculate the refrigerant mass flow rate. This section will attempt to familiarize the user with the modeling assumptions, the equations governing the modeling of the components, the input and output parameters, the operating conditions and physical parameters and the required support files for the simulation of the single stage compressor models.

Modeling Assumptions

The compressor is assumed to be a positive displacement system, wherein the volumetric efficiency of the compressor is assumed to be a function of the ratio of the pressures at the exit and the inlet and the speed of the compressor. The compression process is assumed to be adiabatic with an isentropic efficiency.

Model Derivation for the Single Stage Compressor

The refrigerant mass flow rate is calculated from Equation (A1). Where, the refrigerant density ρ_k is calculated as a function of the inlet refrigerant pressure and

enthalpy [Equation (A2)]. The relationships between the inlet and outlet enthalpies are given by Equations (A3)-(A6).

$$\dot{m}_k = \omega_k V_k \rho_k \eta_{vol} \tag{A1}$$

$$\rho_k = \rho\left(P_{k,in}, h_{k,in}\right) \tag{A2}$$

$$\frac{h_{out,isentropic} - h_{in}}{h_{out} - h_{in}} = \eta_k \tag{A3}$$

$$h_{out,isentropic} = h(P_{out}, s_k) \tag{A4}$$

$$s_k = s(P_{in}, h_{in}) \tag{A5}$$

$$h_{out} = \frac{1}{\eta_k}[h_{out,isentropic} + h_{in}(\eta_k - 1)] \tag{A6}$$

$$\eta_{vol} = f_1(P_{ratio}, \omega_k) \tag{A7}$$

$$\eta_k = f_2(P_{ratio}, \omega_k) \tag{A8}$$

The volumetric and isentropic efficiencies are interpolated as functions of the pressure ratio and compressor speed from semi empirical maps [Equation (A7)-(A8)]. The compressor speed is rate limited in order to capture the limitations of real compressors.

Implementation in MATLAB/Simulink

The following tables list the inputs, physical parameters, operating conditions and required support files for the single stage compressor model.

Table A1: Input variables

Variable	Description	Units
rpm	Compressor speed	RPM
Pk_ri	Refrigerant pressure at the inlet	kPa
Pk_ro	Refrigerant pressure at the outlet	kPa
Hk_ri	Refrigerant enthalpy at the inlet	kJ/kg

Table A2: Physical parameters

Variable	Description	Units
rsr	Rising slew rate for compressor speed	rpm/s
fsr	Falling slew rate for compressor speed	rpm/s
delay	Time delay for compressor speed	s
upperlimit	Maximum percentage valve opening	$-$
lowerlimit	Minimum percentage valve opening	$-$
Vk	Volume of compression chamber	m^3
tau_k	Time constant for evolution of the refrigerant enthalpy at compressor outlet	s
RPM_vector	Operating range vector of compressor speed	rpm
P_ratio_vector	Operating range vector of compressor pressure ratio	$-$
eta_v_matrix	Interpolation matrix for volumetric efficiency, $\eta_{vol} = f(rpm, P_{ratio})$	$-$

Table A3: Operating conditions

Variable	Description	Units
Pk_ri	Refrigerant pressure at compressor inlet	kPa
Pk_ro	Refrigerant pressure at compressor outlet	kPa
Hk_ri	Refrigerant enthalpy at compressor inlet	kJ/kg
Hk_ro	Refrigerant enthalpy at compressor outlet	kJ/kg
mdot	Refrigerant mass flow rate through the compressor	kg/s
rpm	Compressor speed	RPM

Table A4 Support files

Name	Type	Description
CompProp	mat-file	Compressor property maps. The user can used the sample maps defined in this file to point to physical parameter variables like RPM_vector, P_ratio_vector, eta_v_matrix, eta_a_matrix etc.
RefProp_{name}	mat-file	Refrigerant property maps for interpolation. {name} is the type of refrigerant used, e.g. R134a, R410a

APPENDIX B

A complete derivation of the mathematical equation for the heat exchanger modeling is given here. This work has been included in this thesis with permission from Erik Rodriguez [28]. The Finite Control Volume (FCV) approach to the modeling of heat exchangers is available in commercial packages such as EASY5, SINDA/FLUENT , Modelica and e-thermal This document will explain the approach taken to provide FCV models compatible with MATLAB/Simulink environment. While the FCV modeling approach is widely believed to be able to model the heat exchanger dynamics with a lot of detail, thus leading to high accuracy, it is also computationally expensive with respect to both the simulation time and the load on the computer's memory. The simulation time is also a function of the level of discretization (number of control volumes) used in the creation of the models, while it has been observed that for a given set of parameters (e.g. cross-sectional area, length of the heat exchanger, external surface area etc.) there exists a minimum threshold for the number of control volumes required to capture the required dynamics accurately.

Figure B1 shows a FCV heat exchanger model discretized into n control volumes. The k^{th} control volume is assumed to have an internal surface area $A_{i,k}$ external surface area $A_{o,k}$, and a volume V_k. The conservation equations for refrigerant mass, refrigerant energy and wall energy can be applied to each of the control volumes and the governing equations for the heat exchangers can be derived. The goal is to derive

a system of equations of the form shown in Equation (B1), where x is the state vector shown in Equation (B2) and u is the input vector defined by Equation (B3).

$$Z(x,u)\dot{x} = f(x,u) \tag{B1}$$

$$x = [P \quad h_1 \quad \cdots \quad h_k \quad \cdots \quad h_n \quad T_{w,1} \quad \cdots \quad T_{w,k} \quad \cdots \quad T_{w,n}] \tag{B2}$$

$$u = [\dot{m}_{in} \quad \dot{m}_{out} \quad h_{in} \quad T_{air,in} \quad \dot{m}_{air}] \tag{B3}$$

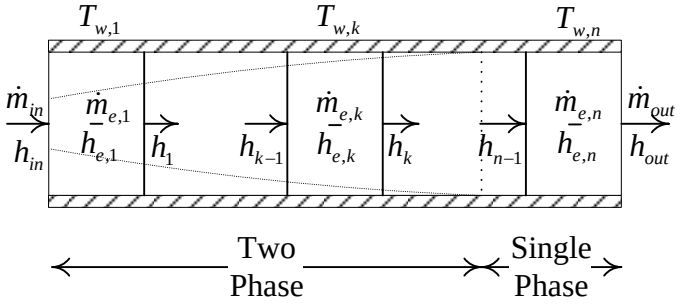

Figure B1: Finite control volume heat exchanger

Modeling Assumptions

The derivation approach uses several modeling assumptions associated with the refrigerant flow in the heat exchanger. The assumptions have been commonly used in past modeling efforts and are stated as follows:

- The heat exchanger is assumed to be a long, thin, horizontal tube.
- The refrigerant flow through the heat exchanger is modeled as a one dimensional fluid flow.
- Axial conduction of refrigerant is negligible.

- Pressure drop along the heat exchanger tube due to momentum change in refrigerant and viscous friction is negligible (refrigerant pressure along the entire heat exchanger tube can be assumed to be uniform). Thus the equation for conservation of momentum is not used.

As stated earlier the governing equations for the heat exchanger models can be derived using the unsteady state conservation equations refrigerant mass, refrigerant energy and wall energy. The equations for conservation of refrigerant mass, energy and wall energy together provide a complete characterization of the dynamics of a heat exchanger. Simplification along with convenience in creating a simulation model can be achieved by expanding the time derivative terms $\dot{U}$ and $\dot{E}_w$ in terms of the state variables defined earlier. The parameters used in the expansion of these terms are given in Table B1.

Table B1: Parameters Used in the Expansion of Conservation Equations

ρ	density of refrigerant
P	pressure of refrigerant
h	enthalpy of refrigerant
p_i	inner perimeter (interior surface area per unit length)
p_o	outer perimeter (outer surface area per unit length)
T_r	temperature of refrigerant
T_w	tube wall temperature

α_i	heat transfer coefficient between tube wall and internal fluid
α_o	heat transfer coefficient between tube wall and external fluid
A_{cs}	cross sectional area of the inside of the tube
$\dot{m}$	mass flow rate of refrigerant flowing along the tube
$\left(C_p \rho V\right)_w$	thermal capacitance of the tube wall per unit length

Model Derivation for FCV Evaporator

The modeling procedure assumes that the refrigerant entering the evaporator is a two phase mixture and the refrigerant exiting the heat exchanger is a superheated vapor. While this is done only for simplifying the documentation, the model itself will not have such limitations. Keeping this in mind the heat exchanger can be assumed to be broadly divided into two regions. To aid the modeling approach it is further assumed that the refrigerant gradually transitions into the superheated vapor phase from the two phase mixture as indicated in Figure B1. It is further assumed that the enthalpy at the outlet in each of the control volumes determines the state of the refrigerant in the entire region, i.e. if the outlet enthalpy for a region is less than or equal to the saturated vapor enthalpy at the evaporator pressure, then the state of the refrigerant in the entire region is assumed to be a two phase mixture. Conversely, if the outlet enthalpy is greater than the saturated vapor enthalpy, then the state of the refrigerant is assumed to be a superheated vapor. These assumptions lead to the presence of a transition region, wherein the refrigerant transitions from a two phase mixture to a superheated vapor. To preserve consistency,

the state of the refrigerant is determined by the original assumption which would lead to the refrigerant being assumed to be a superheated vapor in the case of the evaporator. This scenario allows for some modeling errors since the actual transition boundary might not be reflected by the boundary of the control volume, due to which the accuracy of the model is greater if the refrigerant transitions closer to the outlet boundary of the control region. However, increasing the number of control volume can minimize this error.

Conservation of refrigerant energy

Consider the equation for conservation of refrigerant energy for each control region. The rate of change of internal energy in a control region, $\dot{U}$ is given by Equation (B4), where $\dot{H}_{in}$ is the rate of energy entering the region, $\dot{H}_{out}$ is the rate of energy leaving the region by means of refrigerant mass and $\dot{Q}_w$ is the rate of energy leaving the region through heat transfer to the heat exchanger wall. The fluid flow energy at a point is given by $\dot{H} = \dot{m}h$ where $\dot{m}$ is the mass flow rate of the fluid and h is the enthalpy of the fluid at that point. The wall heat transfer term for a region is defined as $\dot{Q}_w = \alpha_i A_i (T_w - T_r)$ where α_i is the lumped heat transfer coefficient between refrigerant and wall material, A_i is the internal surface area of the heat exchanger wall in that region, T_w and T_r are the lumped wall temperature and refrigerant temperature in that region. Substituting the defined terms in Equation (B4) results in the equations for conservation of refrigerant energy for all the control regions of the heat exchanger as shown in Equation (B5).

$$\dot{U} = \dot{H}_{in} - \dot{H}_{out} + \dot{Q}_w \tag{B4}$$

$$\begin{bmatrix} \dot{U}_1 \\ \vdots \\ \dot{U}_k \\ \vdots \\ \dot{U}_n \end{bmatrix} = \begin{bmatrix} \dot{m}_{in}h_{in} - \dot{m}_1 h_1 + \alpha_{i,1}A_{i,1}(T_{w,1} - T_{r,1}) \\ \vdots \\ \dot{m}_{k-1}h_{k-1} - \dot{m}_k h_k + \alpha_{i,k}A_{i,k}(T_{w,k} - T_{r,k}) \\ \vdots \\ \dot{m}_{n-1}h_{n-1} - \dot{m}_{out}h_n + \alpha_{i,n}A_{i,n}(T_{w,n} - T_{r,n}) \end{bmatrix} \tag{B5}$$

Conservation of refrigerant mass

The equation for conservation of refrigerant mass in each of the control regions is as shown in Equation (B6), which essentially states that the rate of change of refrigerant mass in a given control region is the difference of the refrigerant mass entering and leaving that control volume. All the equations in Equation (B6) can be combined together by adding them and are presented in Equation (B7), where $\dot{m}$ gives the rate of change of total refrigerant mass in the heat exchanger.

$$\begin{bmatrix} \dot{m}_1 \\ \vdots \\ \dot{m}_k \\ \vdots \\ \dot{m}_n \end{bmatrix} = \begin{bmatrix} \dot{m}_{in} - \dot{m}_1 \\ \vdots \\ \dot{m}_{k-1} - \dot{m}_k \\ \vdots \\ \dot{m}_{n-1} - \dot{m}_{out} \end{bmatrix} \tag{B6}$$

$$\dot{m} = \dot{m}_{in} - \dot{m}_{out} \tag{B7}$$

Conservation of wall energy

The conservation of wall energy in a control region is given in Equation (B8) where $\dot{E}_w$ is the rate of change of total energy of the heat exchanger wall in the control region considered, $\dot{Q}_w$ is the rate of energy leaving the region through heat transfer to the

heat exchanger wall and $\dot{Q}_a$ is the rate of energy entering the heat exchanger wall through heat transfer from the external fluid. Substituting the defined terms in Equation (B8), the equations for conservation of tube wall energy for all the control regions of the heat exchanger are presented in Equation (B9).

$$\dot{E}_w = \dot{Q}_a - \dot{Q}_w \tag{B8}$$

$$\begin{bmatrix} \dot{E}_{w,1} \\ \vdots \\ \dot{E}_{w,k} \\ \vdots \\ \dot{E}_{w,n} \end{bmatrix} = \begin{bmatrix} \alpha_{o,1}A_{o,1}(T_{a,1} - T_{w,1}) - \alpha_{i,1}A_{i,1}(T_{w,1} - T_{r,1}) \\ \vdots \\ \alpha_{o,k}A_{o,k}(T_{a,k} - T_{w,k}) - \alpha_{i,k}A_{i,k}(T_{w,k} - T_{r,k}) \\ \vdots \\ \alpha_{o,n}A_{o,n}(T_{a,n} - T_{w,n}) - \alpha_{i,n}A_{i,n}(T_{w,n} - T_{r,n}) \end{bmatrix} \tag{B9}$$

State Transformation

The conservation equation derived in sections B4, B5 and B6 can be combined to form Equation (B10). The equations for conservation of refrigerant energy, refrigerant mass and wall energy can be expressed in terms of the state vector x defined in Equation (B2). To this end, the internal energy is expressed in terms of the refrigerant mass and average internal energy as shown in Equation (B11), whereas the refrigerant mass is expressed in terms of the average density and internal volume as shown in Equation (B12). Further, the density and internal energy can be given as functions of pressure and enthalpy in each of the control volumes. Thus, the time derivatives of these terms can be expanded to include more accessible state variables as shown in Equation (B13).

Further simplification can be achieved by redefining enthalpy as $h_k = u_k + \frac{P}{\rho_k}$ and the partial derivatives as $\left.\frac{\partial u_k}{\partial P}\right|_{h_k} = -\frac{1}{\rho_k} + \frac{P}{{\rho_k}^2}\left.\frac{\partial \rho_k}{\partial P}\right|_{h_k}$ and $\left.\frac{\partial u_k}{\partial h_k}\right|_{P} = 1 + \frac{P}{{\rho_k}^2}\left.\frac{\partial \rho_k}{\partial h_k}\right|_{P}$. These simplifications result in Equations (B14) and (B15). The wall energy can be expressed in terms of the thermal capacitance and wall temperature, the time derivative of which can be expressed as in Equation (B16).

$$\begin{bmatrix} \dot{U}_1 \\ \vdots \\ \dot{U}_k \\ \vdots \\ \dot{U}_n \\ \dot{m} \\ \dot{E}_{w,1} \\ \vdots \\ \dot{E}_{w,k} \\ \vdots \\ \dot{E}_{w,n} \end{bmatrix} = \begin{bmatrix} \dot{m}_{in}h_{in} - \dot{m}_1 h_1 + \alpha_{i,1}A_{i,1}(T_{w,1} - T_{r,1}) \\ \vdots \\ \dot{m}_{k-1}h_{k-1} - \dot{m}_k h_k + \alpha_{i,k}A_{i,k}(T_{w,k} - T_{r,k}) \\ \vdots \\ \dot{m}_{n-1}h_{n-1} - \dot{m}_{out}h_n + \alpha_{i,n}A_{i,n}(T_{w,n} - T_{r,n}) \\ \dot{m}_{in} - \dot{m}_{out} \\ \alpha_{o,1}A_{o,1}(T_{a,1} - T_{w,1}) - \alpha_{i,1}A_{i,1}(T_{w,1} - T_{r,1}) \\ \vdots \\ \alpha_{o,k}A_{o,k}(T_{a,k} - T_{w,k}) - \alpha_{i,k}A_{i,k}(T_{w,k} - T_{r,k}) \\ \vdots \\ \alpha_{o,n}A_{o,n}(T_{a,n} - T_{w,n}) - \alpha_{i,n}A_{i,n}(T_{w,n} - T_{r,n}) \end{bmatrix} \tag{B10}$$

$$U_k = m_k u_k \tag{B11}$$

$$m_k = V_k \rho_k \tag{B12}$$

$$\dot{U}_k = V_k\left[\left(\left.\frac{\partial \rho_k}{\partial P}\right|_{h_k}\dot{P} + \left.\frac{\partial \rho_k}{\partial h_k}\right|_{P}\dot{h}_k\right)u_k + \left(\left.\frac{\partial u_k}{\partial P}\right|_{h_k}\dot{P} + \left.\frac{\partial u_k}{\partial h_k}\right|_{P}\dot{h}_k\right)\rho_k\right] \tag{B13}$$

$$\dot{U}_k = V_k\left(\left.\frac{\partial \rho_k}{\partial P}\right|_{h_k}h_k - 1\right)\dot{P} + V_k\left(\left.\frac{\partial \rho_k}{\partial h_k}\right|_{P}h_k + \rho_k\right)\dot{h}_k \tag{B14}$$

$$\dot{m}_k = \left[\left(\left.\frac{\partial \rho_k}{\partial P}\right|_{h_k}\right)\dot{P} + \left(\left.\frac{\partial \rho_k}{\partial h_k}\right|_{P}\right)\dot{h}_k\right]V_k \tag{B15}$$

$$\dot{E}_{w,k} = \left(C_p \rho V\right)_w \dot{T}_{w,k} \tag{B16}$$

Model in $\boldsymbol{Z(x,u)\dot{x} = f(x,u)}$ form

The resulting equations can be expressed in a slightly modified form of Equation (B1) that includes the mass flows as unknowns as shown in Equation (B17a). Code is included for three separate methods for calculating the state derivatives. The first method involves a matrix inversion to solve for the state derivatives and the intermediate mass flow rates simultaneously. The second method uses a transformation matrix that requires a smaller matrix inversion, and solves for the state derivatives first and then the intermediate mass flows afterwards. The third method performs the algebraic substitution manually (equivalent to the transformation matrix method). Each of these methods is theoretically and numerically equivalent but the second method is more computationally favorable. The elements of the $Z(x,u)$ and $f(x,u)$ for the first method are given in Equations (B17b) to (B30). The transformation equations used to transition from the first method to the second method are given in Equations (B31) to (B38) and the resulting small matrix elements are given in Equations (B39) to (B45).

$$Z(x,u)\begin{bmatrix}\dot{P}\\ \dot{h}\\ \dot{m}\\ \dot{T}_w\end{bmatrix} = f(x,u) \tag{B17a}$$

$$Z(x,u) = \begin{bmatrix}Z_{11} & Z_{12} & Z_{13} & 0\\ Z_{21} & Z_{22} & Z_{23} & 0\\ 0 & 0 & 0 & Z_{34}\end{bmatrix}_{3nX3n} \tag{B17b}$$

$$Z_{11} = \begin{bmatrix} V_1\left(\left.\frac{\partial \rho_1}{\partial P}\right|_{h_1} h_1 - 1\right) \\ \vdots \\ V_k\left(\left.\frac{\partial \rho_k}{\partial P}\right|_{h_k} h_k - 1\right) \\ \vdots \\ V_n\left(\left.\frac{\partial \rho_n}{\partial P}\right|_{h_n} h_n - 1\right) \end{bmatrix}_{nX1} \tag{B18}$$

$$Z_{12} = \begin{bmatrix} Z_{12}^1 & 0 & \cdots & \cdots & 0 \\ 0 & \ddots & \ddots & & \vdots \\ \vdots & \ddots & Z_{12}^k & \ddots & \vdots \\ \vdots & & \ddots & \ddots & 0 \\ 0 & \cdots & \cdots & 0 & Z_{12}^n \end{bmatrix}_{nXn} \tag{B19}$$

$$Z_{12}^1 = V_1\left(\left.\frac{\partial \rho_1}{\partial h_1}\right|_P h_1 + \rho_1\right) \tag{B20}$$

$$Z_{12}^k = V_k\left(\left.\frac{\partial \rho_k}{\partial h_k}\right|_P h_k + \rho_k\right) \tag{B21}$$

$$Z_{12}^n = V_n\left(\left.\frac{\partial \rho_n}{\partial h_n}\right|_P h_n + \rho_n\right) \tag{B22}$$

$$Z_{13} = \begin{bmatrix} h_1 & 0 & \cdots & \cdots & \cdots & 0 \\ -h_1 & h_2 & 0 & \cdots & & \vdots \\ 0 & -h_2 & h_3 & 0 & \cdots & \vdots \\ \vdots & \ddots & \ddots & \ddots & \ddots & \vdots \\ \vdots & & \ddots & \ddots & -h_{n-2} & h_{n-1} \\ 0 & \cdots & \cdots & \cdots & 0 & -h_{n-1} \end{bmatrix}_{nX(n-1)} \tag{B23}$$

$$Z_{21} = \begin{bmatrix} V_1\left(\frac{\partial \rho_1}{\partial P}\Big|_{h_1}\right) \\ \vdots \\ V_k\left(\frac{\partial \rho_k}{\partial P}\Big|_{h_k}\right) \\ \vdots \\ V_n\left(\frac{\partial \rho_n}{\partial P}\Big|_{h_n}\right) \end{bmatrix}_{nX1} \tag{B24}$$

$$Z_{22} = \begin{bmatrix} V_1\left(\frac{\partial \rho_1}{\partial h_1}\Big|_{P}\right) & 0 & \cdots & \cdots & 0 \\ 0 & \ddots & \ddots & & \vdots \\ \vdots & \ddots & V_k\left(\frac{\partial \rho_k}{\partial h_k}\Big|_{P}\right) & \ddots & \vdots \\ \vdots & & \ddots & \ddots & 0 \\ 0 & \cdots & \cdots & 0 & V_n\left(\frac{\partial \rho_n}{\partial h_n}\Big|_{P}\right) \end{bmatrix}_{nXn} \tag{B25}$$

$$Z_{23} = \begin{bmatrix} 1 & 0 & \cdots & \cdots & \cdots & 0 \\ -1 & 1 & 0 & \cdots & & \vdots \\ 0 & -1 & 1 & 0 & \cdots & \vdots \\ \vdots & \ddots & \ddots & \ddots & \ddots & \vdots \\ \vdots & & \ddots & \ddots & -1 & 1 \\ 0 & \cdots & \cdots & \cdots & 0 & -1 \end{bmatrix}_{nX(n-1)} \tag{B26}$$

$$Z_{34} = diag\{(C_p\rho V)_{w,1} \quad \cdots \quad (C_p\rho V)_{w,n}\} \tag{B27}$$

$$f(x,u) = \begin{bmatrix} f_1 \\ f_2 \\ f_3 \end{bmatrix}$$

$$f_1 = \begin{bmatrix} \dot{m}_{in}h_{in} + \alpha_{i,1}A_{i,1}(T_{w,1} - T_{r,1}) \\ \alpha_{i,2}A_{i,2}(T_{w,2} - T_{r,2}) \\ \vdots \\ \alpha_{i,n-1}A_{i,n-1}(T_{w,n-1} - T_{r,n-1}) \\ -\dot{m}_{out}h_n + \alpha_{i,n}A_{i,n}(T_{w,n} - T_{r,n}) \end{bmatrix} \tag{B28}$$

$$f_2 = \begin{bmatrix} \dot{m}_{in} \\ 0 \\ \vdots \\ 0 \\ -\dot{m}_{out} \end{bmatrix} \tag{B29}$$

$$f_3 = \begin{bmatrix} \alpha_{o,1}A_{o,1}(T_{a,1} - T_{w,1}) - \alpha_{i,1}A_{i,1}(T_{w,1} - T_{r,1}) \\ \vdots \\ \alpha_{o,k}A_{o,k}(T_{a,k} - T_{w,k}) - \alpha_{i,k}A_{i,k}(T_{w,k} - T_{r,k}) \\ \vdots \\ \alpha_{o,n}A_{o,n}(T_{a,n} - T_{w,n}) - \alpha_{i,n}A_{i,n}(T_{w,n} - T_{r,n}) \end{bmatrix} \tag{B30}$$

$$Let\ T = \begin{bmatrix} 1 & 1 & \cdots & \cdots & 1 \\ 1 & 0 & \cdots & \cdots & 0 \\ 1 & 1 & 0 & \cdots & 0 \\ \vdots & \ddots & \ddots & \ddots & \vdots \\ 1 & 1 & \cdots & 1 & 0 \end{bmatrix}_{nXn} \tag{B31}$$

$$T = \begin{bmatrix} T_1 \\ T_2 \end{bmatrix} \tag{B32}$$

$$TZ_{23} = \begin{bmatrix} 0^{1X(n-1)} \\ I^{(n-1)X(n-1)} \end{bmatrix} \tag{B33}$$

$$Z_{21}\dot{P} + Z_{22}\dot{h} + Z_{23}\dot{m} = f_2 \tag{B34}$$

$$\dot{m} = (TZ_{23})^T T(f_2 - Z_{21}\dot{P} - Z_{22}\dot{h}_k) \tag{B35}$$

$$Z_{11}\dot{P} + Z_{12}\dot{h} + Z_{13}\dot{m} = f_1 \tag{B36}$$

$$\begin{aligned} &(Z_{11} - Z_{13}(TZ_{23})^T TZ_{21})\dot{P} + (Z_{12} - Z_{13}(TZ_{23})^T TZ_{22})\dot{h} \\ &= f_1 - Z_{13}(TZ_{23})^T T f_2 \end{aligned} \tag{B37}$$

$$(T_1 Z_{21})\dot{P} + (T_1 Z_{22})\dot{h} = T_1 f_2 \tag{B38}$$

$$\hat{Z}_{11} = Z_{11} - Z_{13}(TZ_{23})^T TZ_{21} \tag{B39}$$

$$\hat{Z}_{12} = Z_{12} - Z_{13}(TZ_{23})^T TZ_{22} \tag{B40}$$

$$\hat{f}_1 = f_1 - Z_{13}(TZ_{23})^T T f_2 \tag{B41}$$

$$\hat{Z}_{21} = T_1 Z_{21} \tag{B42}$$

$$\hat{Z}_{22} = T_1 Z_{22} \tag{B43}$$

$$\hat{f}_2 = T_1 f_2 \tag{B44}$$

$$\begin{bmatrix} \hat{Z}_{11} & \hat{Z}_{12} & 0 \\ \hat{Z}_{21} & \hat{Z}_{22} & 0 \\ 0 & 0 & Z_{34} \end{bmatrix} \begin{bmatrix} \dot{P} \\ \dot{h} \\ \dot{T}_w \end{bmatrix} = \begin{bmatrix} \hat{f}_1 \\ \hat{f}_2 \\ f_3 \end{bmatrix} \tag{B45}$$

Implementation of Pressure Drop

Pressure drop calculation is split into two parts: single phase and two-phase. The single phase pressure drop is calculated using the Darcy-Weisbach while the two-phase flow pressure drop is calculated using the Wattlet-Chato pressure drop correlation. The void fraction used in the two-phase acceleration pressure drop calculation is calculated using Zivi's form of the slip-ratio-correlated equation. Pressure drop calculation is implemented by filling in the "Pressure drop calculation" check box in the function block parameters of the FCV heat exchanger model.

Implementation of Flow Conditions

The outlet temperature of the external fluid will vary depending on the flow condition of the heat exchanger external fluid. Conservation of energy is applied to a control region using Equation (B46) where the heat transfer rate from the external fluid is represented by $\dot{Q} = \dot{m} C_p (T_{ai} - T_a)$ where $\dot{m}$ is the mass flow rate of the external fluid, C_p is the specific heat of the external fluid, T_{ai} is the temperature of the external fluid at the inlet of the control region, and T_a is the average external fluid temperature in

the control region. This heat transfer rate is balanced with the heat transfer rate into the heat exchanger wall $\alpha_o A_o(1 - T_{a\mu})(T_a - T_w)$ where α_o is the lumped heat transfer coefficient between external fluid and wall material, A_o is the external surface area of the heat exchanger wall in that region, $T_{a\mu}$ is a weighing factor for calculating average external fluid temperature, and T_w and T_a are the lumped wall temperature and average external fluid temperature in that region. Equation (B46) can be rearranged to solve for the average external fluid temperature in the region as shown in Equation (B47). The external fluid temperature at the outlet of the control region can then be determined using the weighted temperature equation $T_a = T_{a\mu}T_{ai} + (1 - T_{a\mu})T_{ao}$ and rearranging as shown in Equation (B48). The mass flow rate, wall temperature, and inlet temperature values for each control region are based on the selected flow condition. Equations (B49) – (B57) show the mass flow rate, average external fluid temperature, and external fluid outlet temperature for all control regions for cross-flow (Equations (B49) – (B51)), co-flow (Equations (B52) – (B54)), and counter-flow (Equations (B55) – (B57)) conditions where $\dot{m}_{total}$ is the external fluid mass flow rate specified in the operating conditions, and n is the number of control regions. The final external fluid outlet temperature reported by the simulation block is the last value calculated for the outlet temperature for co-flow ($T_{ao,n}$) and counter-flow ($T_{ao,1}$), and is the mean of the outlet temperatures in all regions for cross-flow $\left(\frac{1}{n}\sum_{i=1}^{n} T_{ao,i}\right)$

$$\dot{m}C_p(T_{ai} - T_a) = \alpha_o A_o(1 - T_{a\mu})(T_a - T_w) \tag{B46}$$

$$T_a = \frac{\dot{m}C_pT_{ai} + \alpha_o A_o(1 - T_{a\mu})T_w}{\dot{m}C_p + \alpha_o A_o(1 - T_{a\mu})} \tag{B47}$$

$$T_{ao} = \frac{T_a - T_{a\mu}T_{ai}}{(1 - T_{a\mu})} \tag{B48}$$

$$\dot{m}_k = \frac{\dot{m}_{total}}{n} \tag{B49}$$

$$\begin{bmatrix} T_{a,1} \\ \vdots \\ T_{a,k} \\ \vdots \\ T_{a,n} \end{bmatrix} = \begin{bmatrix} \frac{\dot{m}_1 C_{p,1} T_{ai,1} + \alpha_{o,1} A_{o,1}(1 - T_{a\mu,1})T_{w,1}}{\dot{m}_1 C_{p,1} + \alpha_{o,1} A_{o,1}(1 - T_{a\mu,1})} \\ \vdots \\ \frac{\dot{m}_k C_{p,k} T_{ai,k} + \alpha_{o,k} A_{o,k}(1 - T_{a\mu,k})T_{w,k}}{\dot{m}_k C_{p,k} + \alpha_{o,k} A_{o,k}(1 - T_{a\mu,k})} \\ \vdots \\ \frac{\dot{m}_n C_{p,n} T_{ai,n} + \alpha_{o,n} A_{o,n}(1 - T_{a\mu,n})T_{w,n}}{\dot{m}_n C_{p,n} + \alpha_{o,n} A_{o,n}(1 - T_{a\mu,n})} \end{bmatrix} \tag{B50}$$

$$\begin{bmatrix} T_{ao,1} \\ \vdots \\ T_{ao,k} \\ \vdots \\ T_{ao,n} \end{bmatrix} = \begin{bmatrix} \frac{T_{a,1} - T_{a\mu,1}T_{ai,1}}{(1 - T_{a\mu,1})} \\ \vdots \\ \frac{T_{a,k} - T_{a\mu,k}T_{ai,k}}{(1 - T_{a\mu,k})} \\ \vdots \\ \frac{T_{a,n} - T_{a\mu,n}T_{ai,n}}{(1 - T_{a\mu,n})} \end{bmatrix} \tag{B51}$$

$$\dot{m}_k = \dot{m}_{total} \tag{B52}$$

$$\begin{bmatrix} T_{a,1} \\ T_{a,2} \\ \vdots \\ T_{a,k} \\ \vdots \\ T_{a,n} \end{bmatrix} = \begin{bmatrix} \frac{\dot{m}_1 C_{p,1} T_{ai,1} + \alpha_{o,1} A_{o,1}(1 - T_{a\mu,1})T_{w,1}}{\dot{m}_1 C_{p,1} + \alpha_{o,1} A_{o,1}(1 - T_{a\mu,1})} \\ \frac{\dot{m}_2 C_{p,2} T_{ao,1} + \alpha_{o,2} A_{o,2}(1 - T_{a\mu,2})T_{w,2}}{\dot{m}_2 C_{p,2} + \alpha_{o,2} A_{o,2}(1 - T_{a\mu,2})} \\ \vdots \\ \frac{\dot{m}_k C_{p,k} T_{ao,k-1} + \alpha_{o,k} A_{o,k}(1 - T_{a\mu,k})T_{w,k}}{\dot{m}_k C_{p,k} + \alpha_{o,k} A_{o,k}(1 - T_{a\mu,k})} \\ \vdots \\ \frac{\dot{m}_n C_{p,n} T_{ao,n-1} + \alpha_{o,n} A_{o,n}(1 - T_{a\mu,n})T_{w,n}}{\dot{m}_n C_{p,n} + \alpha_{o,n} A_{o,n}(1 - T_{a\mu,n})} \end{bmatrix} \tag{B53}$$

$$\begin{bmatrix} T_{ao,1} \\ T_{ao,2} \\ \vdots \\ T_{ao,k} \\ \vdots \\ T_{ao,n} \end{bmatrix} = \begin{bmatrix} \dfrac{T_{a,1} - T_{a\mu,1}T_{ai,1}}{(1 - T_{a\mu,1})} \\ \dfrac{T_{a,2} - T_{a\mu,2}T_{ao,1}}{(1 - T_{a\mu,2})} \\ \vdots \\ \dfrac{T_{a,k} - T_{a\mu,k}T_{ao,k-1}}{(1 - T_{a\mu,k})} \\ \vdots \\ \dfrac{T_{a,n} - T_{a\mu,n}T_{ao,n-1}}{(1 - T_{a\mu,n})} \end{bmatrix} \tag{B54}$$

$$\dot{m}_k = \dot{m}_{total} \tag{B55}$$

$$\begin{bmatrix} T_{a,n} \\ T_{a,n-1} \\ \vdots \\ T_{a,n-k+1} \\ \vdots \\ T_{a,1} \end{bmatrix} = \begin{bmatrix} \dfrac{\dot{m}_1 C_{p,1} T_{ai,1} + \alpha_{o,n} A_{o,n} (1 - T_{a\mu,1}) T_{w,n}}{\dot{m}_1 C_{p,1} + \alpha_{o,n} A_{o,n} (1 - T_{a\mu,1})} \\ \dfrac{\dot{m}_2 C_{p,2} T_{ao,n} + \alpha_{o,n-1} A_{o,n-1} (1 - T_{a\mu,2}) T_{w,n-1}}{\dot{m}_2 C_{p,2} + \alpha_{o,n-1} A_{o,n-1} (1 - T_{a\mu,2})} \\ \vdots \\ \dfrac{\dot{m}_k C_{p,k} T_{ao,n-k+2} + \alpha_{o,n-k+1} A_{o,n-k+1} (1 - T_{a\mu,k}) T_{w,n-k+1}}{\dot{m}_k C_{p,k} + \alpha_{o,n-k+1} A_{o,n-k+1} (1 - T_{a\mu,k})} \\ \vdots \\ \dfrac{\dot{m}_n C_{p,n} T_{ao,2} + \alpha_{o,1} A_{o,1} (1 - T_{a\mu,n}) T_{w,1}}{\dot{m}_n C_{p,n} + \alpha_{o,1} A_{o,1} (1 - T_{a\mu,n})} \end{bmatrix} \tag{B56}$$

$$\begin{bmatrix} T_{ao,n} \\ T_{ao,n-1} \\ \vdots \\ T_{ao,n-k+1} \\ \vdots \\ T_{ao,1} \end{bmatrix} = \begin{bmatrix} \dfrac{T_{a,n} - T_{a\mu,1}T_{ai,1}}{(1 - T_{a\mu,1})} \\ \dfrac{T_{a,n-1} - T_{a\mu,2}T_{ao,n}}{(1 - T_{a\mu,2})} \\ \vdots \\ \dfrac{T_{a,n-k+1} - T_{a\mu,k}T_{ao,n-k+2}}{(1 - T_{a\mu,k})} \\ \vdots \\ \dfrac{T_{a,1} - T_{a\mu,n}T_{ao,2}}{(1 - T_{a\mu,n})} \end{bmatrix} \tag{B57}$$

Implementation of Heat Exchanger Type

The FCV Heat Exchanger model is capable of acting as either an evaporator or condenser depending upon the specifications set by the user in the operating conditions. The heat exchanger type selected affects the heat transfer coefficient correlation method used. The Wattlet-Chato correlation is used for an evaporator while the Dobson correlation is used for a condenser. Other than this the model execution remains exactly the same for both heat exchanger types.

Implementation in MATLAB\Simulink

The following tables list the inputs, physical parameters, operating conditions and required support files for FCV heat exchanger model.

Table B2: Input variables

Variable	Description	Units
mdot_i	Mass flow rate of refrigerant at the inlet of heat exchanger	kg/s
mdot_o	Mass flow rate of refrigerant at the outlet of heat exchanger	kg/s
H_ri	Enthalpy of refrigerant at the inlet of heat exchanger	kJ/kg
T_ai1	Temperature of external fluid at the inlet of heat exchanger	^oC
m_air1	Mass flow rate of external fluid at the inlet of heat exchanger	kg/s

Table B3: Physical parameters

Variable	Description	Units
Mass1	Total mass of heat exchanger	kg
Cpw1	Specific heat of heat exchanger material	$kJ/kg/K$
Diameter1	Hydraulic diameter of refrigerant passage	m
L_total1	Total length of refrigerant passage	m
A_i1	Total Internal surface area of the heat exchanger	m^2
A_o1	Total external surface area of the heat exchanger	m^2
A_cs1	Cross sectional area of refrigerant passage	m^2

Table B4: Operating conditions

Variable	Description	Units
n_1	Number of control volumes	$-$
m_air1	Mass flow rate of external fluid	kg/s
mdot	Mass flow rate of refrigerant	kg/s
P	Refrigerant pressure in the heat exchanger	kPa
H_ri	Refrigerant enthalpy at heat exchanger inlet	kJ/kg
H_ro	Refrigerant enthalpy at heat exchanger outlet	kJ/kg
T_ai1	External fluid temperature at heat exchanger inlet	^oC
T_ao1	External fluid temperature at heat exchanger outlet	^oC

Cp_ext1	Specific heat of external fluid	$kJ/kg/K$
T_a_mu1	Weighting factor for calculating average external fluid temperature	–
Slip	Two-phase region slip ratio for calculating void fraction	–
CJF_data1	Colburn J-factor data for external heat transfer for the heat exchanger	–
Ext_Fluid1	Fluid data for external heat transfer for the heat exchanger	–
ext_flow_var	External fluid flow condition (1=cross-flow, 2=co-flow, 3=counter-flow)	–
HX_var	Heat exchanger type (1=evaporator, 2=condenser)	–

Table B5: Support files

Name	**Type**	**Description**
H_COLBURN_JFACTOR	m-file	Air side heat transfer correlation
H_EVAP_WATTLET	m-file	Refrigerant side heat transfer correlation for evaporating two-phase flows
H_COND_DOBSON	m-file	Refrigerant side heat transfer correlation for condensing two-phase flows
H_1PH_GNIELINSKI	m-file	Refrigerant side heat transfer correlation for single phase flows
F_1PH_CHURCHILL	m-file	Churchill friction factor correlation

MassEnergyBalance_FCV	m-file	Steady state solver
MassEnergyBalance_FCV_solution	m-file	Steady state parameter calculator
RefProp_{name}	mat-file	Refrigerant property maps for interpolation. {name} is the type of refrigerant used, e.g. R134a, R410a

Implementation of Heat Exchanger Type

The FCV Heat Exchanger model is capable of acting as either an evaporator or condenser depending upon the specifications set by the user in the operating conditions. The heat exchanger type selected affects the heat transfer coefficient correlation method used. The Wattlet-Chato correlation is used for an evaporator while the Dobson correlation is used for a condenser. Other than this the model execution remains exactly the same for both heat exchanger types.

Implementation in MATLAB\Simulink

The following tables list the inputs, physical parameters, operating conditions and required support files for FCV heat exchanger model.

Table B6: Input variables

Variable	Description	Units
mdot_i	Mass flow rate of refrigerant at the inlet of heat exchanger	kg/s

mdot_o	Mass flow rate of refrigerant at the outlet of heat exchanger	kg/s
H_ri	Enthalpy of refrigerant at the inlet of heat exchanger	kJ/kg
T_ai1	Temperature of external fluid at the inlet of heat exchanger	^oC
m_air1	Mass flow rate of external fluid at the inlet of heat exchanger	kg/s

Table B7: Physical parameters

Variable	**Description**	**Units**
Mass1	Total mass of heat exchanger	kg
Cpw1	Specific heat of heat exchanger material	k$J/kg/K$
Diameter1	Hydraulic diameter of refrigerant passage	m
L_total1	Total length of refrigerant passage	m
A_i1	Total Internal surface area of the heat exchanger	m^2
A_o1	Total external surface area of the heat exchanger	m^2
A_cs1	Cross sectional area of refrigerant passage	m^2

Table B8: Operating conditions

Variable	**Description**	**Units**
n_1	Number of control volumes	$-$
m_air1	Mass flow rate of external fluid	kg/s
mdot	Mass flow rate of refrigerant	kg/s
P	Refrigerant pressure in the heat exchanger	kPa

H_ri	Refrigerant enthalpy at heat exchanger inlet	kJ/kg
H_ro	Refrigerant enthalpy at heat exchanger outlet	kJ/kg
T_ai1	External fluid temperature at heat exchanger inlet	^oC
T_ao1	External fluid temperature at heat exchanger outlet	^oC
Cp_ext1	Specific heat of external fluid	$kJ/kg/K$
T_a_mu1	Weighting factor for calculating average external fluid temperature	–
Slip	Two-phase region slip ratio for calculating void fraction	–
CJF_data1	Colburn J-factor data for external heat transfer for the heat exchanger	–
Ext_Fluid1	Fluid data for external heat transfer for the heat exchanger	–

Table B9: Support files

Name	**Type**	**Description**
H_COLBURN_JFACTOR	m-file	Air side heat transfer correlation
H_EVAP_WATTLET	m-file	Refrigerant side heat transfer correlation for evaporating two-phase flows
H_COND_DOBSON	m-file	Refrigerant side heat transfer correlation for condensing two-phase flows
H_1PH_GNIELINSKI	m-file	Refrigerant side heat transfer correlation for single phase flows

F_1PH_CHURCHILL	m-file	Churchill friction factor correlation
MassEnergyBalance_FCV	m-file	Steady state solver
MassEnergyBalance_FCV_solution	m-file	Steady state parameter calculator
RefProp_{name}	mat-file	Refrigerant property maps for interpolation. {name} is the type of refrigerant used, e.g. R134a, R410a

Finite Control Volume Heat Exchangers in Series

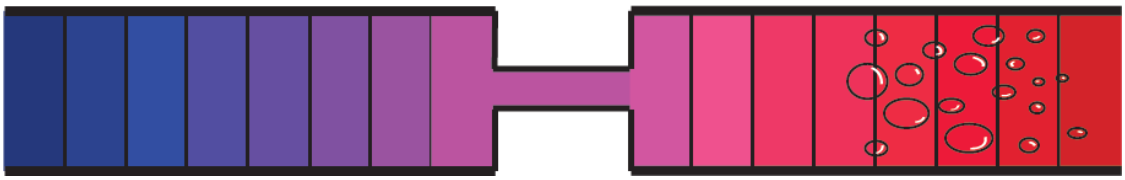

Simulink Icon for Finite Control Volume Evaporators in Series

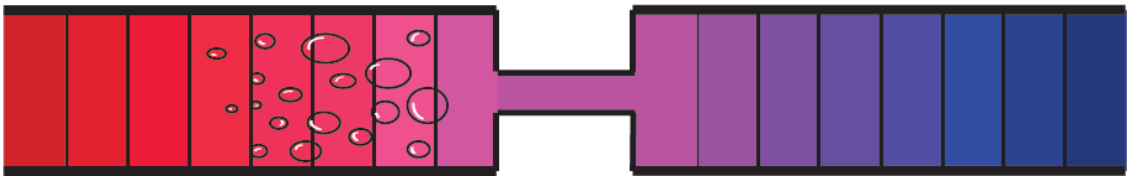

Simulink Icon for Finite Control Volume Condensers in Series

The model for the FCV heat exchangers in series is identical to that of the single FCV heat exchanger except for the addition of the following inputs, physical parameters, and operating conditions.

Table B10: Additional input variables

Variable	Description	Units
T_ai2	Temperature of external fluid at the inlet of second heat exchanger	^oC
m_air2	Mass flow rate of external fluid at the inlet of second heat exchanger	kg/s

Table B11: Additional physical parameters

Variable	Description	Units
Mass2	Total mass of second heat exchanger	kg
Cpw2	Specific heat of second heat exchanger material	$kJ/kg/K$
Diameter2	Hydraulic diameter of second refrigerant passage	m
L_total2	Total length of second refrigerant passage	m
A_i2	Total Internal surface area of the second heat exchanger	m^2
A_o2	Total external surface area of the second heat exchanger	m^2
A_cs2	Cross sectional area of second refrigerant passage	m^2

Table B12: Additional operating conditions

Variable	Description	Units
n_2	Number of control volumes for second heat exchanger	–
m_air2	Mass flow rate of external fluid for second heat exchanger	kg/s
T_ai2	External fluid temperature at second heat exchanger inlet	^oC
T_ao2	External fluid temperature at second heat exchanger outlet	^oC
Cp_ext2	Specific heat of external fluid for second heat exchanger	$J/kg/K$
T_a_mu2	Weighting factor for calculating average external fluid temperature for second heat exchanger	–
CJF_data2	Colburn J-factor data for external heat transfer for the second heat exchanger	–
Ext_Fluid2	Fluid data for external heat transfer for the second heat exchanger	–

Table B13 Additional parameters used in the accumulator/receiver conservation equations

$\dot{m}_{rec}$	rate of change of total mass of refrigerant inside accumulator/receiver
$\dot{m}_n$	mass flow rate of refrigerant at accumulator/receiver inlet
h_{rec}	enthalpy of refrigerant at accumulator/receiver outlet
UA_{rec}	external heat transfer coefficient of accumulator/receiver
T_{rec}	average temperature of accumulator/receiver

T_{amb}	ambient temperature
ρ_g	vapor density of two-phase refrigerant at pressure P
ρ_f	liquid density of two-phase refrigerant at pressure P
V_g	volume occupied by vapor in accumulator/receiver
V_f	volume occupied by liquid in accumulator/receiver
m_g	mass of vapor in accumulator/receiver
m_f	mass of liquid in accumulator/receiver
u_g	vapor internal energy of two-phase refrigerant at pressure P
u_f	liquid internal energy of two-phase refrigerant at pressure P

$$\dot{U}_{rec} = \dot{m}_n h_n - \dot{m}_{out} h_{rec,out} - UA_{rec}(T_{rec} - T_{amb}) \tag{B58}$$

$$\dot{m}_{rec} = \dot{m}_n - \dot{m}_{out} \tag{B59}$$

The state vector, x, is expanded to include the total mass of refrigerant inside accumulator/receiver, m_{rec}. The $\dot{m}$ element of the time derivative of the state vector is also expanded to include the mass flow rate of the refrigerant at the accumulator/receiver inlet ($\dot{m}_n$). The resulting equations can be expressed in a slightly modified form of Equation (B17a) as shown in Equation (B60). The modified elements of $Z(x,u)$ and $f(x,u)$ are given in Equations (B17b) to (B28).

$$Z(x,u)\begin{bmatrix} \dot{P} \\ \dot{h} \\ \dot{m} \\ \dot{T}_w \\ \dot{m}_{rec} \end{bmatrix} = f(x,u) \tag{B60}$$

$$Z(x,u)=\begin{bmatrix} Z_{11} & Z_{12} & Z_{13} & 0 & 0 \\ Z_{21} & Z_{22} & Z_{23} & 0 & 0 \\ 0 & 0 & 0 & Z_{34} & 0 \\ Z_{41} & 0 & Z_{43} & 0 & Z_{45} \\ 0 & 0 & Z_{53} & 0 & Z_{55} \end{bmatrix}_{(3n+2)X(3n+2)} \tag{B61}$$

$$f(x,u)=\begin{bmatrix} f_1 \\ f_2 \\ f_3 \\ f_4 \\ f_5 \end{bmatrix} \tag{B62}$$

$$Z_{13}=\begin{bmatrix} h_1 & 0 & \cdots & \cdots & \cdots & 0 \\ -h_1 & h_2 & 0 & \cdots & & \vdots \\ 0 & -h_2 & h_3 & 0 & \cdots & \vdots \\ \vdots & \ddots & \ddots & \ddots & \ddots & \vdots \\ 0 & \cdots & \cdots & \cdots & -h_{n-1} & h_n \end{bmatrix}_{nXn} \tag{B63}$$

$$Z_{23}=\begin{bmatrix} 1 & 0 & \cdots & \cdots & \cdots & 0 \\ -1 & 1 & 0 & \cdots & & \vdots \\ 0 & -1 & 1 & 0 & \cdots & \vdots \\ \vdots & \ddots & \ddots & \ddots & \ddots & \vdots \\ 0 & \cdots & \cdots & \cdots & -1 & 1 \end{bmatrix}_{nXn} \tag{B64}$$

$$Z_{41}=\left[\frac{d\rho_g}{dP}V_g u_g+\frac{d\rho_f}{dP}V_f u_f+\frac{du_g}{dP}m_g+\frac{du_f}{dP}m_f - \left(\frac{\rho_g u_g-\rho_f u_f}{\rho_g-\rho_f}\right)\left(\frac{d\rho_g}{dP}V_g+\frac{d\rho_f}{dP}V_f\right)\right]_{1X1} \tag{B65}$$

$$Z_{43}=[0 \quad \dots \quad 0 \quad -h_n]_{1Xn} \tag{B66}$$

$$Z_{45}=\left[\left(\frac{\rho_g u_g-\rho_f u_f}{\rho_g-\rho_f}\right)\right]_{1X1} \tag{B67}$$

$$Z_{53}=[0 \quad \dots \quad 0 \quad -1]_{1Xn} \tag{B68}$$

$$Z_{55}=[1]_{1X1} \tag{B69}$$

$$f_1 = \begin{bmatrix} \dot{m}_{in} h_{in} + \alpha_{i,1} A_{i,1} (T_{w,1} - T_{r,1}) \\ \alpha_{i,2} A_{i,2} (T_{w,2} - T_{r,2}) \\ \vdots \\ \alpha_{i,n-1} A_{i,n-1} (T_{w,n-1} - T_{r,n-1}) \\ \alpha_{i,n} A_{i,n} (T_{w,n} - T_{r,n}) \end{bmatrix}_{nX1} \tag{B70}$$

$$f_2 = \begin{bmatrix} \dot{m}_{in} \\ 0 \\ \vdots \\ 0 \end{bmatrix}_{nX1} \tag{B71}$$

$$f_4 = \left[-\dot{m}_{out} h_{rec,out} - UA_{rec} (T_{rec} - T_{amb}) \right]_{1X1} \tag{B72}$$

$$f_5 = [-\dot{m}_{out}]_{1X1} \tag{B73}$$

Table B14 shows the additional operating conditions required for the FCV with accumulator/receiver model.

Table 14: Additional operating conditions

Variable	Description	Units
V_rec	Volume of the accumulator/receiver	m^3
UA_rec	External heat transfer coefficient of receiver	$kJ/K/s$
minv_rec	Initial mass of refrigerant in the receiver	kg
Tamb	Ambient temperature	^oC